SYNTHESIS AND CHARACTERIZATION OF LANTHANIDE COMPLEXES FOR USE IN NEAR-INFRARED LIGHT EMITTING DIODES

By

ALISON STEELE KNEFELY

A DISSERTATION PRESENTED TO THE GRADUATE SCHOOL
OF THE UNIVERSITY OF FLORIDA IN PARTIAL FULFILLMENT
OF THE REQUIREMENTS FOR THE DEGREE OF
DOCTOR OF PHILOSOPHY

UNIVERSITY OF FLORIDA

2005

This document is dedicated to my grandparents RADM and Mrs. Richard A. Paddock and Mr. and Mrs. George M. Knefely, Sr., my parents Dr. and Mrs. George M. Knefely, Jr. and my loving husband Charles Robert Sides.

ACKNOWLEDGMENTS

First of all, I would like to thank my advisor, Jim Boncella, for all of his guidance, understanding and support throughout my graduate career. I would like to also thank him for the opportunity to work at Los Alamos National Lab, where I had the privilege to meet and work with other great scientists. I would like to thank Tony Burrell for taking me under his wing at LANL and for sharing his knowledge of porphyrin chemistry and electrochemistry. I would like to thank all the people who made it a smooth transfer to and from the lab, especially Bill Tumas, Bev Ortiz and Deb Allison-Truijillo. I would like to thank my dear friends and colleagues, especially Edel Minogue, Paul and Isabel Plieger, Gavin Collis, Piyush Shulka and the Burrell and Boncella families who not only helped in chemistry, but made me a part a family, provided tennis partners and made living in Los Alamos enjoyable and memorable.

I would like to thank Kirk Schanze and all the members of the group who provided a bench, hood, desk and a group of great people with whom to work. I would like to thank Lisa McElwee-White and all of the group members who provided a glove box and solvent system for me to use. I would like to thank the former members of the Boncella group, especially Elon Ison, Tim Foley and Tom Cameron, for all of their friendship and guidance. I would like to thank all the collaborators who have come together to make this work possible, especially Khalil Abboud, Brian Scott, John Reynolds, Paul Holloway, Ben Harrison, Garry Cunningham, T.S. King , Nisha Ananthakrishnan and Fengui Guo. I would like to thank my undergraduate research advisor, R. Chris

Schnabel. Without his love for chemistry, I would not have developed a taste for synthetic chemistry and without his guidance, I would not have pursued a career in chemistry.

I would like to thank my parents whose love and support have carried me through all of these years. I thank my entire family, the Knefelys, Paddocks, Stumpfs and Sides, for all of their encouragement. Finally, I would like to thank my husband Rob for giving me the love, strength and laughter to finish and make it a fun ride.

TABLE OF CONTENTS

TABLE

Table page

LIST OF FIGURES

Abstract of Dissertation Presented to the Graduate School
of the University of Florida in Partial Fulfillment of the
Requirements for the Degree of Doctor of Philosophy

SYNTHESIS AND CHARACTERIZATION OF LANTHANIDE COMPLEXES FOR USE IN NEAR-INFRARED LIGHT EMITTING DIODES

By

Alison Steele Knefely

December 2005

Chair: James M. Boncella
Major Department: Chemistry

The synthesis and characterization of a series of new lanthanide porphyrin and phthalocyanine complexes was investigated in order to study the luminescence properties of these complexes for polymer light emitting diodes. These lanthanide complexes consist of the near-infrared emitting lanthanides (Ln=Pr^{3+}, Nd^{3+}, Ho^{3+}, Tm^{3+}, Yb^{3+}), a macrocyclic chromophore to sensitize the emission of the lanthanide ion, and a capping ligand to encapsulate and shield the lanthanide from solvent molecules that affect emission efficiency. Lanthanide complexes were synthesized with a variety of chromophores and capping ligands to study the effects of different molecules on device efficiency.

The procedure to synthesize LnTPP(X)(DME) complexes provided a high yielding approach to new lanthanide porphyrin complexes that serve as the starting material for a variety of lanthanide-porphyrin complexes *via* a salt metathesis reaction, replacing the halide and solvent molecules with multidentate ancillary ligands. Lanthanide

monoporphyrinate complexes, LnTPP (TPP=tetraphenylporphyrin) were synthesized and characterized with the capping ligands hydrotris(pyrazolyl)borate (Tp), (cyclopentadienyl)tris(diethylphosphinito)cobalt(I), K(LOEt), and (hydroxy)quinolate (Q) to study the effects of capping ligands on device efficiency. Effects of varying the chromophore were also studied with the synthesis of lanthanide complexes of tetra(2,3,4-trimethoxyphenyl)porphyrin (TmPP), tetra(4-pyridyl)porphyrin (TPyP), tetra(3-ethylhexyloxypheny)porphyrin (TPPoeh) and phthalocyanine (Pc). These complexes were isolated in high yields and characterized by 1-D and 2-D NMR spectroscopy, UV/Vis spectroscopy and elemental anaylsis. Photoluminescent studies on Ln(porphyrin)L complexes showed NIR emission with quantum efficiencies ranging from 4.1%-0.91%. Electroluminescent studies using devices blended with polystyrene and Ln(porphyrin)L complexes produced NIR emission with quantum efficiencies ranging from 0.01%- 0.03%.

Studies were then conducted on the effects of incorporating the Ln-porphyrin complex into a polymer backbone. A ytterbium-vinylporphyrin complex was copolymerized with *t*-butylstyrene and trifluoroethyl methacrylate to give a copolymer with 1 mol% of the lanthanide complex and a weight average molecular weight (M_w) and a number average molecular weight (M_n) of ~ 200,000 and 90,000, respectively. Polymers containing trispyrazole borate (Tp) units were synthesized by Prof. Frieder Jaekle's group, at Rutgers University, and yielded the Yb-TPP incorporated polymer. Absorption and NIR emission studies showed typical LnTPP absorption and Yb-emission.

CHAPTER 1
INTRODUCTION

Organic and polymeric light emitting diodes (OLEDs and PLEDs) represent a rapidly growing field as industry and academia pursue the development of new, inexpensive, durable, flexible and efficient light sources. These materials are able to produce light through electroluminescence, a process in which an applied electric field generates an excited species that radiatively decays. Research has developed OLEDs and PLEDs that produce light across the entire visible region with device efficiency, brightness and lifetime rapidly approaching commercial target figures (Figure 1.1).[1]

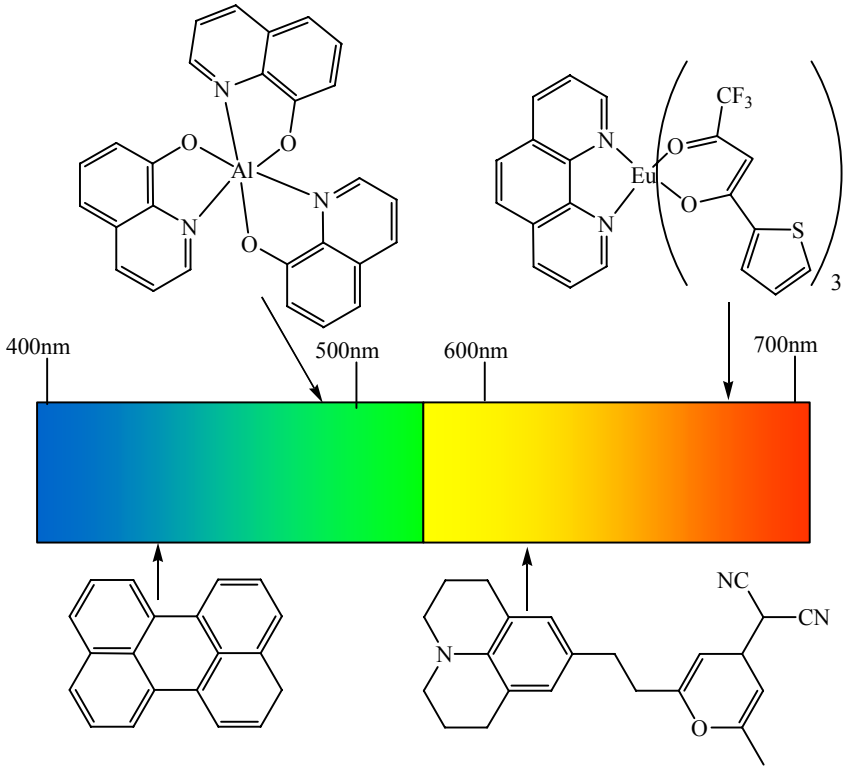

Figure 1.1: Examples of compounds used as emitters in OLEDs.[2]

The first efficient electroluminescence from an organic solid was demonstrated in the early 1960s using anthracene crystals.[3] Crystals 1-5 mm thick emitted blue light with quantum efficiencies ~ 8%, but with operating voltages between 50-1000 V.[4] Improvement in device construction and operation occurred in 1987 with the construction of the first vacuum deposited multi-layer device.[5] The device consisted of a double layer of organic thin film, with one layer capable of only monopolar transport and the other layer capable of luminescence. Devices using an aromatic diamine as the first organic layer and 8-hydroxyquinoline aluminum (AlQ_3) as the luminescent material produced high brightness green light with voltages as low as ~10 V (Figure 1.2).

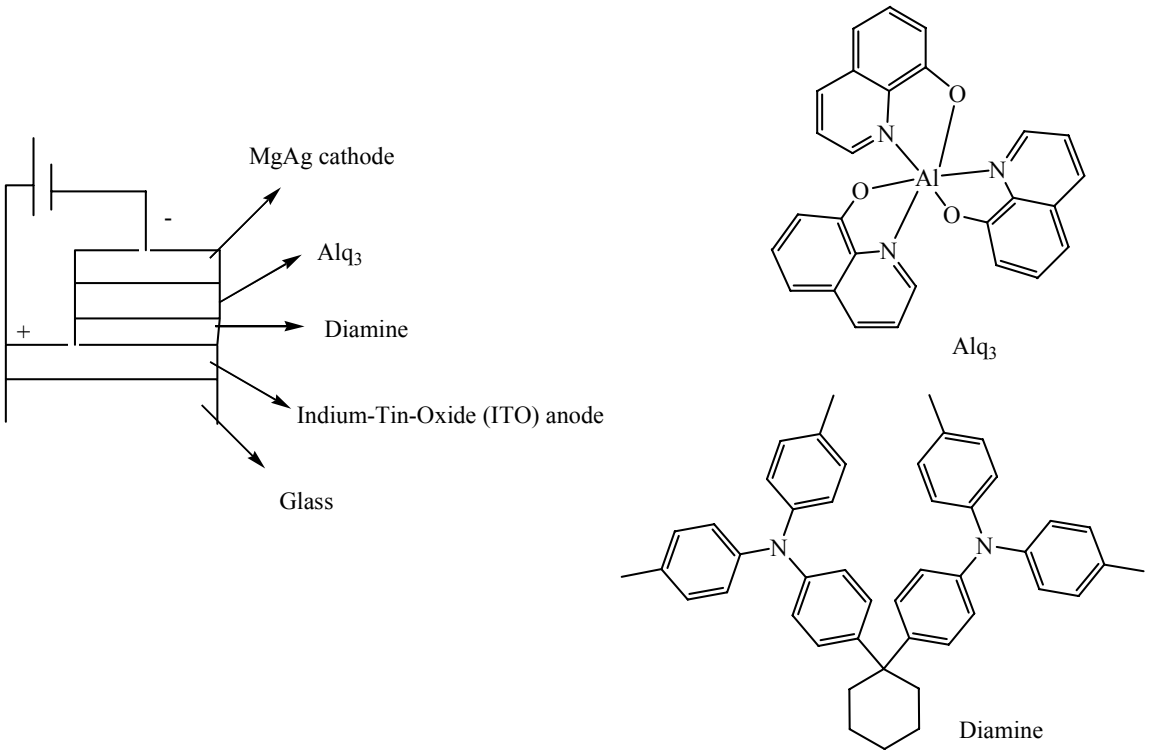

Figure 1.2: Configuration of multi-layer device and molecular structures.

Since the development of organic thin film electroluminescence by Tang in the 1980s,[6] there has been much interest in organic, as well as conjugated polymer (CP) thin films as new materials for light emitting diodes (LEDs). With the construction of a

device using poly(*p*-phenylene vinylene), Borroughes *et al*. showed that polymeric thin films can produce efficient devices.[7] Polymer based LEDs (PLEDs) have many advantages over current inorganic devices such as low costs, easy processing and the ability to emit in wavelengths that span the visible spectrum.[8]

The simplest device configuration consists of a single organic/polymeric layer in between an anode and a cathode. With an applied electric field, holes from the anode and electrons from the cathode are driven into the emissive layer, where they recombine to form an excited state of the polymer that decays either radiatively or non-radiatively. The cathode is a low work function material that injects electrons into the lowest unoccupied molecular orbital (LUMO) of the emissive layer and is typically a metal such as calcium, magnesium, or aluminum. The anode is a high work function material that injects holes into the highest occupied molecular orbital (HOMO) of the emissive layer. Indium-tin-oxide (ITO) is a commonly used anode because of its good transmission properties over the desired wavelength range.

In a single layer device, the organic/polymeric layer serves as the emitting source as well as the charge carrier and should therefore have high photoluminescence quantum efficiency and the ability to transport holes and electrons. Single layered devices, however, exhibit low quantum efficiencies and short operational lifetimes caused by enhanced quenching at the electrode-organic interface as well as deterioration of the organic layers.[4,9] Because a single material having all the necessary properties for optimal device performance does not exist, additional layers can be added to the LED to improve the charge transport, quantum efficiency of emission and stability of the device.[10] A typical multilayer device is comprised of an anode (ITO), a hole transport

layer, emitting layer, electron transport layer and a cathode (Figure 1.3). More elaborate device construction strategies have also been used.

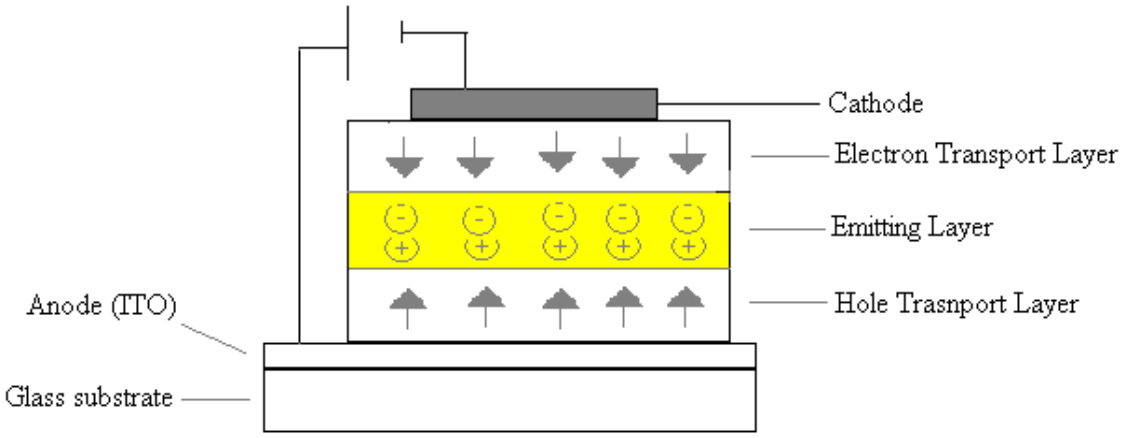

Figure 1.3: Configuration of a typical multi-layer device.

An effective hole-transport layer should have a low ionization potential for efficient injection of holes from the anode, a higher exciton energy level than the emissive layer for confining excitons within the emissive layer and should be transparent to the radiation emitted from the device.[10] A commonly used polymer is poly(3,4-ethylenedioxythiophene) doped with polystyrene sulfonic acid (Figure 1.4). The introduction of an electron-transport layer helps control charge injection, transport, and recombination in the emissive layer of the device. The electron transport material should have a high ionization potential to efficiently block holes and high electron mobility to transport electrons to the emissive layer. Oxadiazoles such as 2-(4-biphenyl)-5-(4-*t*-butylphenyl)-1,3,4-oxidiazole (PBD) and metal chelates such as AlQ_3 are the most widely used electron transport materials (Figure 1.4).[11]

Conjugated polymers (CP) typically used for emission include a yellow-green emitter poly(*p*-phenylene vinylene) (PPV), the first CP used in a PLED,[7] an orange-red

emitter poly(2-(2'-ethylhexyloxy)-5methoxy-1,4-phenylene vinylene) (MEH-PPV) and a blue emitter poly(*p*-phenylene) derivative, PPP-OR11 (Figure 1.5).

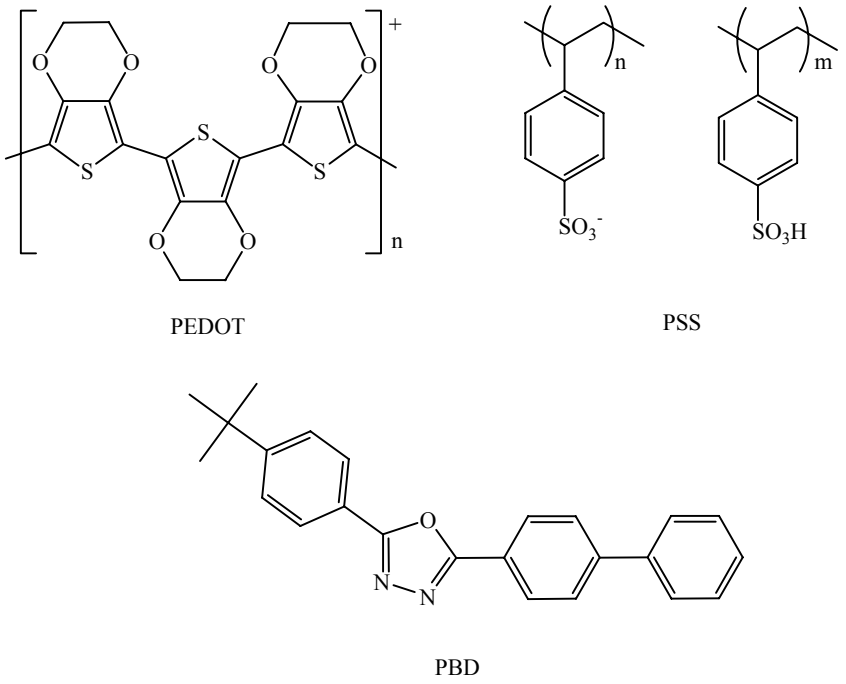

Figure 1.4: Common organic molecules for hole and electron transport.

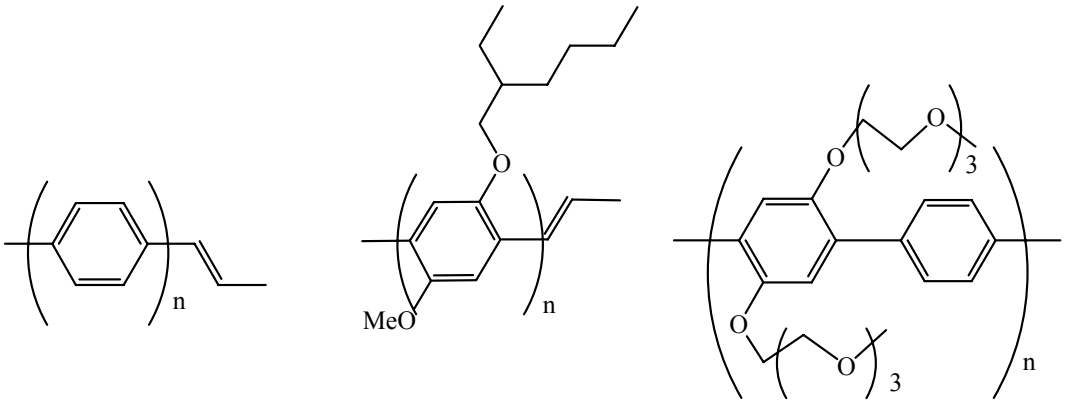

Figure 1.5: Commonly used conjugated polymers for emission in device construction.

While there has been much research devoted to the improvement of the luminescence and efficiencies of PLEDs, there are some inherent problems with pure PLEDs. When recombination occurs, the spin wave function (S) of the excited molecule

can either be a singlet (S=0) or triplet (S=1). In organic materials, the triplet state decays non-radiatively.[1] Statistically, 75% of injected charges are in the triplet state, limiting organic device efficiencies to about 25%.[10] Another problem is that CPs have broad emission spectra, with a typical full width at half max of 50-200 nm,[12] which gives rise to poor color purity. Consequently, PLEDs do not have the ability to produce finely tuned emission with maximum efficiencies.

In order to combat these problems of pure PLEDs, recent work has focused on blending polymers with materials with significant spin-orbit coupling, which facilitates inter-system crossing and allows triplet state emission. Organometallic compounds have been found to be prime examples of good triplet state emitters and therefore successful dopants for polymer devices. The dopant can harvest energy from the polymer by Förster energy transfer (induced dipole mechanism) or Dexter energy transfer (an electron exchange mechanism) (Figure 1.6) or direct charge trapping and exciton formation on the dopant itself.[2,13] Efficient energy transfer from host to dopant depends on the quantum yield of emission by the donor (D*), the light absorbing ability of the acceptor (A) and the overlap of the emission spectrum of D* and the absorption spectrum of A.

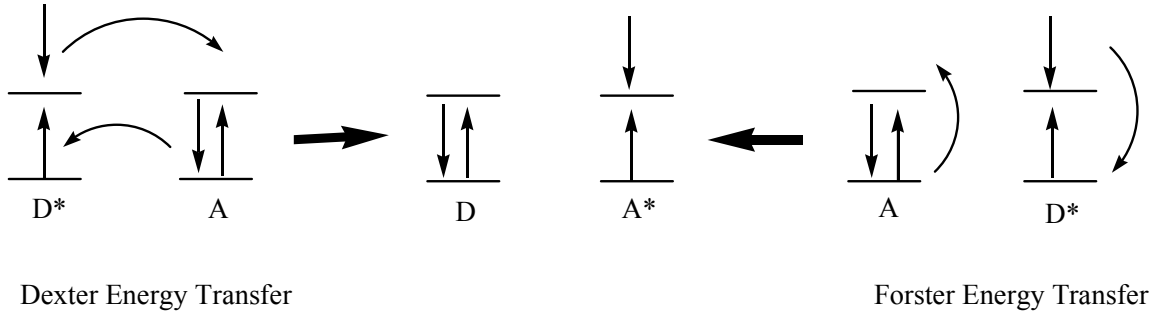

Figure 1.6: Scheme of Dexter and Forster energy transfer mechanisms.

Recently published reports show that devices constructed with blends of platinum (Pt) and iridium (Ir) complexes have high luminescence effieciences with the ability to

tune the emission color through much of the visible region by simply changing the ligands of the complex.[1] Thompson and coworkers have synthesized a series of Ir-(acetylacetonate) complexes that give green, yellow and red electroluminescence with external quantum efficiencies ranging from 6%-12% (Figure 1.7).[14]

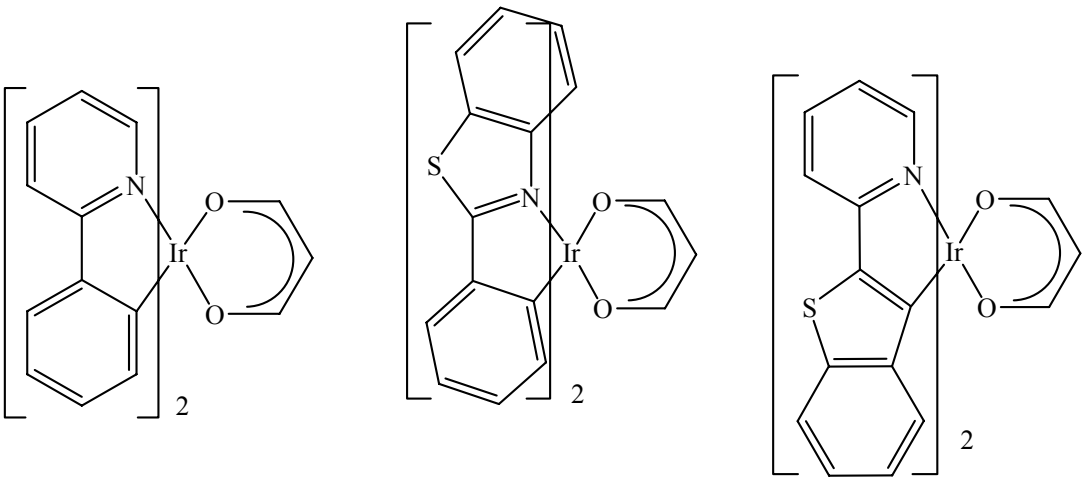

ppy$_2$Ir(acac) Green

bt$_2$Ir(acac) Yellow

btp$_2$Ir(acac) Red

Figure 1.7: Ir(acac) dopants for OLEDs.

With unique optical properties such as line like emission, long luminescence lifetimes and a wide spectral range (from blue to near-infrared), the trivalent lanthanides have also been used as dopants in LEDs.[15] The optical properties are governed by the 4*f*-orbitals, which are shielded from external forces by the 5*p* and 5*s* orbitals. The 4*f*-orbials only weakly interact with the ligands bound to the metal center, leading to small ligand field splitting and thus sharp emission spectra at certain wavelengths regardless of the ligand. The *f-f* transitions, however, are forbidden and consequently the lanthanides have rather low molar absorptivity coefficients and must be sensitized to produce intense emission. The process of sensitized emission,[16] known as the antenna effect, begins with the ligand absorbing energy, undergoing inter-system crossing from singlet to triplet state

and then transferring the energy to the lanthanide metal center (Figure 1.8). The excited state of the antenna must, therefore, be higher in energy than the emissive level of the lanthanide metal center.

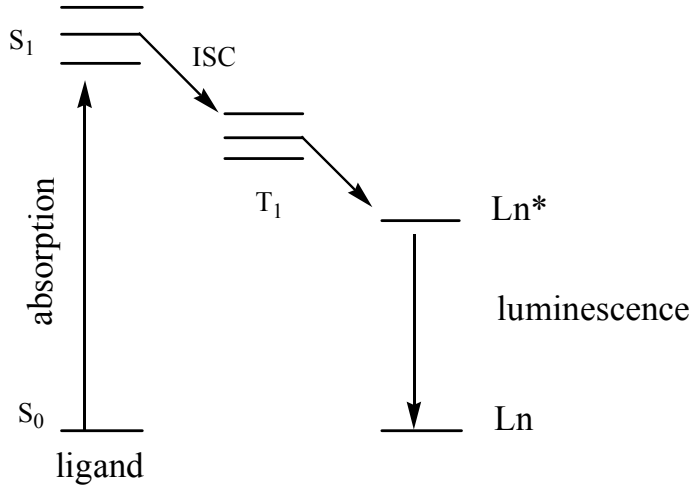

Figure 1.8: Energy transfer from chromophore to lanthanide metal center for sensitized emission.

The first reports of devices using lanthanide complexes as the emitting species used Eu(thenoyltrifluoroacetonate)$_3$ (Eu(TTFA)$_3$) and Tb(acac)$_3$ to produce red and green emission, respectively.[17,18] Since these reports, there have been many studies examining a variety of Tm^{3+} complexes for blue light[19] and Eu^{3+} and Tb^{3+} complexes for sharp emission of red, green and white light.[10,20-23]

Interest in NIR/IR emitting devices for such uses as telecommunication and sensors has brought the blending of CPs with lanthanides to the attention of many research groups including ours. Figure 1.9 shows the normalized luminescence spectra of the near-infrared emitting lanthanides.

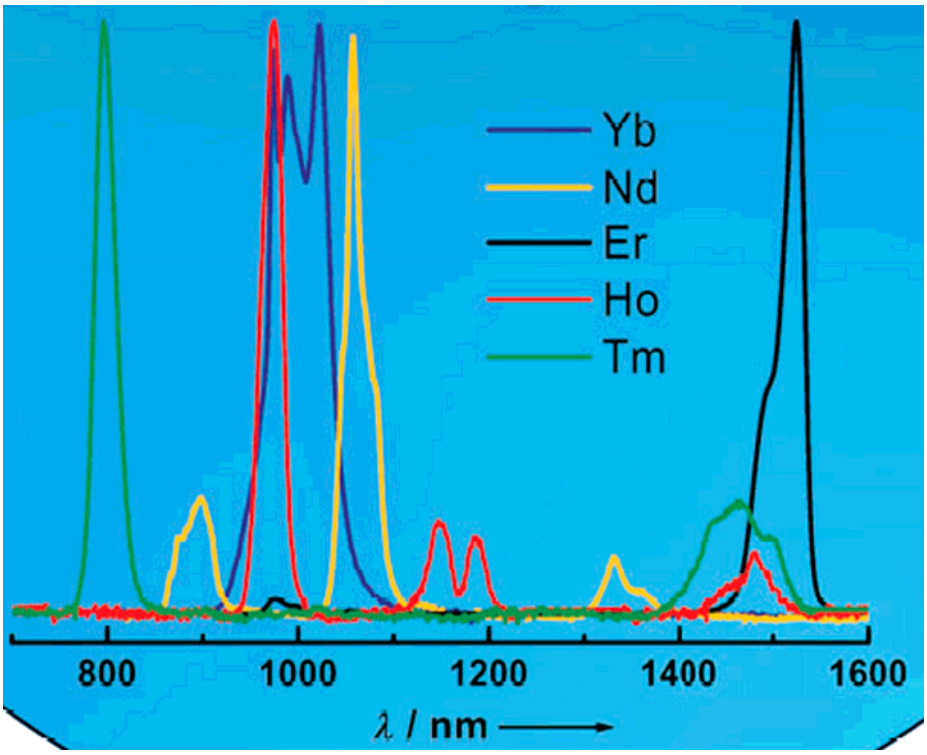

Figure 1.9: Normalized luminescence of Yb^{3+}, Nd^{3+}, Er^{3+}, Ho^{3+} and Tm^{3+}.[24]

Recent reports show NIR emission from devices made with blends of a CP and Er (acetylacetonato)$_3$(1,10-phenanthroline) to give 1.54 μm emission[25] and a Nd(lissamine) complex to produce typical Nd^{3+} luminescence at 890, 1060 and 1340 nm.[26] The low – lying radiative levels of the lanthanide ions are easily quenched by the vibrational energy of O-H and C-H molecules from solvents or ligands; thus, ligands bound to the lanthanides should not only contain a chromphore that can readily excite the lanthanide, but should also encapsulate the ion to shield it from solvent molecules. In efforts to improve device luminescence and efficiencies, our group has become interested in synthesizing lanthanide complexes of nitrogen-based macrocycles for use in NIR LEDs. The following chapters discuss the synthesis and characterization of a series of new lanthanide porphyrin and phthalocyanine complexes. The use of these compounds in

PLED devices and the characterization of the performance of these devices are also presented.

CHAPTER 2
LANTHANIDE TETRAPHENYLPORPHYRIN COMPLEXES: SYNTHESIS, CHARACTERIZATION AND LUMINESCENCE STUDIES

Introduction

Porphyrins are interesting molecules because their large π systems give them properties that allow them to be used in photodynamic therapy, areas of light harvesting, catalysis and optics.[27] As highly conjugated molecules, porphyrins are promising organic molecules for the design of efficient luminescent materials. Forrest *et al.* have used tetraphenylporphyrin (TPP) as the red emitter in light emitting diodes (LED),[28,29] while other groups have examined platinum porphyrin complexes as emissive dopants in LEDs.[12,29-32]

The small absorption coefficients of the lanthanides make light absorption and emission an inefficient process for these metal ions and require that sensitization by a coordinating ligand be used for efficient light absorption and emission. Contributing factors to the luminescence intensity are the intensity of the ligand absorption and the efficiency of ligand-to-metal energy transfer.[33] With a molar absorptivity ~300,000 and triplet energies typically around 12,000 cm^{-1}-17,000 cm^{-1}, studies show that TPP efficiently absorbs light and transfers energy to the metal ions.[34-36] These studies also reveal that lanthanide-porphyrin complexes possess rapid rates of energy transfer from the porphyrin to the lanthanide ion.

The intense Soret band of lanthanide porphyrin complexes leads to facile singlet excitation, while the presence of the lanthanide ion gives rise to facile inter-system

crossing to the low energy triplet state that can readily excite the emissive states of the lanathanide ion.[37-39] Meanwhile, the highly delocalized π system of these complexes is suitable for efficient hole-transport[40,41] through the bulk material. This combination of properties makes TPP a proficient ligand for energy transfer to near-infrared emitting lanthanide ion.

Previous Synthetic Procedures

The first synthesis of lanthanide-monotetraphenylporphyrin (LnTPP) complexes was reported by Wong *et al.* in 1974.[42] Lanthanide-monoporphyrinate complexes have been studied for their use as NMR shift reagents,[42-44] and as probes in the area of clinical and molecular biology,[45,46] but difficulties in their syntheses have stunted the growth of research in this field. As the accepted LnTPP synthesis, Wong's procedure involves the reaction between $Ln(acac)_3$ and the free base tetraphenylporphyrin (H_2TPP) in refluxing trichlorobenzene. While progress of the reaction monitored by UV/Vis spectroscopy shows a yield of greater than 90%, the LnTPP(acac) compound is isolated by column chromatography, leading to product decomposition and isolated yields of 10-30%. With the use of this method, Yb- and Er-porphyrin complexes were synthesized and found to be viable as NIR lumophores in NIR LEDs.[39] These results stimulated our interest in finding a high yielding synthetic procedure that would allow us to access complexes with a variety of ligands that might have improved luminescent properties.

Since the first reported synthetic procedure for lanthanide monoporphyrinate complexes, there have been few reports of new procedures that improve conditions or yields with most research utilizing Wong's procedure.[37,47-49] In 1999, an alternate procedure generating a hydrated LnTPP(Cl) complex was published.[50] The disadvantage

of this synthetic procedure is that the complexes are coordinated to several equivalents of water. Since the excited state of the lanthanide ion is effectively quenched by vibrational energy transfer to solvents or ligands containing O-H groups, this synthetic procedure is not amenable for use in near IR emissive systems.

Recently our lab has developed a high yielding synthetic procedure for lanthanide tetraphenylporphyrin chloride complexes[51] *via* a salt metathesis reaction between tetraphenylporphyrin dianion and anhydrous $LnCl_3$. Reaction of these compounds in refluxing toluene gave the lanthanide tetraphenylporphyrin chloride (LnTPPCl(DME)) in yields greater than 75%. Progress of the reaction can be monitored by UV/Vis spectrometry as the Soret band shifts from 417 nm of free TPP to 422 nm for metalloporphyrin. The complexes are then easily isolated by simple filtration and recrystallization. This synthetic approach was successfully applied to ytterbium, thulium, erbium and holmium complexes (Figure 2.1).

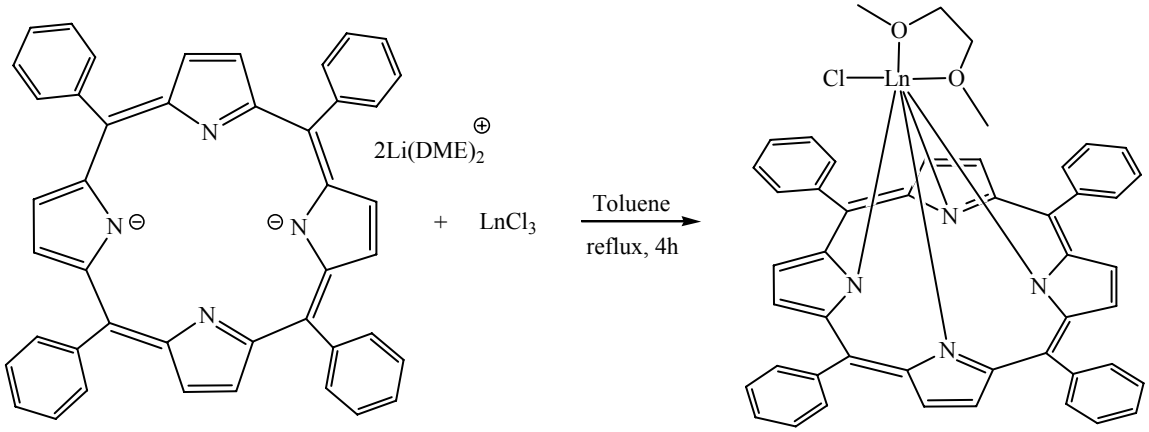

Figure 2.1: Synthesis of LnTPPCl(DME) where Ln = Ho, Er, Tm, and Yb.

These complexes were then used to synthesize a series of sterically saturated monoporphyrinate lanthanide complexes *via* a second salt metathesis reaction, replacing the chloride ion and solvent molecule with an ancillary ligand (Figure 2.2). Addition of

potassium acetylacetonate to the Yb complex in dimethoxyethane gave the YbTPP(acac) complex in yields greater than 90%.

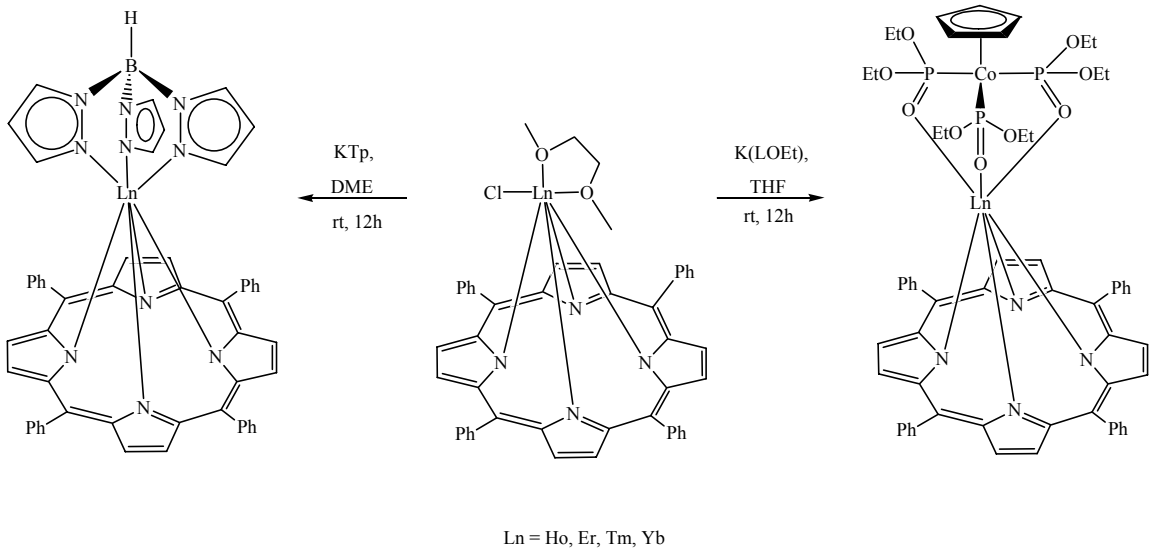

Figure 2.2: Synthesis of LnTPP(L) complexes (Ln= Ho, Er, Tm,Yb and L= Tp,L(OEt)).

Synthesis of Nd and Pr Complexes

In order to complete the series of near-IR emitting lanthanides, the same synthetic routes used to synthesize LnTPPCl(DME) complexes of the smaller lanthanides Er, Ho, Tm, and Yb were used to try to make the complexes of the larger lanthanides, neodymium (Nd) and praseodymium (Pr). After four hours of refluxing the $LnCl_3$ with the TPP anion in dry toluene, the UV/Vis spectrum of the reaction mixture showed free TPP with an absorbance peak at 415 nm and no evidence of metallated porphyrin. The reaction was then refluxed for twelve hours with the same results and no isolation of product.

Half-Sandwich Complexes

Inspired by the recent work of the Bianconi group,[52] we attempted another synthetic route to obtain Nd and Pr porphyrin compounds. Bianconi recently reported the synthesis of neodymium tris(1-pyrazolyl)borate diiode ($NdTpI_2(THF)_2$), and we pursued

the displacement of the iodide ligands with TPP dianion as an alternative route to the desired complexes, NdTPPTp and PrTPPTp.

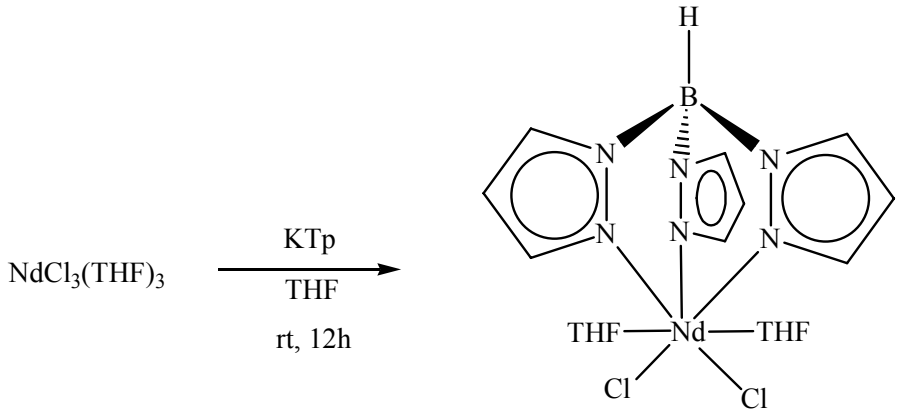

Figure 2.3: Synthesis of $NdTpCl_2(THF)_2$.

In an attempt to make the analogous chloride complex, $NdTpCl_2(THF)_2$, $NdCl_3(THF)_3$ was treated with KTp (Figure 2.3). After stirring for twelve hours, the resulting blue solution was filtered, the solvent removed under reduced pressure and the product was extracted with methylene chloride. Layering the CH_2Cl_2 solution with pentane gave an immediate blue precipitate, which had proton NMR shifts corresponding to the Tp protons at -0.55 ppm, 7.64 ppm and 13.2 ppm. The proton NMR, however, was significantly different from the proton NMR of the diiodide complex in that the Tp peaks had different chemical shifts and there were no peaks associated with coordinated THF. The Biaconi group reported[52] the synthesis of ytterium Tp chloride and bromide complexes, but only the iodide complex of neodymium. These results suggested that perhaps the chloride ions were not large enough to satisfy the coordination sphere of neodymium and the complex was not a half sandwich but perhaps a dimer or higher aggregate. Attempts to obtain crystals of this compound were unsuccessful.

LnTPPI(DME) Complexes

Given the differences in the behavior of the chloride and iodide complexes, the complexes $NdI_3(THF)_4$ **(1)** and $PrI_3(THF)_4$ **(2)** were prepared according to the literature procedure used for $CeI_3(THF)_4$ as shown in equation 2.1.[53]

$$Ln^0 + 3CH_3CH_2I \xrightarrow{THF} LnI_3(THF)_n \qquad (2\text{-}1)$$

The lanthanide triiodide complexes **1** and **2** were used in salt metathesis reactions with $Li_2TPP(DME)_2$ (Figure 2.4). After refluxing the lanthanide triiodide and TPP dianion in toluene for four hours, the UV/Vis of the reaction mixture showed an absorption at ~425 nm corresponding to metallated TPP. The solution was then separated from KI by hot filtration and after layering with pentane, the complexes NdTPPI(DME) **(3)** and PrTPPI(DME) **(4)** precipitated in 74% and 72% yields, respectively.

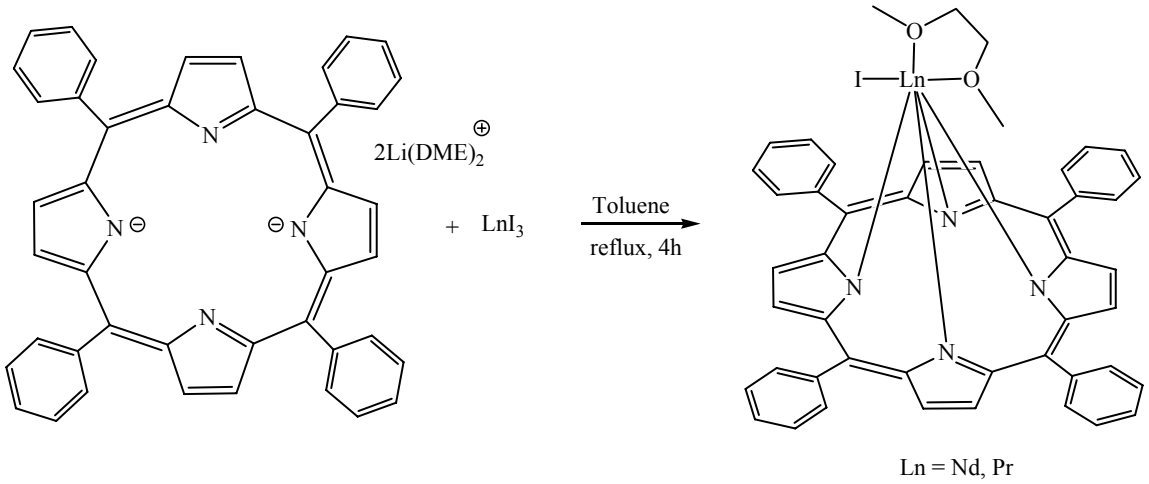

Figure 2.4: Synthesis of **3** and **4**.

In order to study the phosphorescence of TPP in our devices, we synthesized gadolinium and lutetium porphyrin complexes whose metal centered excited states are too high in energy to be sensitized by TPP. Similar to the previously stated procedure, GdTPPCl(DME) **(5)** and LuTPPCl(DME) **(6)** were synthesized by reaction of the lanthanide trichloride with the dilithiated TPP compound.

Single crystals of NdTPP(I)$(THF)_2$ were grown by slow diffusion of pentane into a saturated solution of THF and were analyzed by X-ray crystallography. The thermal ellipsoid plot of the solid–state structure of the neodymium complex with selected atom labels is shown in figure 2.5. The crystal structure shows that the lanthanide ion is seven coordinate with the metal ion bonded to the four nitrogens of the porphyrin ring, one iodide and two oxygens from coordinating THF molecules. The metal ion is too large to fit into the porphyrin cavity and so the porphyrin ring adopts a domed conformation to maximize the Ln-N interactions. The average Nd-N bond length is 2.436(1) Å and the Nd atom sits 1.286(6) Å above the mean plane of the coordinating nitrogens on the porphyrin ring.

Single crystals of LuTPPCl(DME) **(6)** suitable for X-ray structure determination were grown from a saturated solution of CH_2Cl_2 layered with pentane. The thermal ellipsoid plot of the solid–state structure of the lutetium complex with selected atom labels is also shown in figure 2.4. Similar to the Nd complex, the LuTPPCl(DME) complex is seven coordinate with the metal ion bonded to the four nitrogens of the porphyrin ring, as well as one chloride ion and two oxygens from the coordinating DME molecule. The ionic radius of the Lu ion is about 0.15 Å smaller than the Nd ion, giving rise to shorter averaged metal-ligand bond distances. The average Lu-N bond length is 2.306(1) Å and the Lu ion sits 1.098(0) Å above the mean plane defined by the nitrogen atoms of the porphyrin ring.

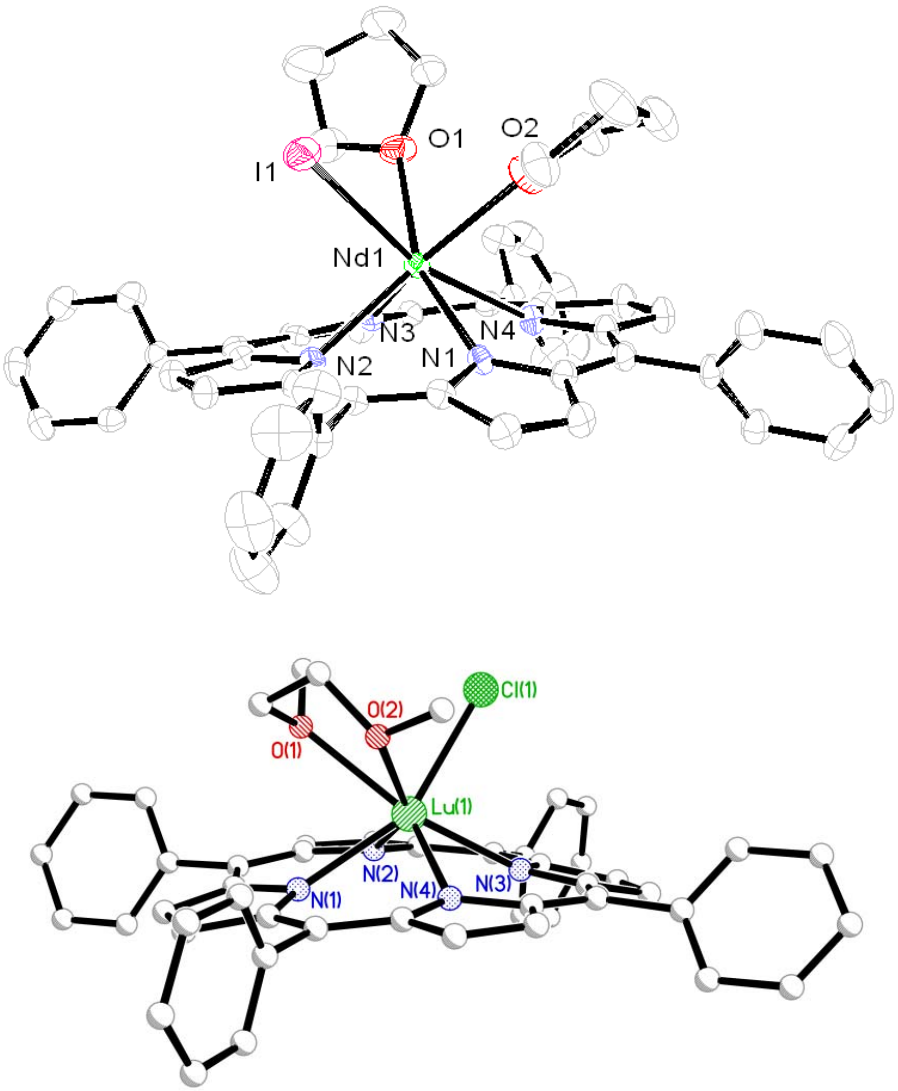

Figure 2.5: Thermal ellipsoid plots of the molecular structure of NdTPPI(DME) (top) and LuTPPCl(DME) **(6)** (bottom), showing selected atom labels, drawn at the 50 % probability level. The hydrogen atoms have been excluded for clarity.

LnTPP(L) Complexes

The LnTPPX(DME) compounds have been used to synthesize a series of sterically saturated monoporphyrin lanthanide complexes *via* a second salt metathesis reaction, replacing the halide and solvent molecule with a mutlidentate, monoanionic ancillary ligand. The low-lying emissive levels of these lanthanide ions are easily quenched by molecular vibrations, especially O-H and C-H oscillators.[54-56] In order to enhance the

luminescence properties of the complex, the ancillary ligand must provide enough steric bulk to prevent quenching agents such as water from interacting with the metal. Furthermore, the polydentate, monoanionic axial ligand saturates the coordination sphere of the metal center while maintaining a neutral complex. The complexes that we have used to fill the remaining coordination sites of the metal are hydrotris (pyrazolyl) borate (Tp), (cyclopentadienyl)tris(diethylphosphinito)cobalt (K(LOEt)), and (hydroxy)quinolate (Q) ligands.

LnTPP(Tp) complexes

Similar to cyclopentadienide ligands, Tp ligands are one of the most common supporting ligands in transition metal and lanthanide chemistry,[57] with the first lanthanide-polypyrazolylborate complex published by Bagnall in the 1970s.[58] The binding of the monoanionic ligand occurs in a tridentate fashion with the nitrogens of the pyrazolyl binding to the lanthanide. The binding properties of this ligand are easily tuned by simple manipulation of the 3- and 5-substituents of the pyrazolyl rings. Synthesis of LnTp complexes is a simple salt metathesis reaction involving a lanthanide halide or triflate and the potassium or sodium salt of the ligand to give a mono-, bis-, or tris-ligand complexes, depending on the steric bulk of the ligand.

The LnTPP(Tp) complexes of holmium, erbium, thulium and ytterbium were synthesized previously by Foley.[51,59] Recently Wong *et al.* published another synthetic route for the NdTPP(Tp) complex, prepared by reaction of the Ln(Porphyrin)$(H_2O)_3Cl$ with KTp.[60] The analogous praseodymium, neodymium,[59] gadolinium and lutetium complexes were synthesized by reaction of the potassium salt of Tp (KTp) with LnTPPX(DME) (where X = I for Pr and Nd and X = Cl for Gd and Lu) in DME , giving the desired LnTPPTp (Figure 2.6). The reaction was performed under an inert

atmosphere to prevent the hydrolysis of the LnTPP bonds. After stirring at room temperature for twelve hours, the products were extracted with CH_2Cl_2 and were then isolated as purple crystalline solids in high yields by recrystallization from a mixture of CH_2Cl_2 and pentane. The purity of the bulk material was confirmed by elemental analyses and the molecular structure of NdTPPTp **(7)** was determined by X-ray crystallography.

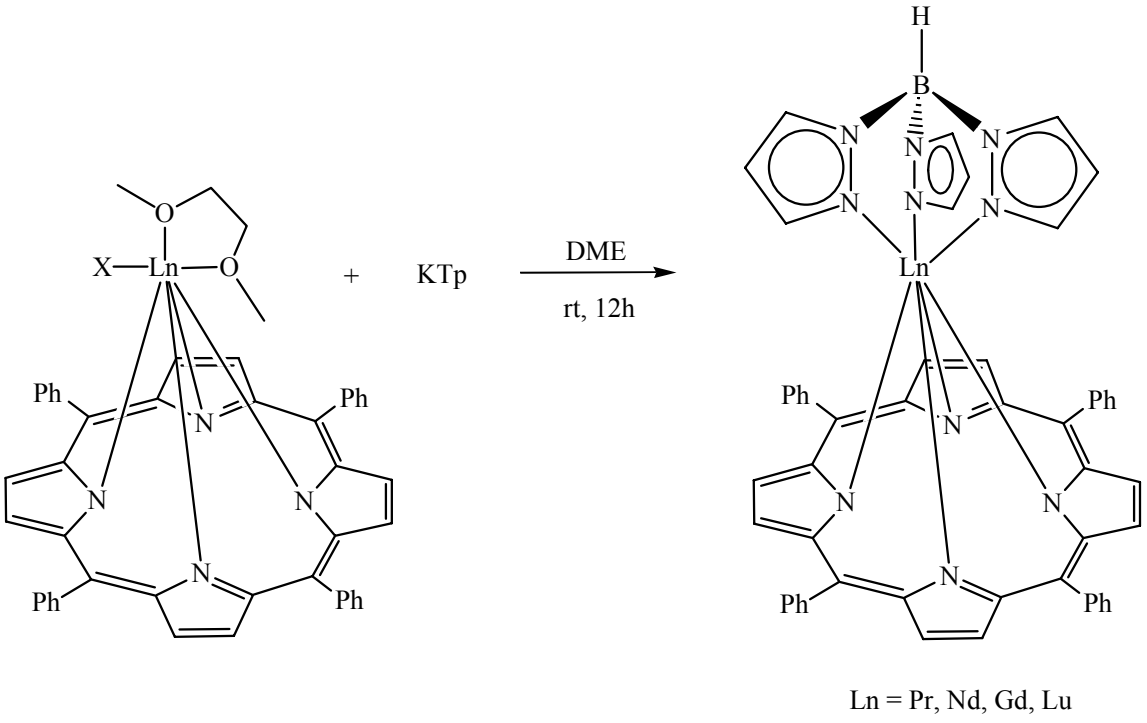

Figure 2.6: Synthesis of LnTPP(Tp) where Ln = Pr, Nd, Gd, Lu.

Slow diffusion of pentane into a saturated CH_2Cl_2 solution gave X-ray diffraction quality crystals of NdTPPTp **(7)** (Figure 2.7). The coordination geometry of the metal ion is best described as a distorted capped trigonal prism with the trigonal prism being composed of three of the porphyrin N atoms and the three pyrazolyl N atoms with the capping group being the final porphyrin N atom. The distortion in the structure is due to the different bond lengths between Nd and the nitrogens atoms of the porphyrin group.

The distances of Nd-N(4) and Nd-N(1), which are 2.458 Å and 2.447 Å respectively, are slightly longer than the Nd bond between N(2) and N(3), which are 2.427 Å and 2.421 Å, respectively. The center of the Nd atom is 1.302(4) Å above the center of the mean plane defined by the pyrrole nitrogens of the porphyrin and 1.891(7) Å below the mean plane defined by the pyrazolyl nitrogen plane. The pyrrole rings deviate from the mean plane defined by the pyrrole nitrogens by 17.0°, 8.9°, 15.3° and 5.1° for the rings containing N(1), N(2), N(3) and N(4) respectively. The porphyrin becomes puckered in order to accommodate the large metal, causing these deviations from the mean plane.

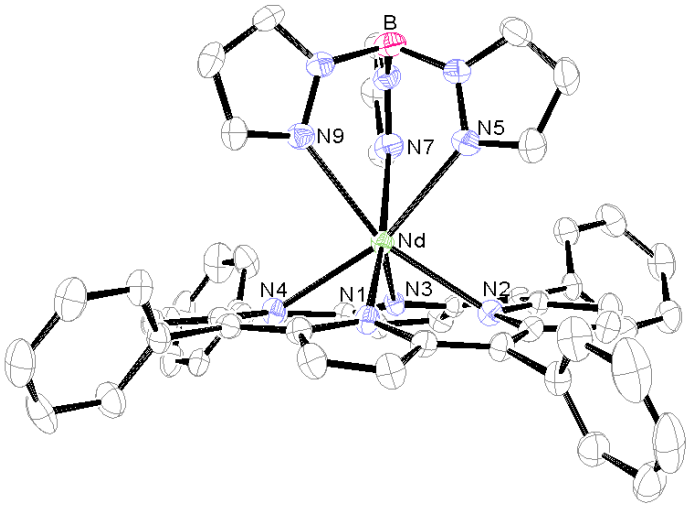

Figure 2.7: Thermal ellipsoid plot of NdTPPTp **(7)** showing selected atom labels drawn at the 50 % probability level. The hydrogen atoms have been excluded for clarity.

LnTPP(LOEt) complexes

The tripodal ligand $[(C_5H_5)Co\{P(O)(OEt)_2\}_3]$ was first reported in 1974[61] by Klaui and has been shown to be a versatile compound in the synthesis of heterobimetallic complexes. Coordination occurs through the oxygen atoms to form a tridentate ligand that has been demonstrated by Klaui *et al.* to form stable coordination compounds with

many metal ions including lanthanide ions.[62] Edelmann *et al.* have recently reported the first organolanthanide-LOEt complex by reaction of $[(\eta^8\text{-}C_8H_8)Sm(\mu\text{-}Cl)(THF)]_2$ with Na(LOEt) to obtain $(\eta^8\text{-}C_8H_8)Sm(LOEt)$.[63]

The synthetic procedure for preparing LnTPP(LOEt) is similar to that used for the TP complexes. The synthesis and crystal structure of the ErTPP(LOEt) and YbTPP(LOEt) complexes have been reported by Wong *et al.*[64,65] This procedure, however takes 48 hours and the desired products must be isolated and purified by column chromatography. The procedure developed by our lab synthesizes the same product in a one pot, 12 hour reaction in DME using simple recrystallization techniques to isolate LnTPP(LOEt) (Ln= Ho, Er, Tm, Yb) in high yields.[59] The LOEt complexes of Nd and Pr were synthesized using THF as the solvent. The reaction of K(LOEt) and NdTPPI(DME) in DME led to low yields, with the proton NMR spectrum showing free ligand (Figure 2.8).

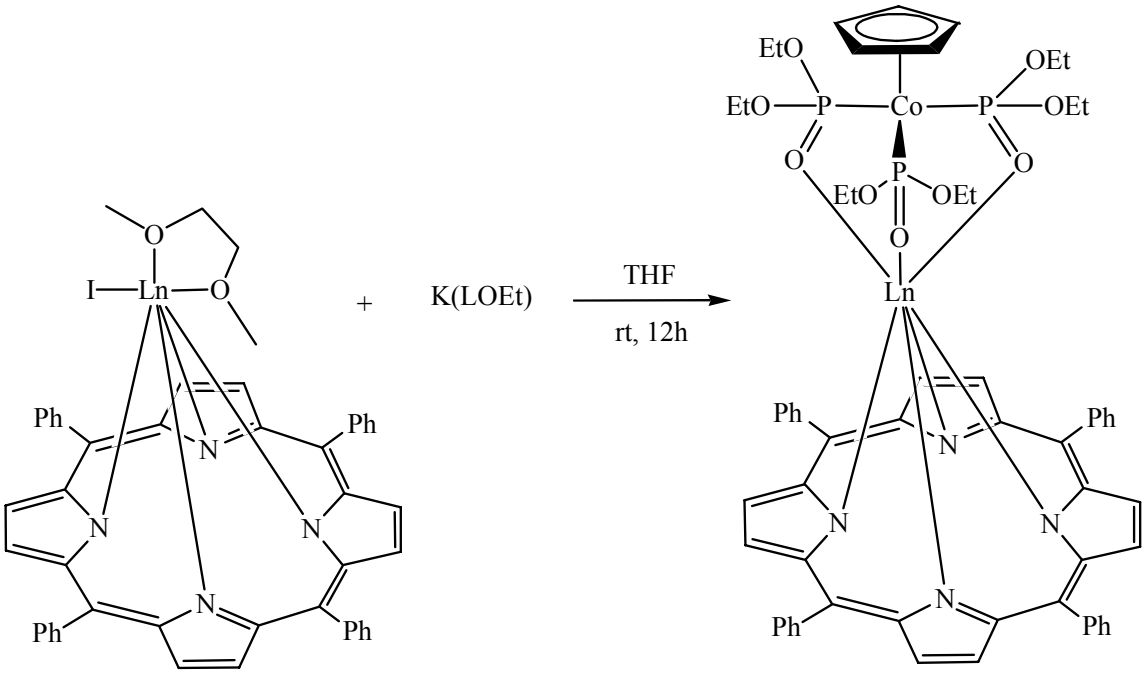

Figure 2.8: Synthesis of LnTPP(LOEt), where Ln = Nd **(11)**, Pr **(12)**.

LnTPP(quinolate) complexes

Whether used as an emitting layer or an electron transport layer, tris-(8-hydroxyquinoline)aluminum (AlQ_3) is one of the most frequently used materials for organic light emitting devices.[66,67] The incorporation of this known electron transporter into blends of our lanthanide porphyrin complexes resulted in a significant increase in device efficiency.[38] AlQ_3 likely increases the electron transport properties of the material, thereby improving the charge carrier balance in the devices. Inspired by this work, we synthesized a lanthanide porphyrin complex with quinolate capping ligands

The procedure for the synthesis of the YbTPP(Q)THF **(13)** complex was analogous to the TP and LOEt procedures. The potassium salt of quinlone (KQ) was added to YbTPPCl(DME) in THF under an inert atmosphere for twelve hours to give the desired product (Figure 2.9).

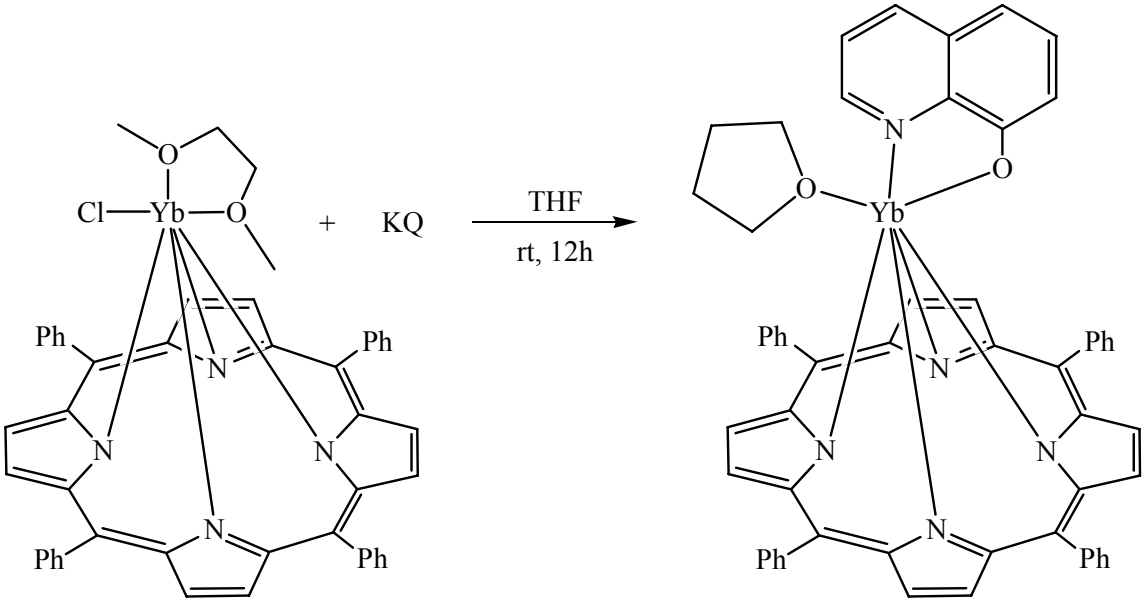

Figure 2.9: Synthesis of YbTPP(Q)THF **(13)**.

Crystals suitable for X-ray diffraction were grown from THF solutions of the complex layered with pentane. The crystal structure of **13** (figure 2.10) illustrates that the

complex is a monomer with a coordination number of seven around the metal center. The ytterbium sits 1.102(5) Å above the plane of the porphyrin and has an average Yb-N bond distance of 2.331(3) Å. The bond distances on the ligand are 2.180(2) Å and 2.538(3) Å for Yb-O(1) and Yb-N(5), respectively. The quinolate ligand is not bulky enough to shield the lanthanide from solvent coordination as seen by the coordinating THF molecule with a bond distance of 2.397(3) Å for Yb-O(2).

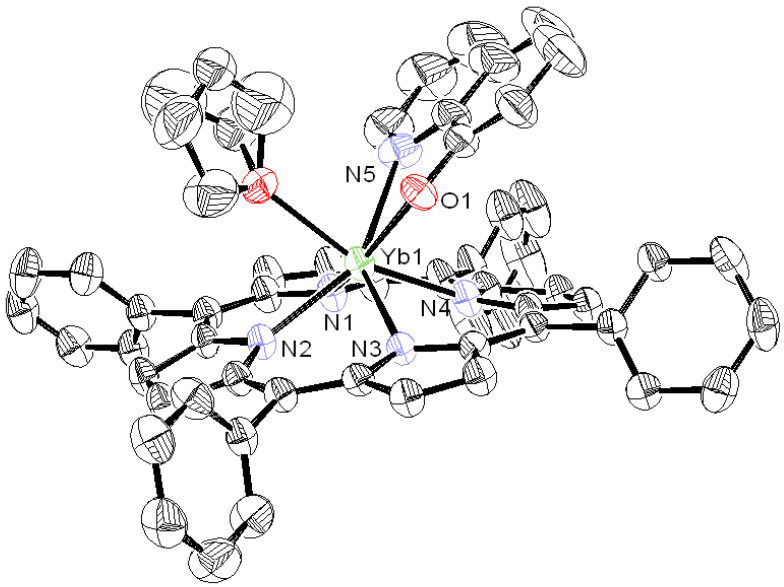

Figure 2.10: Thermal ellipsoid plot of YbTPP(Q)THF **(13)** showing selected atom labels drawn at the 50 % probability level. The hydrogen atoms have been excluded for clarity.

NMR Studies

In this section, the proton 1-D and 2-D NMR spectroscopy results will be discussed. Despite their paramagnetic nature, lanthanide complexes can give NMR spectra having narrow line widths with large spectral windows due to the nature of the f-electron paramagnetism.[43,68] The paramagnetic shifts are dependent on the electronic structure of the lanthanide ion as well as the position of the resonating nuclei with respect

to the metal. Because of the uncertainty of the paramagnetic shifts of these new compounds, the proton peaks cannot be assigned as easily as in diamagnetic materials. However, the use of the relative integrals as well as simple 2-D NMR experiments has allowed us to do a complete assignment of the proton NMR spectra of these compounds.

NdTPPTp

The 1-D proton NMR spectrum of **7** is shown in figure 2.11. Assuming the rotation of the phenyl rings on the porphyrin is slow compared to the time scale of the experiment,[68,69] there should be nine proton peaks. Of these nine peaks, five of the peaks correspond to the protons from the phenyl rings and have an integration of four, three of the peaks correspond to the Tp protons and have an integration of three and the ninth peak corresponds to the pyrrole protons and has an integration of eight. (The B-H proton of the Tp group is almost never observed, even in diamagnetic compounds, due to quadrapolar broadening from the boron atom). The spectrum, however, only shows eight peaks with integrated ratios (labeled A-H) of 3:4:8:7:4:4:3. Studies have shown that paramagnetic complexes have a significant temperature dependence of their resonance shifts.[43] Lauffer *et al*. showed that with lanthanide complexes of diethylenetriaminepentaacetate, overlapping singlets at room temperature can be observed at low temperatures.[70] Variable temperature NMR studies (Figure 2.12) in the range of 20° to 50° C show that peak D splits into two peaks, D_a and D_b, with relative integrations of 4 and 3 respectively. Using the integrals, peaks A, D_b and H are assigned to the Tp protons while peaks B, D_a, E, F and G are assigned to the protons on the phenyl ring and peak C is assigned to the protons on the pyrrole.

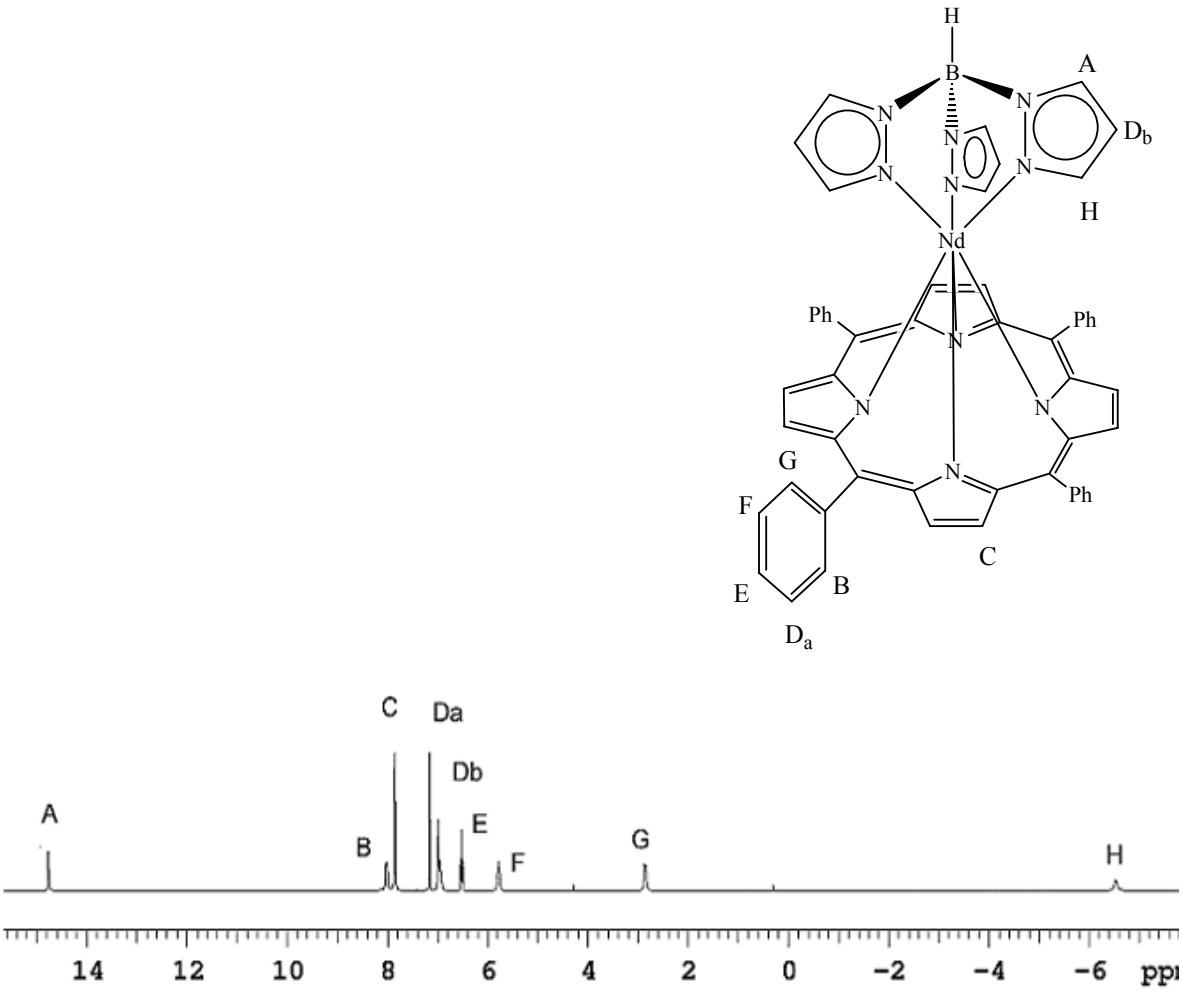

Figure 2.11: ^{1}H NMR of NdTPPTp **(7)**.

By running a COSY NMR experiment, we were able to observe the proton couplings that are obscured by the line width in the 1-D NMR spectrum. By looking at the reference peaks along the horizontal or vertical axes and their cross peaks off the diagonal, the proton-proton correlations are seen and used in peak assignment. The 2-D spectra of **7** (figure 2.13) show a cross peak between peaks A and D_b with no other couplings, confirming the Tp assignment of these two protons.

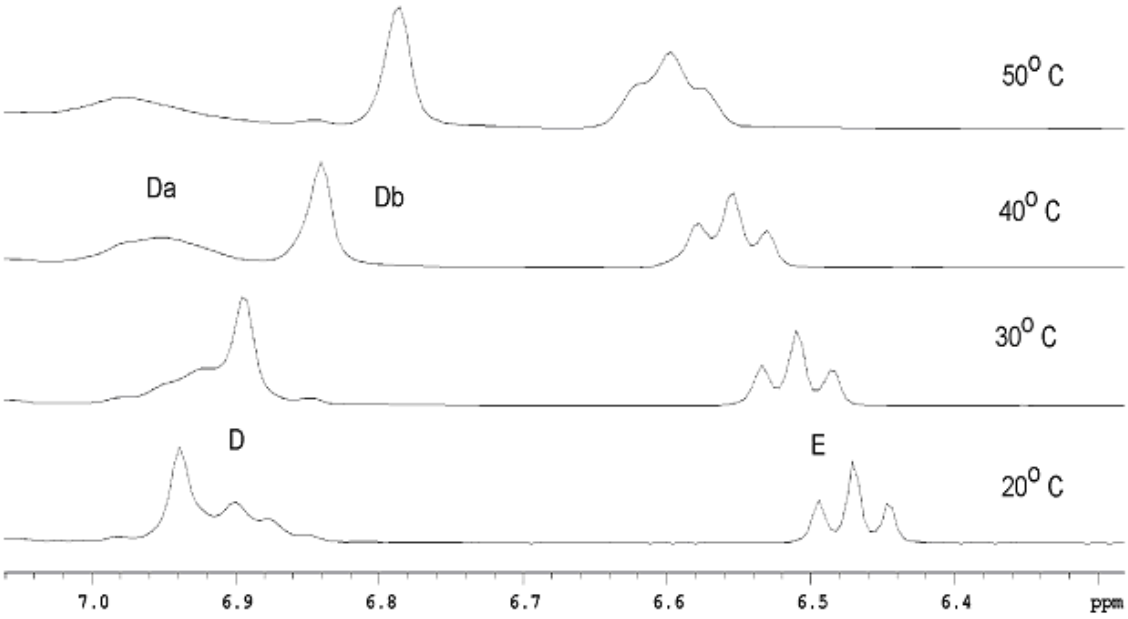

Figure 2.12: Variable temperature NMR of the phenyl region of NdTPPTp **(7)** from 20°-50°.

Because of its proximity to the paramagnetic nucleus the relaxation time of peak H is too fast to allow the appearance of the crosspeaks between H and either D_b or A in the NMR spectrum. So, peak H is assigned the proton nearest the metal because it is shifted significantly upfield and, with a half width of 22.4 Hz, it is the broadest Tp peak. The expanded area of the COSY spectrum (figure 2.13) shows correlations between peaks B and D_a, D_a and E, E and F, and F and G. Because of their correlations with only peaks D_a and F respectively, peaks B and G are assigned the *ortho* protons on the phenyl ring. The half width of peak G is 15.6 Hz while the half width of peak B is 15.0 Hz, so G is assigned to the proton pointing towards the metal and Tp. The rest of the assignments were made using the same logic, with peak F being the *meta* proton pointing towards the metal and D_a pointing away and E being the *para* proton.

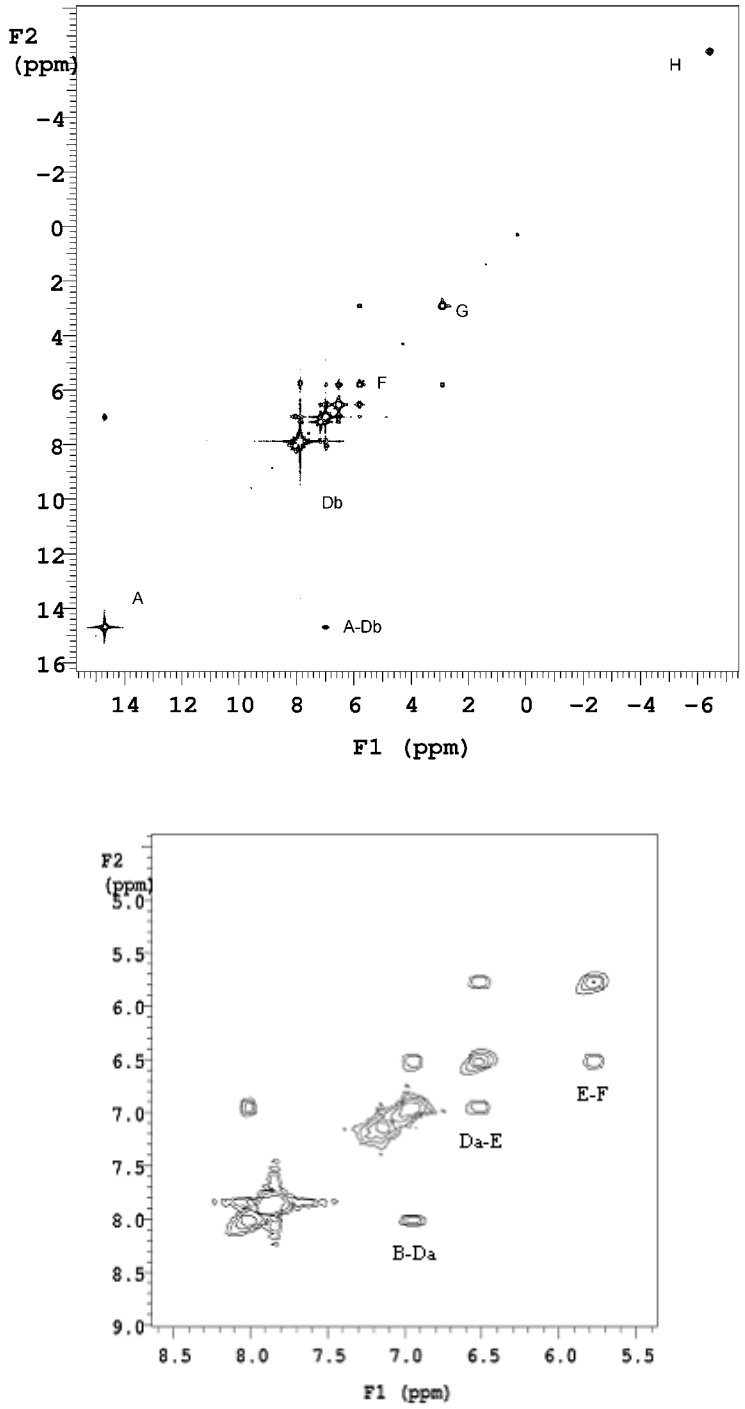

Figure 2.13: Full COSY NMR of NdTPPTp **(7)** (top), expansion from 8.5-5.5 ppm (bottom).

NdTPP(LOEt)

One and two-dimensional NMR experiments were used to analyze the LOEt complexes as well. The 1-D proton NMR spectrum (figure 2.14) shows nine peaks for NdTPP(LOEt) (**11**). Similar to the analysis of **7**, the peaks can be assigned to protons *via* their relative integrations. Starting with peak A at 10.16 ppm, the integrated ratios are 5:4:8:4:4:4:12:18. There is one peak with an integration of 5, which is expected for the Cp protons, two peaks with integrations of 12 and 18,which are the methylene and methyl protons on the LOEt ligand respectively, and then there are the expected number of peaks and integrations for the phenyl and pyrrole protons. The COSY spectra of NdTPP(LOEt) (**11**) (figures 2.15 and 2.16) show that peaks H and I are coupled to each other, supporting the ethoxy group assignment. While not observed in the 1-D NMR, the 2-D NMR spectrum shows the inequivalence of the diastereotopic protons on the methylene group. Looking at the expanded region, the cross peaks show that peaks B and G are the ortho protons, C and F are the meta protons and peak E is the para proton. Because peak G is broader than peak B, it is assigned the ortho proton closest to neodymium. The half widths of G and B were 25.3 Hz and 24.1 Hz, respectively.

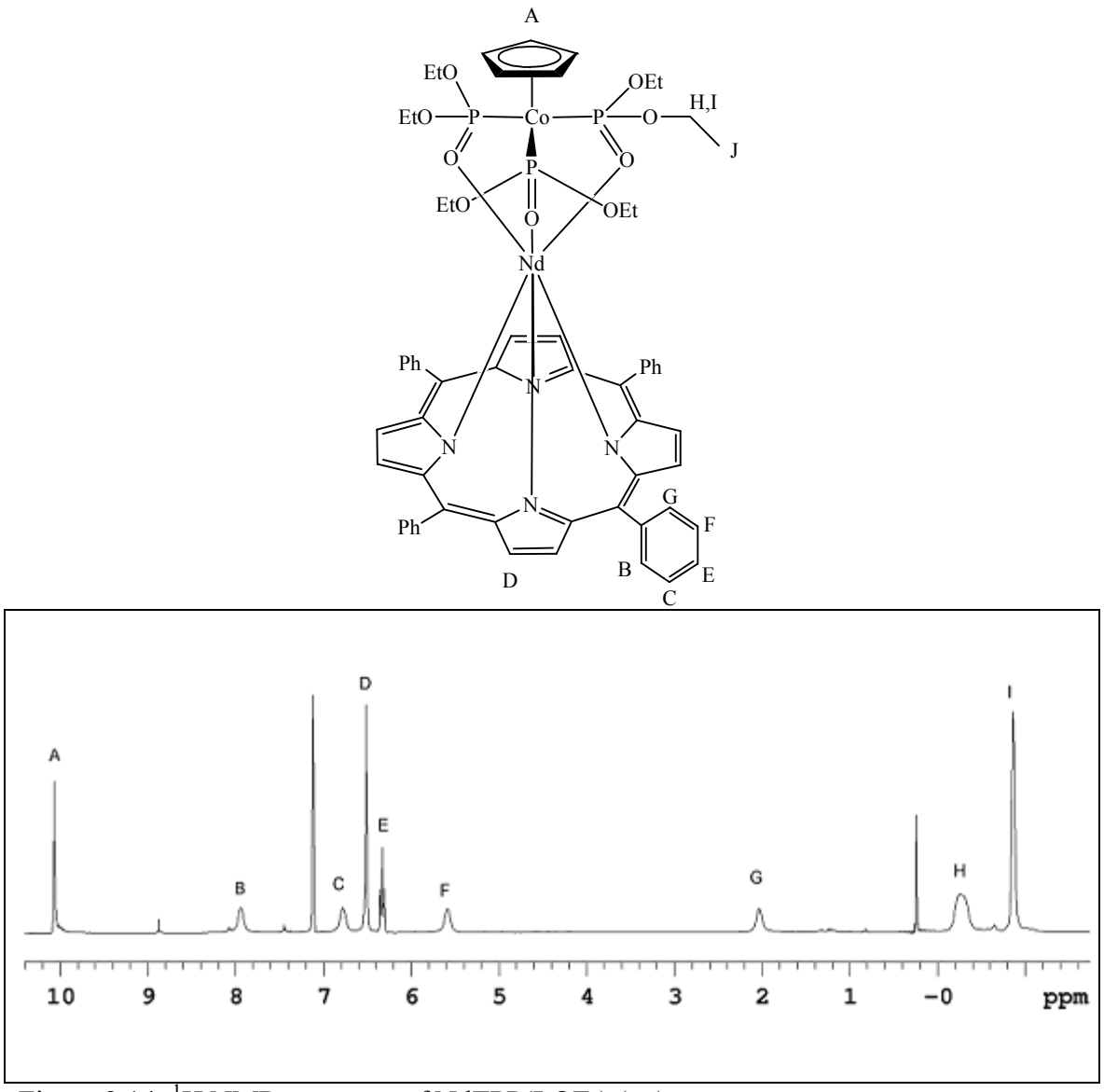

Figure 2.14: ^{1}H NMR spectrum of NdTPP(LOEt) (**11**).

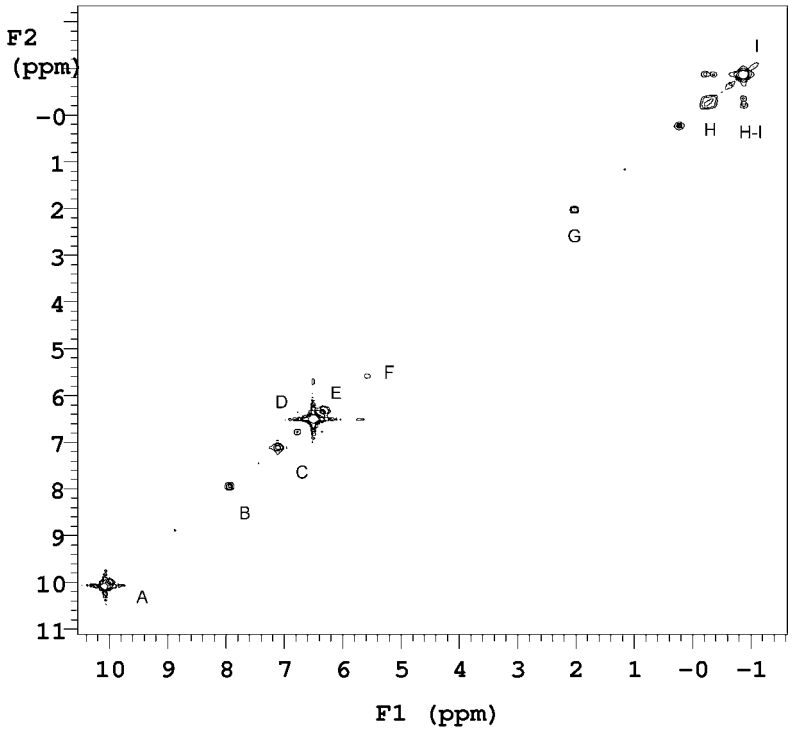

Figure 2.15: COSY NMR of NdTPP(LOEt) (**11**).

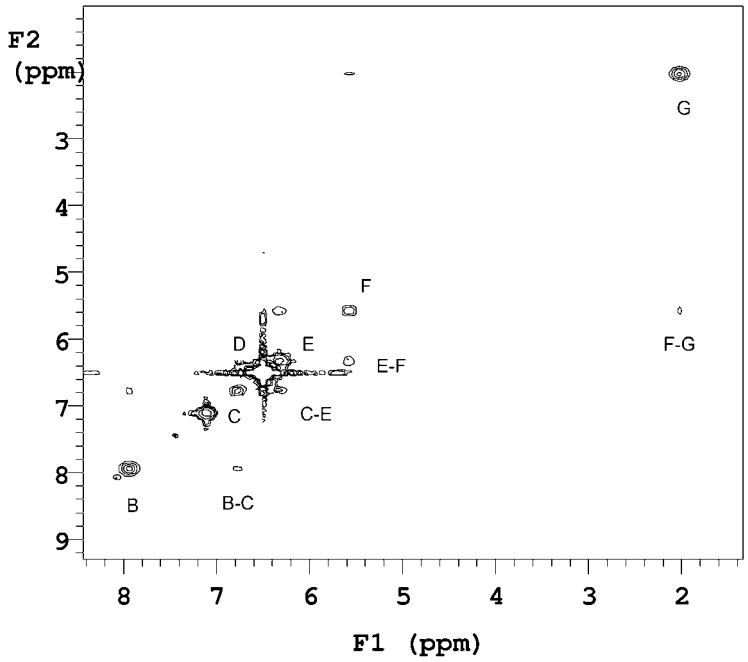

Figure 2.16: COSY NMR of NdTPP(LOEt) (**11**)**,** expansion from 8-2ppm.

LnTPP(L) Photoluminescence and Electroluminescene Studies

After the syntheses and full characterization of the LnTPP(L) complexes, the photoluminescence (PL) and electroluminescence (EL) properties of these compounds were examined. Recent work[39] has shown that formulation of the EL device materials can be guided by PL studies. Due to the lengthy process of device construction, PL studies were carried out on blends of polymer and the lanthanide complexes to determine if the complexes would be luminescent. PL studies on NdTPPTp, performed by Ben Harrison, showed NIR emission around 900 nm, 1069 nm and 1300 nm, which are the $^4F_{3/2} \rightarrow {}^4I_{9/2}$, $^4I_{11/2}$, and $^4I_{13/2}$ transitions of Nd (figure 2.17). The quantum efficiency (ϕ_{em}) was determined to be 2.4 %.[59] PL studies of NdTPP(LOEt) had similar results (figure 2.17).[59] Reported quantum efficiencies of other Nd-complexes range from 0.4 %[71] to 1.0 %.[72]

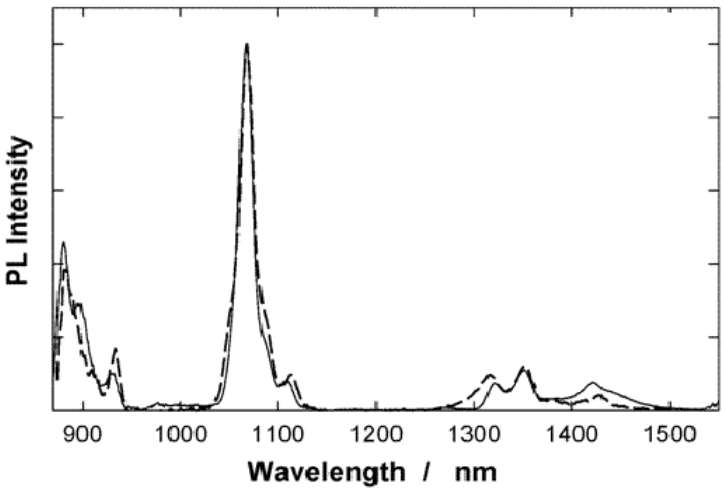

Figure 2.17: PL emission NdTPPL (solid lines, L = Tp, dashed lines, L = LOEt).

PL studies of the Pr complexes showed no NIR luminescence and therefore no devices were made with these complexes. Lack of emission is not surprising in that the

energy states that are below the $^3\pi$-π^* of the TPP ligand are closely spaced (separations of 2000-4000 cm^{-1}), causing nonradiative decay to be efficient.[59]

The device construction is shown in figure 2.18. The hole transport layer, PEDOT-PSS, was spin coated onto ITO covered glass, followed by the active layer (consisting of the lanthanide complex blended with polystyrene (PS)) and then finally the calcium layer as well as a layer of aluminum to prevent oxidation of the calcium.

While most of the device construction used the conjugated polymer, PPP-OR11,[73] our labs have demonstrated the fabrication of NIR-LEDs using blends of our lanthanide porphyrin complexes in non-conjugated host polymers, where the porphyrin serves as not only the charge carrier but also luminescent material (figure 2.19).[73,74]

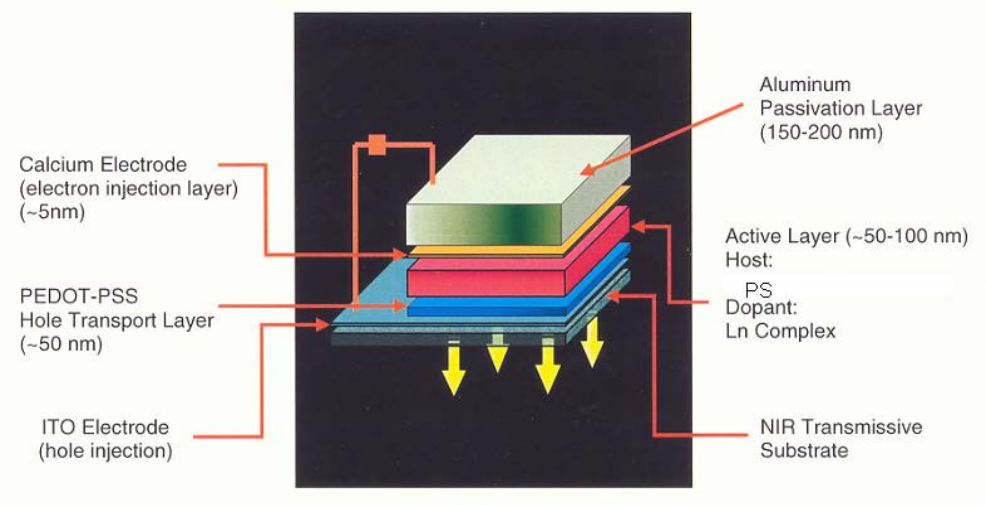

Figure 2.18: Device architecture.

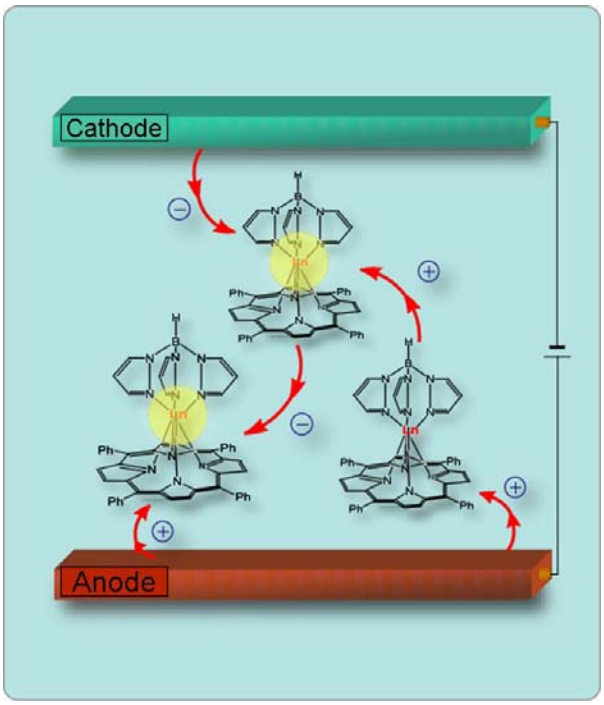

Figure 2.19: Charge hopping cartoon.

Devices made with blends of NdTPP(LOEt) and PS (2:1 weight ratio, complex:polymer) turned on at about 4 V and were able to operate efficiently at 9 V, producing NIR emission around 900 nm, 1069 nm and 1300 nm, which are the $^4F_{3/2} \rightarrow {}^4I_{9/2}$, $^4I_{11/2}$, and $^4I_{13/2}$ transitions of Nd (figure 2.20).[74]

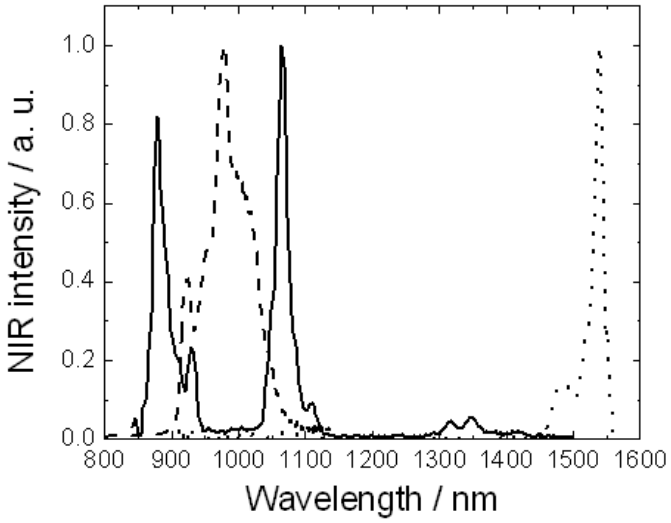

Figure 2.20: Electroluminescence emission of Ln(TPP)(LOEt) in polystyrene measured at 9 V. Ln = Nd (solid line), Yb (dashed line) and Er (dotted line).[74]

The quantum efficiency of blends with YbTPPTP, polystyrene and the known electron transporter, 8-hydroxyquinoline aluminum (AlQ_3) is ten times higher than devices without AlQ_3. Through these studies, we have found that LnTPP(L) is more efficient in the transport of holes and, therefore, creates a charge imbalance and low device efficiencies. There have been many studies on the poor ability of lanthanides to transport charge carriers, especially electrons.[21,75,76] With hopes of improved charge balance, PL and EL studies of YbTPP(Q)THF **(13)** were conducted by Garry Cunningham. PL studies showed NIR emission with a predominant peak ~ 980 nm. The quantum efficiency was calculated to be 0.0091 in CH_2Cl_2, which is significantly lower than efficiencies found for our other YbTPPL complexes.[59] Devices made with **13** emitted ~970 nm with a quantum efficiency of 0.00002-0.00004, depending on device loading of the complex. Again, these efficiencies are found to be lower than efficiencies previously reported for YbTPPL complexes.[73] As seen in the crystral structure of **13**, the capping ligand does not complete the coordination sphere of Yb and is not sterically hindering enough to prevent solvents, such as THF, from coordinating to the complex. It is likely that the proximity of the C-H bonds in the coordinated THF molecules provides efficient pathways for nonradiative decay, thus lowering the quantum efficiency of the complex.

Summary and Conclusions

In summary, novel neodymium and praseodymium complexes of tetraphenylporphyrin have been synthesized, thus completing the series of NIR emitting lanthanide porphyrin complexes. Through a simple salt metathesis reaction with the corresponding triiodides and dilithioTPP complexes, LnTPPI(DME) of Nd and Pr complexes were cleanly isolated in good yields. Analogous compounds of gadolinium

and lutetium were synthesized in the same fashion. From these starting materials, the lanthanide compounds were easily complexed with a number of ancillary ligands including Tp, LOEt and quinolate. These compounds have been fully characterized through crystallography, proton and COSY NMR studies, with proton peak assignment accomplished by integration of the 1-D proton spectrum and from proton correlations observed in the 2-D spectrum.

Recent work has demonstrated that devices do not require conjugated polymers and that blends of the lanthanide complexes with nonconjugated polymers produce NIR emission. PL studies found that devices blended with Nd complexes give NIR emission with a quantum efficiency of about 0.0024, while Pr complexes do not emit in the NIR. The NdTPPL complexes produce NIR emission with quantum efficiencies higher than published reports, supporting the design of emitting Ln complex consisting of the porphyrin sensitizing molecule and ancillary capping ligand.

PL and EL studies carried out with blends of NdTPP(L) and PS show that the TPP complex acts as the charge carrier that is more efficient in hole transport. Synthesis of the YbTPPQ was an attempt to balance the charge transfer in the emissive layer. However, the capping ligand is not sterically encumbering enough to hinder solvent coordination, facilitating nonradiative decay pathways and lowering device efficiency.

Experimental

Materials and Reagents

Unless otherwise stated, all syntheses were carried out on a double manifold Schlenk line under an atmosphere of nitrogen or in a N_2 filled glovebox. Glassware was oven dried prior to use. Methylene chloride, dimethoxyethane, chloroform and dimethlyforamide were purchased from Fisher Scientific and were dried with an

appropriate drying agent.[77] Pentane, tetrahydrofuran and toluene were purchased from Aldrich Chemicals and dried by passing through a column of activated alumina. Following dehydration, all solvents were degassed and stored over 4 Å molecular sieves in resealable ampoules with fitted Teflon valves. 8-hydroxyquinoline was purchased from Aldrich and used as received. The complexes (Cyclopentadienyl)tris(diethylphospinito)cobalt(I) (LOEt),[78] hydridotris(1-pyrazolyl)borate (Tp^H),[79] $TPNdCl_2THF$,[52] $(LOEt)NdCl_2THF$,[52] TPP,[80] Li_2TPP,[81] and YbTPPCl(DME)[51] were synthesized following literature procedures. Potassium 8-hydroxyquinoline (KQ) was synthesized by reacting 8-hydroxyquinoline with potassium hydride in THF. Elemental analyses were performed at the University of California, Berkley, Micro-Mass Facility or University of Florida Spectroscopic Services. Proton NMR spectra were measured at 300 MHz at room temperature, unless otherwise stated and on Varian Gemini 300, VXR 300, Mercury 300 or Bruker 300 NMR machines. Chemical shifts were referenced to residual solvent peaks and are reported relative tetramethylsilane. The spectral window was also different for each metal complex and was determined by expanding the window until peak positions remained unchanged. COSY spectra were run using the standard parameters of the instrument. All UV/VIS spectra were run in 1 cm path length quartz cuvettes in CH_3Cl unless stated otherwise. The samples were prepared and run under N_2 on a double-beam Cary-100 UV-visible spectrometer.

Synthesis

$NdI_3(THF)_4$ (1)

In a round bottom flask equipped with a side arm, Nd metal (4.98 g, 0.0346 mol) was washed with dry THF (3 x 30 mL). Dried and degassed ethyliodide (22 ml, 0.27

mol) was then added along with 30 mL of THF. After refluxing under N_2 for 20 hours, the brown solution was cooled and the THF removed *in vacuo*. Soxhelt extraction of the brown solid was performed in *ca.* 100 mL of THF under N_2 for 3 days. Following the completion of the extraction, the THF was removed, giving **1** as a blue solid in 46% yield (13 g, 0.016 mol).

$PrI_3(THF)_4$ (2)

Using the same procedure for **1**, Pr metal (2.97 g, 0.0211 mol) and CH_3CH_2I (13.1 ml, 0.169 mol) were refluxed under N_2 in dry THF (30 mL) giving **2** as yellow solid in 38% yield (6.1 g, 0.0075 mol).

NdTPPI(DME) (3)

$NdI_3(THF)_4$ (0.51 g, .61 mmol) and $Li_2TPP(DME)$ (0.499 g, 0.615 mmol) were added together in the dry box. About 40 mL of dry toluene was then added and the purple solution was refluxed under N_2. The reaction was followed by UV/VIS spectrometry (a peak at 425 nm with no peaks at ~415 nm indicated completion). After refluxing for four hours, the solution was filtered while hot via cannula. The residue was then washed with CH_3Cl (2 x 20 mL) and the toluene and CH_3Cl solutions were combined and reduced in volume to 10 mL. The solution was then layered with *ca*. 20 mL of pentane. After 12 hours, the solution was filtered, leaving a red/purple solid (0.443 g, 0.455 mmol) in 74% yield. ^1H NMR (300 MHz, CD_2Cl_2): δ 8.95($\nu_{1/2}$ = 5.78 Hz, 8H, *H*-pyrrole), 8.12($\nu_{1/2}$ = 17.33 Hz, 4H, *o*-C_6H_5 TPP), 7.56 ($\nu_{1/2}$ = 19.32 Hz, 4H, *m*-C_6H_5 TPP), 7.31 ($\nu_{1/2}$ = 5.71 Hz, 4H, *p*-C_6H_5 TPP), 6.92 ($\nu_{1/2}$ = 19.49 Hz, 4H, *m*-C_6H_5 TPP) 4.90 ($\nu_{1/2}$ = 18.72 Hz, 4H, *o*-C_6H_5 TPP*)*, -5.42 ($\nu_{1/2}$ = 217 Hz, 10H, DME). UV/VIS (CH_2Cl_2) λ_{max} (log ε): 422 (5.45), 514(3.95), 552(4.37), 590(3.95) nm. Anal. Calcd. for $C_{48}H_{38}N_4NdIO_2$: C, 59.19; H, 3.93; N, 5.75. Found: C, 57.31; H, 4.02, N, 5.52.

PrTPPI(DME) (4)

In the same fashion as **3**, PrTPPI(DME) was synthesized by refluxing $PrI_3(THF)_4$ (0.5 g, 0.1 mmol) and Li_2TPP (0.501 g, 0.108 mmol) in *ca.* 30 mL of toluene for four hours. The purple solid was isolated in 74% yield (0.44g, .451mmol). ^{1}H NMR (300 MHz, CDCl3): δ7.73 ($\nu_{1/2}$ = 16.19 Hz, 4H, *o*-C_6H_5 TPP)), 6.81($\nu_{1/2}$ = 18.66 Hz, 4H, *m*-C_6H_5 TPP), 6.29 ($\nu_{1/2}$ = 5.07 Hz, 4H, *p*-C_6H_5 TPP,), 5.53 ($\nu_{1/2}$ = 5.7 Hz, 8H, *H*-pyrrole), 5.33($\nu_{1/2}$ = 18.79 Hz, 4H, *m*-C_6H_5 TPP) 0.78 ($\nu_{1/2}$ = 17.79 Hz, 4H, *o*-C_6H_5 TPP). UV/VIS (CH_2Cl_2) λ_{max} (log ε): 424 (5.45), 514(3.95), 552(4.37), 590(3.95) nm. Anal. Calcd. for $C_{48}H_{38}N_4PrIO_2$: C, 59.39; H, 3.92; N, 5.77. Found: C, 58.99; H, 3.96; N,5.84.

GdTPP(Cl)DME (5)

In the glove box, $Li_2TPP(DME)$ (0.75 g, 0.80 mmol) and $GdCl_3$ (0.22 g, 0.80 mmol) were added to a Schlenk flask. Dry toluene (*ca.* 30ml) was then added and the green/blue solution was refluxed under N_2 for 3 hours, over time the color changed to red. After refluxing, the solution was removed *in vacuo* and the compound extracted with $CHCl_3$ (3 x 30 mL). The chloroform solution was reduced to *ca*. 20 mL and then layered with hexane (30 mL) to give purple crystalline material in 55% yield (0.4 g, 0.5 mmol). UV/VIS (CH_2Cl_2) λ_{max} (log ε): 425(5.46), 514(4.47), 552(4.87) nm. Anal. Calc. for $C_{48}H_{38}N_4GdClO_2$: C, 64.23; H, 4.25; N, 6.25. Found: C,65.06; H, 4.12; N, 6.12.

LuTPP(Cl)DME (6)

In the same fashion of **5**, LuTPPCl(DME) was synthesized by refluxing $LuCl_3$ (0.51 g, 1.7 mmol) and $Li_2TPP(DME)$ (1.58 g, 1.77 mmol) in *ca.* 30 mL of toluene for 3 hours. After the color change of the solution from green/blue to red, the solution was removed *in vacuo* and the compound was extracted with CH_2Cl_2 (3 x 30 mL) and filtered. The CH_2Cl_2 solution was reduced in volume to *ca*. 20 mL and then layered with hexane

(30 mL) to give purple crystalline material in 63% yield (0.99 g, 1.09 mmol). ^{1}H NMR (C_6D_6): δ9.09(s, 8H), 8.47(m, 4H), 8.07(m, 4H), 7.57(m, 12H). UV/VIS (CH_2Cl_2) λ_{max} (log ε): 420(4.80), 510(3.75), 548(3.961), 585(3.57) nm. Anal. Calc. for $C_{48}H_{38}N_4LuClO_2$: C, 63.13; H, 4.16; N, 6.14. Found: C, 59.49; H, 3.78; N, 5.71.

NdTPPTp (7)

To a solution of **3** (0.15 g, 0.15 mmol) in dry DME (30 mL), was added KTP (0.041 g, 0.15 mmol). The reaction mixture was left to stir for twelve hours at room temperature. The solution was removed *in vacuo* and the purple compound was extracted with *ca*. 30 mL of CH_2Cl_2, leaving a white residue of KI. The volume of the red/purple solution was reduced to 10 mL and then layered with pentane (10 mL). After being cooled to -10^0 C for 12 hours, the solution was filtered, leaving a purple solid. The mother liquor was reduced in volume (*ca.*10 mL) to allow more product to precipitate. Recrystallization of the combined solids from CH_2Cl_2/pentane gave X-ray quality crystals in 64% yield (0.093 g, 0.096 mmol). ^{1}H NMR (C_6D_6): δ 14.65($\nu_{1/2}$ = 5.61 Hz, 3H, *H*-Tp), 7.97($\nu_{1/2}$ = 15.05 Hz, 4H, *o*-C_6H_5 Tpp), 7.82($\nu_{1/2}$ = 4.25 Hz, 8H, *H*-pyrrole), 6.93($\nu_{1/2}$ = 5.08 Hz, 7H, *m*-C_6H_5 Tpp, *H*-Tp), 6.47($\nu_{1/2}$ = 3.25 Hz, 4H, *p*-C_6H_5 Tpp), 5.75($\nu_{1/2}$ = 16.88 Hz, 4H, *m*-C_6H_5 Tpp), 2.88($\nu_{1/2}$ = 15.66 Hz, 4H, *o*-C_6H_5 Tpp), -6.23($\nu_{1/2}$ = 22.41 Hz, 3H, *H*-Tp). UV/VIS (CH_3Cl), λ_{max} (log ε) = 425(5.29), 555(4.36) nm. Anal Calc. for $C_{53}H_{38}BN_{10}Nd$: C, 65.76; H, 3.93; N, 14.47. Found: C, 65.67; H, 3.96; N, 14.33.

PrTPPTp (8)

Following the same procedure for **7**, **4** (0.150 g, 0.155 mmol) and KTP (0.041 g, 0.15 mmol) were stirred together in dry DME (30 mL) for twelve hours at room

temperature. After recrystallization from CH_2Cl_2/pentane, 49% (0.073 g, 0.076 mmol) of product was collected. ^{1}H NMR (C_6D_6): δ 18.08($\nu_{1/2}$ = 4.89 Hz, 3H, *H*-Tp), 8.13($\nu_{1/2}$ = 14.81 Hz, 4H, *o*-C_6H_5 Tpp), 6.63($\nu_{1/2}$ = 5.09 Hz, 7H, *m*-C_6H_5 Tpp, *H*-Tp), 5.90($\nu_{1/2}$ = 3.97 Hz, 4H, *p*-C_6H_5 Tpp), 5.36($\nu_{1/2}$ = 3.69 Hz, 8H, *H*-pyrrole), 4.64($\nu_{1/2}$ = 17.51 Hz, 4H, *m*-C_6H_5 Tpp), -0.47($\nu_{1/2}$ = 14.09 Hz, 4H, *o*-C_6H_5 Tpp), -13.87($\nu_{1/2}$ = 11.23 Hz, 3H, *H*-Tp). UV/VIS (CH_3Cl), λ_{max} (log ε) = 424(5.30), 516(3.78), 555(4.34), 592(3.84) nm. Anal. Calc. for $C_{53}H_{38}BN_{10}Pr$: C, 65.86; H, 3.93; N, 14.50. Found: C, 66.30; H, 3.91; N, 14.23.

GdTPPTp (9)

Following the procedure used to synthesize NdTPPTp, KTp (0.067 g, 0.26 mmol) was added to a solution of GdTPPCl(DME) (0.24 g, 0.26 mmol) in toluene (*ca.* 20 mL). The reaction was stirred overnight at room temperature. The purple solution was removed *in vacuo* and the crude material was extracted with CH_2Cl_2 (*ca.* 30 mL). The solution was filtered and layered with pentane (*ca.* 30 mL) to give the product in 55% yield (0.14 g, 0.14 mmol). UV/VIS (CH_2Cl_2), λ_{max} (log ε) = 424(5.72), 513(4.33), 552(4.57), 590(4.33) nm. Anal. Calc. for $C_{53}H_{38}BN_{10}Gd$: C, 64.76; H, 3.86; N, 14.25. Found: C, 64.63; H, 3.71; N, 12.99.

LuTPPTp (10)

In the same manner as GdTPPTp, LuTPPCl(DME) (0.1 g, 0.10 mmol) and KTP (0.027 g, 0.109 mmol) were mixed in toluene for twelve hours. After recrystalization from CH_2Cl_2/pentane, 60% (0.059g, 0.06mmol) yield was recovered. ^{1}H NMR (C_6D_6): δ8.98(s, 8H), 8.29(m, 4H), 7.79(m, 4H), 7.43(m, 12H), 6.38(s, 4H), δ =5.53(s, 3H), 5.25(s, 3H). UV/VIS (CH_2Cl_2), λ_{max} (log ε) = 421(5.12), 513(4.67), 550(4.93), 588(4.66)

nm. Anal. Calc. for $C_{53}H_{38}BN_{10}Lu$: C, 63.61; H, 3.80; N, 14.00. Found: C, 63.43; H, 3.51; N, 13.91.

NdTPP(LOEt) (11)

To a stirring solution of **3** (0.125 g, 0.128 mmol) in dry THF (30 mL) was added K(LOEt) (0.075 g, 0.125 mmol). The purple solution was stirred for twelve hours at room temperature. The solvent was then removed *in vacuo* and the product was extracted into 30 mL of toluene. The volume of toluene was reduced to about 10 mL and layered with *ca.* 10 mL of pentane. After 24 hours at -78^0C, the purple precipitate was isolated by filtration and recrystallized from CH_2Cl_2/pentane. The crystals were washed with pentane (3 x 10 mL) to give **11** in 30% yield (0.05 g, 0.04 mmol). ^{1}H NMR(C_6D_6): δ 10.13($\nu_{1/2}$ = 3.28 Hz, 5H, *H*-Cp), 7.98($\nu_{1/2}$ = 19.35 Hz, 4H, *o*-C_6H_5 Tpp), 6.80($\nu_{1/2}$ = 20.88 Hz, 4H, *m*-C_6H_5 Tpp), 6.53($\nu_{1/2}$ = 4.32 Hz, 8H, *H*-pyrrole), 6.35($\nu_{1/2}$ = 3.22 Hz, 4H, *p*-C_6H_5 Tpp), 5.61($\nu_{1/2}$ = 20.32 Hz, 4H, *m*-C_6H_5 Tpp), 2.02($\nu_{1/2}$ = 20.63 Hz, 4H, *o*-C_6H_5 Tpp), -0.26($\nu_{1/2}$ = 47.23 Hz, 12H, -OC*H*$_2$CH$_3$), -0.83($\nu_{1/2}$ = 11.27, 18H, OCH$_2$C*H*$_3$). UV/VIS (CH_3Cl), λ_{max} (log ε) = 427(5.42), 518(3.93), 560(4.30), 599(3.97) nm. Anal. Calc. for $C_{61}H_{63}CoN_4O_9P_3Nd$: C, 56.83; H, 4.69; N, 4.35. Found: C, 55.13; H, 4.81; N, 3.90.

PrTPP(LOEt) (12)

The same procedure as **11** was used. PrTPPI(DME) (0.2 g, 0.2 mmol) and K(LOEt) (0.121 g, 0.206 mmol) were reacted to give **12** in 30% yield (0.08g, 0.062mmol). ^{1}H NMR (C_6D_6): δ14.92($\nu_{1/2}$ = 1.79 Hz, 5H, *H*-Cp), 7.96($\nu_{1/2}$ = 23.50 Hz, 4H, *o*-C_6H_5 Tpp), 6.28($\nu_{1/2}$ = 26.26 Hz, 4H, *m*-C_6H_5 Tpp), 5.45($\nu_{1/2}$ = 3.21 Hz, 4H, *p*-C_6H_5 Tpp), 3.96($\nu_{1/2}$ = 26.20 Hz, 4H, *m*-C_6H_5 Tpp), 3.04($\nu_{1/2}$ = 2.47 Hz, 8H, *H*-pyrrole), -2.16($\nu_{1/2}$ = 13.98

Hz, 18H,-OCH$_2$C*H$_3$*), -2.39($\nu_{1/2}$ = 30.25 Hz, 6H, -OC*H$_2$*CH$_3$), -2.59($\nu_{1/2}$ = 27.79 Hz, 6H, -OC*H$_2$*CH$_3$), -3.02($\nu_{1/2}$ = 25.20 Hz, 4H, *o*-C$_6$H$_5$ Tpp). UV/VIS (CH_3Cl), λ_{max} (log ε) = 425(5.14), 520(3.90), 559(4.35), 600(4.03) nm. Anal Calc. for $C_{61}H_{63}CoN_4O_9P_3Pr$: C, 56.93; H, 4.78; N, 4.33. Found: C, 55.73; H, 4.96; N, 3.84.

YbTppQ(THF) (13)

In the glove box, K(8-hydroxyquinolate) (KQ) (0.02 g, 0.01 mmol) was added to a solution of YbTPPCl(DME) (0.1 g, 0.01 mmol) in THF (30 mL) and stirred for 12 hours. The solvent was removed under reduced pressure and the resultant solid was extracted with CH_2Cl_2 (3 x 30 mL). The solution was reduced to *ca.* 10 mL and layered with *ca.* 20 mL of pentane, giving **13** as a purple crystalline solid (0.08 g, 57%). Crystals suitable for single crystal X-ray diffraction studies were grown from a saturated solution of THF (10 mL) that was layered with pentane (20 mL). UV/VIS (CH_2Cl_2) λ_{max} (log ε): 422 (5.43), 512 (3.93), 552 (4.26), 589 (3.95) nm. Anal. Calc. for $C_{57}H_{42}N_5O_2Yb$: C, 68.21; H, 4.19; N, 6.90. Found: C, 67.48; H, 4.45; N, 6.97.

X-ray

NdTPPI(THF)$_2$

Data were collected at 173 K on a Siemens SMART PLATFORM equipped with A CCD area detector and a graphite monochromator utilizing MoK_α radiation (λ = 0.71073 Å). Cell parameters were refined using up to 8192 reflections. A full sphere of data (1850 frames) was collected using the ω-scan method (0.3° frame width). The first 50 frames were remeasured at the end of data collection to monitor instrument and crystal stability (maximum correction on I was < 1 %). Absorption corrections by integration were applied based on measured indexed crystal faces.

The structure was solved by the Direct Methods in *SHELXTL5,* and refined using full-matrix least squares. The non-H atoms were treated anisotropically, whereas the hydrogen atoms were calculated in ideal positions and were riding on their respective carbon atoms. The asymmetric unit consists on the complex and a disordered thf molecule. The THF molecule could not be modeled properly, thus program SQUEEZE, a part of the PLATON package of crystallographic software, was used to calculate the solvent disorder area and remove its contribution to the overall intensity data. The complex has its iodine and two THF ligands disordered about a 2-fold rotation axis perpendicular to the plane of the macrocycle but only the Iodine atom of the minor part could be seen due to its small site occupation factor (refined to 5% then fixed in the final cycles of refinement). A total of 548 parameters were refined in the final cycle of refinement using 21110 reflections with $I > 2\sigma(I)$ to yield R_1 and wR_2 of 4.06% and 10.31%, respectively. Refinement was done using F^2.

LuTPPCl(DME)

The crystal was mounted in a nylon cryoloop from Paratone-N oil under argon gas flow. The data were collected on a Bruker SMART APEX II charge-coupled-device (CCD) diffractometer, with KRYO-FLEX liquid nitrogen vapor cooling device. The instrument was equipped with graphite monochromatized MoKα X-ray source (λ= 0.71073 Å), with MonoCap X-ray source optics. A hemisphere of data was collected using ω scans, with 5-second frame exposures and 0.3º frame widths. Data collection and initial indexing and cell refinement were handled using APEX II software. Frame integration, including Lorentz-polarization corrections, and final cell parameter calculations were carried out using SAINT+ software. The data were corrected for

absorption using the SADABS program. Decay of reflection intensity was monitored *via* analysis of redundant frames. The structure was solved using Direct methods and difference Fourier techniques. All hydrogen atom positions were idealized, and rode on the atom they were attached to. The final refinement included anisotropic temperature factors on all non-hydrogen atoms. Structure solution, refinement, graphics, and creation of publication materials were performed using SHELXTL.

NdTPPTP

Data were collected at 173 K on a Siemens SMART PLATFORM equipped with A CCD area detector and a graphite monochromator utilizing MoK_α radiation ($\lambda = 0.71073$ Å). Cell parameters were refined using up to 8192 reflections. A full sphere of data (1381 frames) was collected using the ω-scan method (0.3° frame width). The first 50 frames were remeasured at the end of data collection to monitor instrument and crystal stability (maximum correction on I was < 1 %). Absorption corrections by integration were applied based on measured indexed crystal faces. The structure was solved by Direct Methods in *SHELXTL5,* and refined using full-matrix least squares. The non-H atoms were treated anisotropically, whereas the hydrogen atoms were calculated in ideal positions and were riding on their respective carbon atoms. The asymmetric unit consists of two complexes and a pentane molecule disordered over a center of inversion. The disorder is resolved where only the methyl groups are disordered. A total of 1208 parameters were refined in the final cycle of refinement using 12451 reflections with $I > 2\sigma(I)$ to yield R_1 and wR_2 of 3.69% and 6.42%, respectively. Refinement was done using F^2.

YbTppQ(THF)

Data were collected at 173 K on a Siemens SMART PLATFORM equipped with A CCD area detector and a graphite monochromator utilizing MoK_α radiation (λ = 0.71073 Å). Cell parameters were refined using up to 8192 reflections. A full sphere of data (1850 frames) was collected using the ω-scan method (0.3° frame width). The first 50 frames were remeasured at the end of data collection to monitor instrument and crystal stability (maximum correction on I was < 1 %). Absorption corrections by integration were applied based on measured indexed crystal faces.

The structure was solved by the Direct Methods in *SHELXTL5,* and refined using full-matrix least squares. The non-H atoms were treated anisotropically, whereas the hydrogen atoms were calculated in ideal positions and were riding on their respective carbon atoms. Atoms C56 and C57 of the coordinated thf were disordered and were refined isotropically in two parts, second part being C56' and C57'. The asymmetric unit consists of the complex, an uncoordinated thf and a pentane molecule. The THF and pentane molecules were disordered and could not be modeled properly, thus program SQUEEZE, a part of the PLATON package of crystallographic software, was used to calculate the solvent disorder area and remove its contribution to the overall intensity data. A total of 585 parameters were refined in the final cycle of refinement using 24756 reflections with $I > 2\sigma(I)$ to yield R_1 and wR_2 of 3.98% and 9.20%, respectively. Refinement was done using F

CHAPTER 3
LANTHANIDE SUBSTITUTED TETRA(ARYL)PORPHYRIN AND PHTHALOCYANINE COMPLEXES : SYNTHESIS, CHARACTERIZATION AND LUMINESCENCE STUDIES

We have demonstrated that devices produce NIR emission when made with blends of the lanthanide porphyrin complexes in non-conjugated host polymers such as polystyrene. In these devices the porphyrin complex must serve as the charge carrier. These studies have also demonstrated that LnTPP is more efficient in the transport of holes and, therefore, creates a charge imbalance in the active layer of the device. This imbalance leads to charge recombination outside the active layer and thus low device efficiencies. In order to enhance device performance, we must enhance the charge balance in our active layer by enhancing the electron transport. In this chapter, the synthesis and characterization of substituted lanthanide-porphyrin and phthalocyanine complexes will be discussed as will the effect of the substituents on device efficiency.

Substituted Tetra(aryl)porphyrins

Much work has been done with studying the substituent effects on the redox properties of substituted tetraphenylporphyrins.[82,83] These studies found that electron-withdrawing and electron-donating groups affect the reduction and oxidation potentials of the porphyrins as well as the rate of electron transfer. Kadish *et al.* found that when electron-withdrawing substituients were placed on the phenyl rings of TPP, reductions were easier and oxidations were more difficult.[83] Korovin *et al.*[84] studied the effects of porphyrins with different aromatic substituents on the luminescence of ytterbium compounds. They reported that the quantum yields of porphyrins with pyridine or

quinoline *meso*-subsituents are higher than in the case of phenyl substituents. By incorporating methoxy, alkoxy and pyridyl groups into our porphyrin complexes, we sought to study the effects of both electron donating and withdrawing groups on our device efficiency. The goal was to indentify a lanthanide complex that would promote balanced injection, transport and recombination of charge carriers.

Synthesis

The synthesis of the ytterbium monoporphyrinate complexes began with the reaction of the dilithiated porphyrins with $Yb(Cl)_3(THF)_3$ under anhydrous, oxygen free conditions to give the metallated porphyrin (Figure 3.1).[51] The Yb(porphyrin)Cl complexes, YbTmPP(Cl)DME **(14)**, YbTPPoeh(Cl)DME **(19)**, and YbTPyP(Cl)DME **(22)** were then allowed to react with the potassium salt of the desired axial ligand to give the final products Yb(TmPP)Tp **(15)**, Yb(TPPoeh)Tp **(20)** and Yb(TPyP)L$(OEt)_3$ **(23)**, (Figure 3.2).[85]

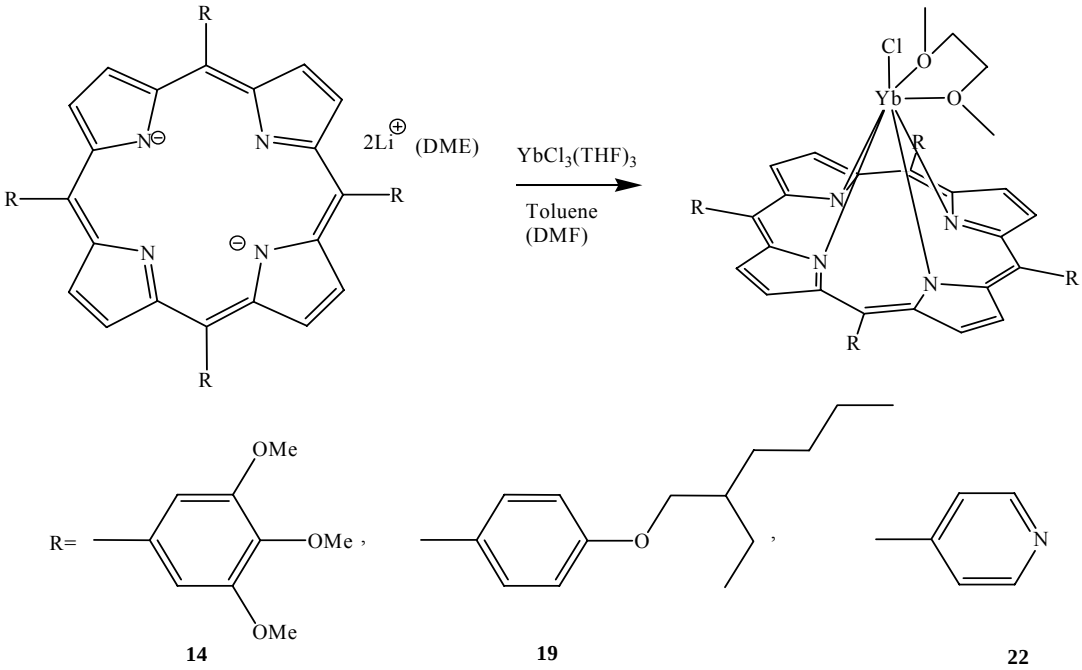

Figure 3.1: Synthesis of YbTmPP(Cl)DME **(14)**, YbTPPoeh(Cl)DME **(19)**, and YbTPyP(Cl)DME **(22)**.

The reaction to metallate the substituted porphyrin ligands with ytterbium proceeded smoothly via nucleophilic displacement of chloride from $YbCl_3$. Differences in the solubility of the reactants and products necessitated differences in the reported procedures. For example, the TpyP compounds were found to be insoluble in most solvents and the syntheses of these compounds were carried out in dry DMF. After stirring Li_2TpyP(DMF) **(21)** with $Yb(Cl_3)(THF)_3$ in DMF at reflux to give YbTPyPCl(DMF), the solution was removed *in vacuo* and the crude material washed several times with DME to remove any soluble impurities. Addition of the axial ligand, LOEt, alleviated the solubility issues of the TpyP compounds. Once the halide was replaced with LOEt, the compound was cleanly isolated in high yields by fractional recrystallization from CH_2Cl_2. On the other hand, the TPPeoh complexes were found to be extremely soluble in most organic solvents, including pentane. These compounds were isolated as oils by extracting the residues of the reactions with pentane and subsequent solvent removal under reduced pressure.

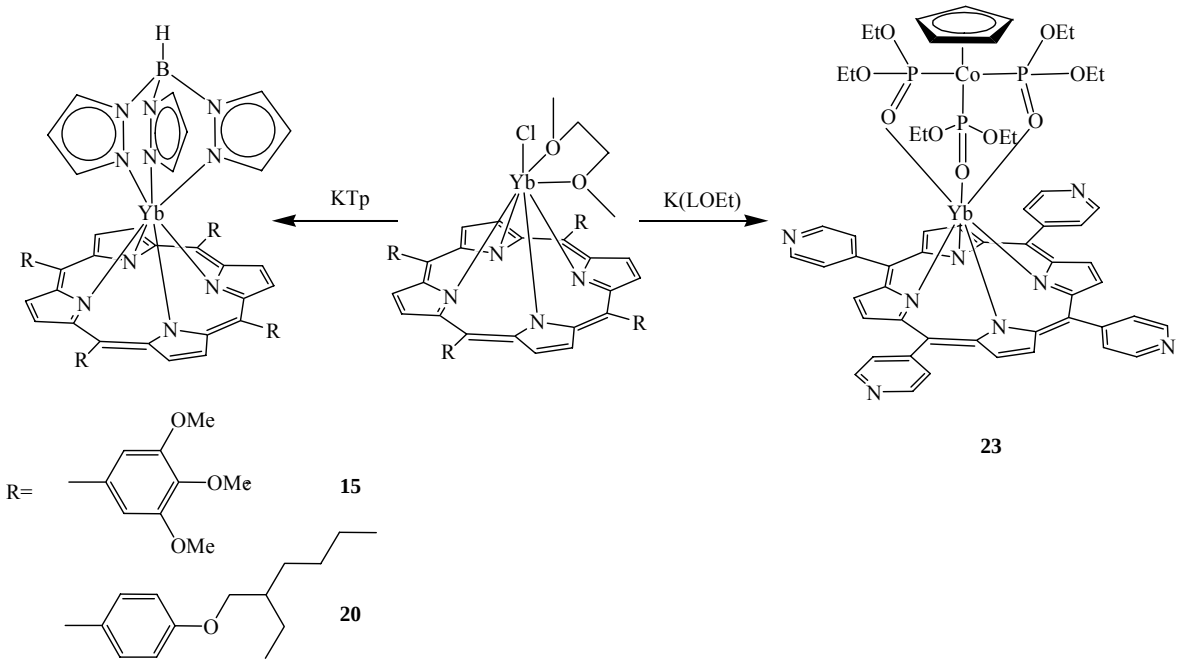

Figure 3.2: Synthesis of Yb(TmPP)Tp **(15)**, Yb(TPPoeh)Tp **(20)** and Yb(TPyP)L(OEt)$_3$ **(23)**.

NMR Studies

The complexes were characterized by proton NMR, UV/VIS spectroscopy as well as by elemental analysis. Uncertainty about the magnitude of the contact and pseudocontact shift in these new paramagnetic compounds adds difficulty to assigning the NMR peaks, but using the relative integration of the peaks and what we have learned from similar structures [85] facilitated assignment of the spectra. The proton NMR spectra of YbTmPP(Cl)DME **(14)** and Yb(TPyP)L(OEt)$_3$ **(23)** are shown in figures 3.3 and 3.4, respectively. Assuming that rotation of the phenyl rings on the porphyrin ligand is slow on the NMR timescale,[68,85] compound **14** should have eight peaks. Of the eight, three correspond to the methoxy groups on the phenyl ring and have an integration of 12 each, two with a relative integral of 4 each correspond to the protons on the phenyl rings, two with relative integrals of 6 and 4, correspond to the coordinated DME and one with an integration of 8 is assigned to the pyrrole protons on the porphyrin. Using these

integrations, peaks A and C were assigned to the protons on the phenyl ring, peaks D, E and F were assigned to the methoxy groups on the phenyl ring while the remaining peaks, G and H, arise from the coordinated DME. Similar to the analysis of compound **14**, the proton peaks in the NMR spectrum of **23** were assigned to protons *via* their relative integrations. Of the nine peaks, two are the diasteriotopic protons of the methylene on the L(OEt) ligand and have integrations of 6, one with an integration of 18 represents the methyl protons on the ligand, one with an integration of 5 is the Cp ring. There are four peaks assigned to the pyridyl ring and one to the pyrrole with integrations of 4 and 1, respectively (Figure 3.4).

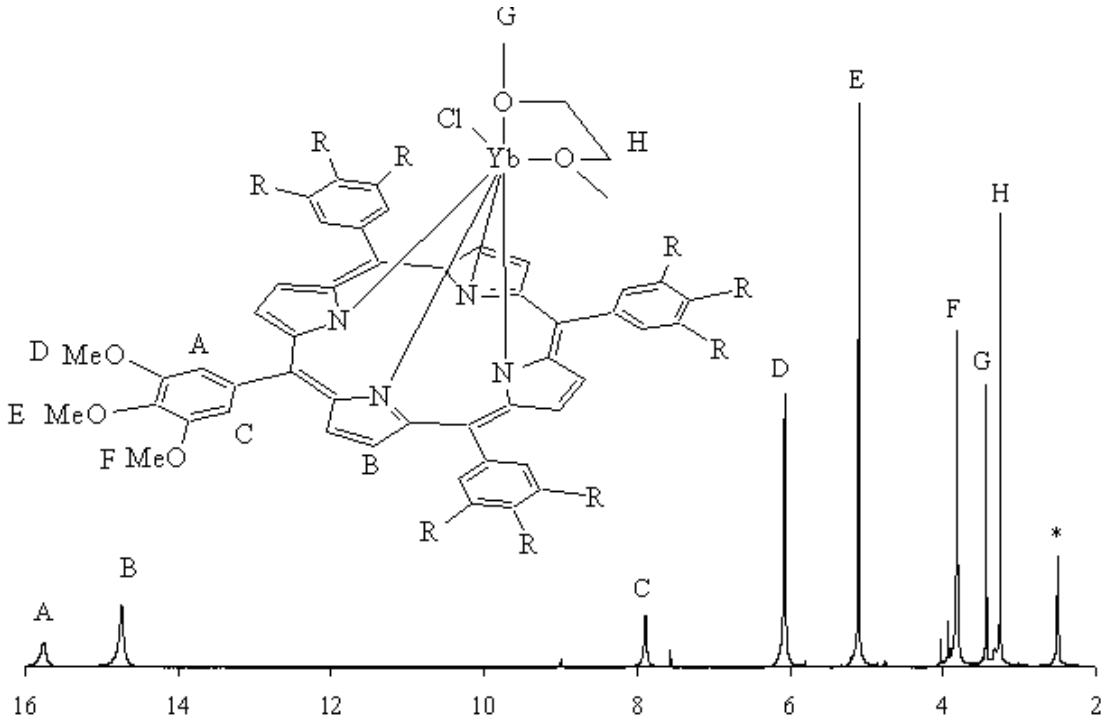

Figure 3.3: Proton NMR spectrum of Yb(TmPP)Cl(DME) (**14**) in DMSO-d_6 (*).

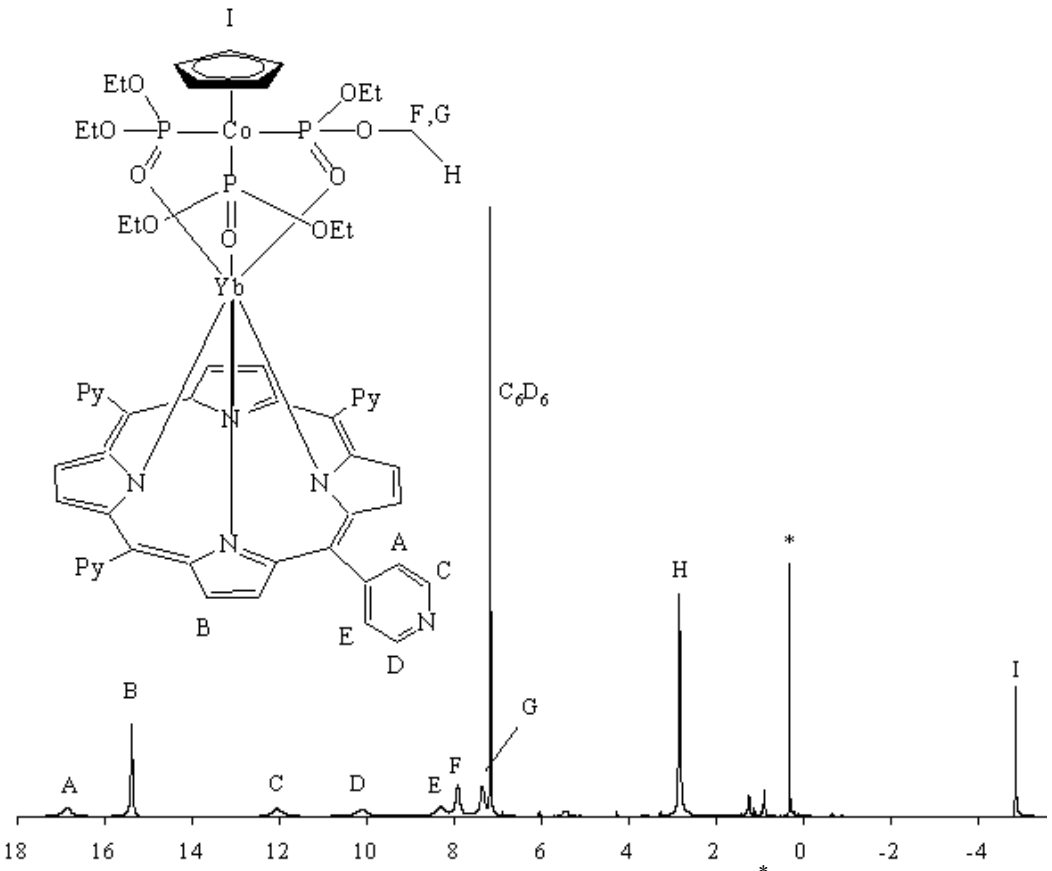

Figure 3.4: Proton NMR of Yb(TPyP)L(OEt)$_3$ **(23)** in C_6D_6(* denotes silicon grease impurity).

Electrochemistry

Cyclic voltammetry is a useful technique for electrochemical studies of new systems and provides valuable information on rates of oxidations/reductions as well as the HOMO/LUMO band gap of the compound. While CH_2Cl_2 for example, is a common solvent used in organic electrochemistry, it can only be used for potentials as high 1.8 V and as low as –1.9 V vs. Ag/Ag^+. Ionic liquids, on the other hand allow a much wider potential window for electrochemical studies. Furthermore, these solvents have the added advantage of not requiring a supporting electrolyte since they are inherently strong ionic conductors.[86,87]

The electrochemical characterization studies of the lanthanide-porphyrin complexes along with their free base porphyrins were performed in the ionic liquid, 1-Butyl-1-methyl-pyrrolidium bis(trifluoromethyl)sulfonamide ([BMP^+]-[NTF^-]) (Figure 3.5) in order to increase the available potential window (Figure 3.6). Electrochemical investigations were performed in a three-electrode cell with a platinum counter wire, platinum working disk and silver wire pseudo-reference electrode. Additionally, ferrocene (Fc) was used as an internal reference standard. The insolubility of compound Yb(TPPoeh)Tp **(20)** in [BMP^+]-[NTF^-] prevented the study of its electrochemistry.

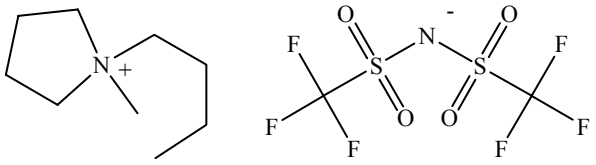

Figure 3.5: 1-Butyl-1-methyl-pyrrolidium bis(trifluoromethyl)sulfonamide ([BMP^+]-[NTF^-]), ionic liquid used for electrochemical studies.

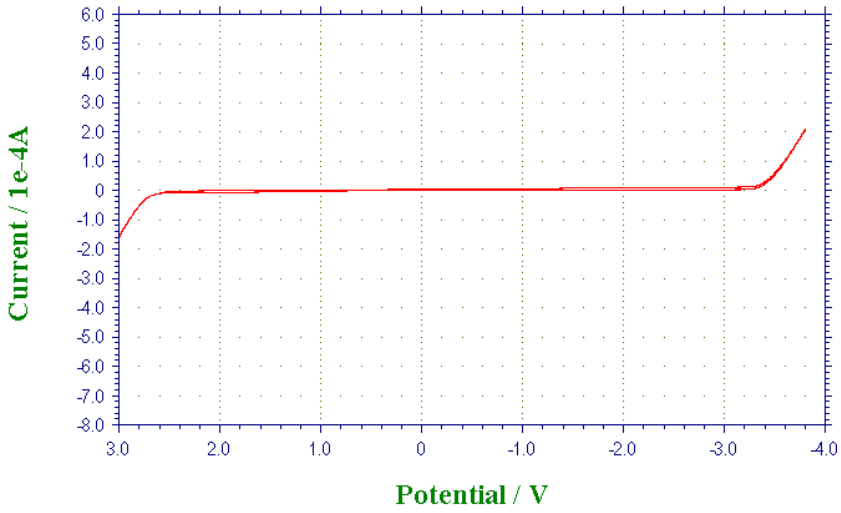

Figure 3.6: Cyclic voltamogram of [BMP^+]-[NTF^-].

A cyclic voltammogram is characterized by several important parameters. These observables include the peak currents (i_{pa} and i_{pc}) and the corresponding peak potentials

(E_{pa} and E_{pc}) and provide the basis for analyzing the cyclic voltammetric response. A typical reduction process is expressed as:

$$O + ne^- \rightleftharpoons R^{n-}$$

If R^{n-} is easily oxidized back to O upon reversing the direction of the potential scan, the process is said to be Nernstian reversible, giving the characteristic current versus potential plot seen in figure 3.7. From a CV, the potentials at which redox reactions occur, the reversablilty and stability of the oxidized and reduced species as well as the HOMO/LUMO band gaps can be determined. Under ideal conditions, for a mass-transport limited reversible process the peak potential separation (E_{pa} - E_{pc}) is equal to 59/n mV (at 25º C) for all scan rates, the peak current ratio (i_{pa}/i_{pc}) is equal to 1 for all scan rates and the peak current function increases linearly as a function of the square root of the scan rate. The average of E_{pa} and E_{pc} gives $E_{1/2}$ of the redox waves. The band gap is thus the difference between the first oxidation/reduction wave and the $E_{1/2}$of the first reduction/oxidation wave.

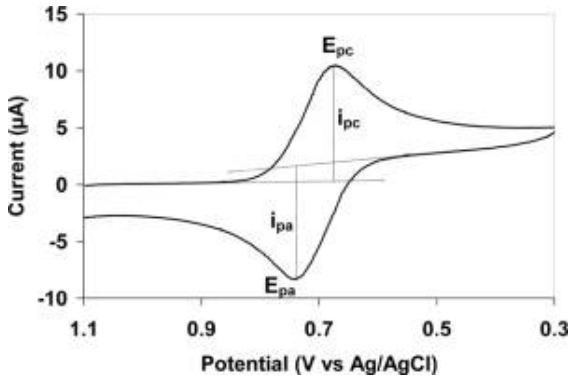

Figure 3.7: CV of a reversible reduction and reoxidation.

Previously reported cyclic voltammograms of LnTPP(acac) complexes consisted of two oxidation waves with $E_{1/2}$ of 0.7 and 0.9 V and two reduction waves with $E_{1/2}$ of

–1.32 and –1.68 V (vs. SCE).[47] Those waves correspond to four reversible one-electron transfer process, with the electrode mechanism shown in figure 3.8.

$$[\text{LnTPP(acac)}]^{2+} \overset{e^-}{\rightleftharpoons} [\text{LnTPP(acac)}]^{+} \overset{e^-}{\rightleftharpoons} \text{LnTPP(acac)} \overset{e^-}{\rightleftharpoons} [\text{LnTPP(acac)}]^{-} \overset{e^-}{\rightleftharpoons} [\text{LnTPP(acac)}]^{2-}$$

Figure 3.8: Electrode reaction mechanism of LnTPP(acac).

The cyclic voltammogram of TmPP in [BMP^+]-[NTF^-] at a scan rate of 0.1 V/s is shown in figure 3.9. The first reduction/oxidation wave, peak B is reversible with a i_{pc}/i_{pa} equal to one and E_{pa} - E_{pc} equal to 79 mV (under the conditions, the peak potential difference is equal to 110 mV for the Fc/Fc^+ coupling, a well established completely reversible process). The $E_{1/2}$ for TmPP were determined to be –1.54 V and –1.78 V for the two reduction waves and 0.66 V for the oxidation wave. The band gap is 2.2 eV.

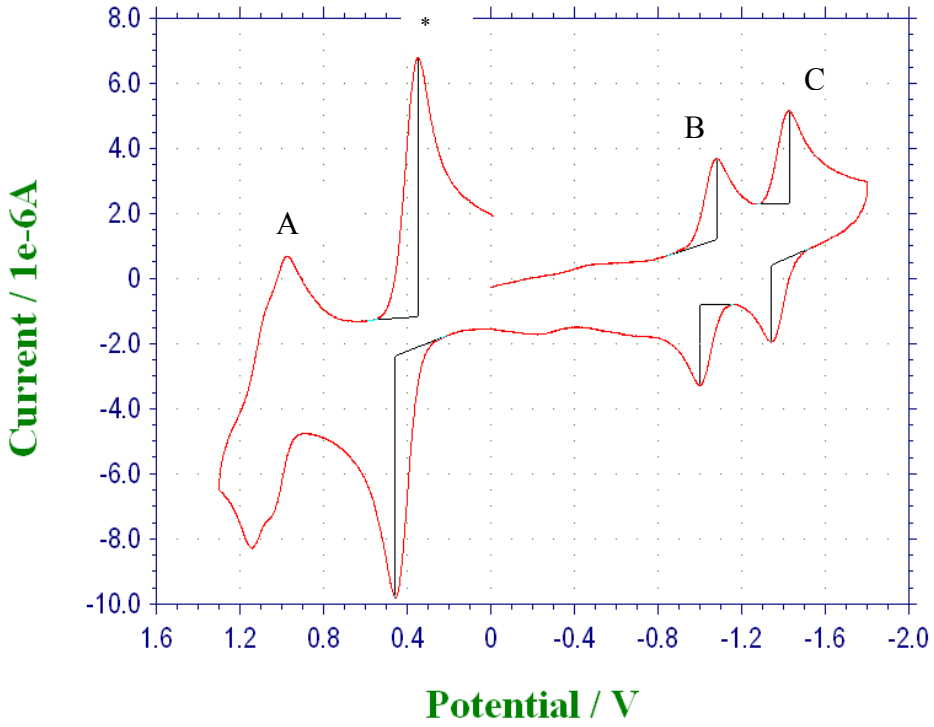

Figure 3.9: CV of TmPP in ionic liquid with a scan rate of 0.1 V/s (* indicates Fc/Fc^+).

Figure 3.10 shows a similar cyclic voltammogram of the complex YbTmPPTp (**15**) in [BMP^+]-[NTF^-] at a scan rate of 0.3 V/s. Similar to LnTPP(acac) complexes, there are two reduction waves, however there is only one oxidation wave. The first reduction/oxidation wave, peak B is reversible with a i_{pc}/i_{pa} equal to one and E_{pa} - E_{pc} equal to 250 mV (under the conditions, the peak potential difference is equal to 260 mV for the Fc/Fc^+ coupling, a well established completely reversible process). Compared to YbTPP(acac) with $E_{1/2}$ of –1.76V and 0.28 V (vs. Fc/Fc^+) for the first reduction and oxidation, respectively, the $E_{1/2}$ for complex **15** were determined to be –1.52 V and –1.97 V for the two reduction waves and 0.68 V for the oxidation wave. The band gap is 2.2 eV.

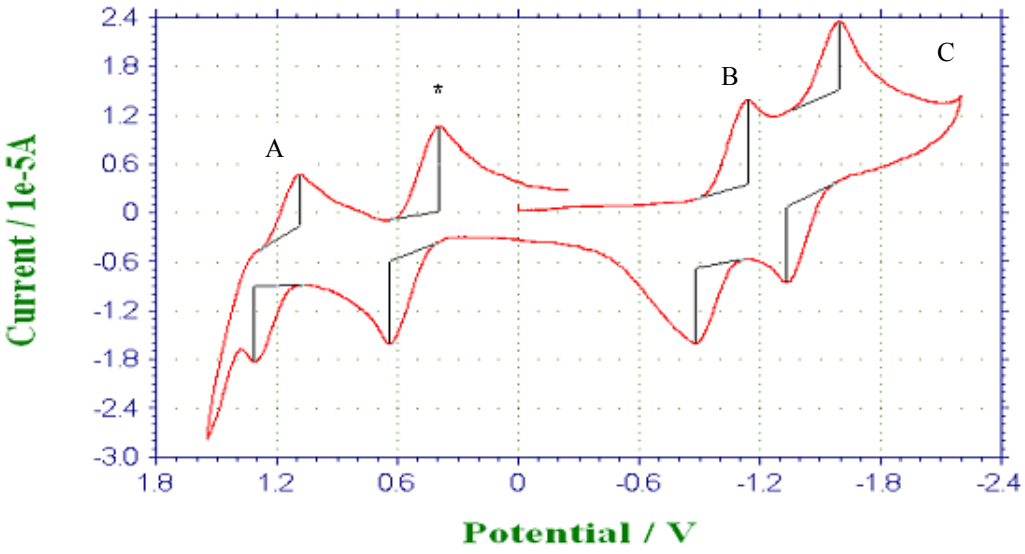

Figure 3.10: Cyclic voltammogram of **15** in ionic liquid with a scan rate of 0.3 V/s (* indicates Fc/Fc^+).

The cyclic voltammogram of the free base porphyrin, TPyP is shown in figure 3.11.

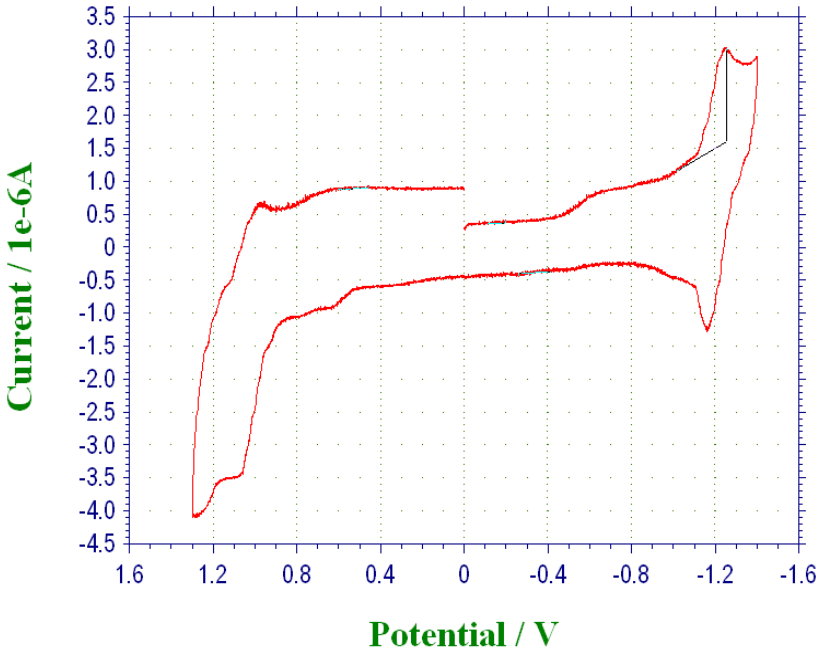

Figure 3.11: Cyclic voltammogram of TPyP in ionic liquid with a scan rate of 0.3 V/s.

There is one irreversible reduction/oxidation peak with $E_{1/2}$ determined to be –1.62 V. There is also one irreversible oxidation/reduction peak and the $E_{1/2}$ was determined to be 0.71 V.

The cyclic voltammogram of the reduction and the oxidation for YbTPyP(LOEt) (**23**) is in figure 3.12. In the reduction half, there are two reduction/oxidation waves, A and B. Peak A is reversible with i_{pc}/i_{pa} equal to one and E_{pa} - E_{pc} equal to 85 mV (under the conditions, the peak potential difference is equal to 131 mV for the Fc/Fc^{+} coupling). There are no reversible oxidation waves present, however, there are several poorly resvolved irreversible waves at 0.22 V and 0.85 V. The $E_{1/2}$ were determined to be –1.69 V and –2.12 V for the two reduction wave. The band gap is 1.9 eV.

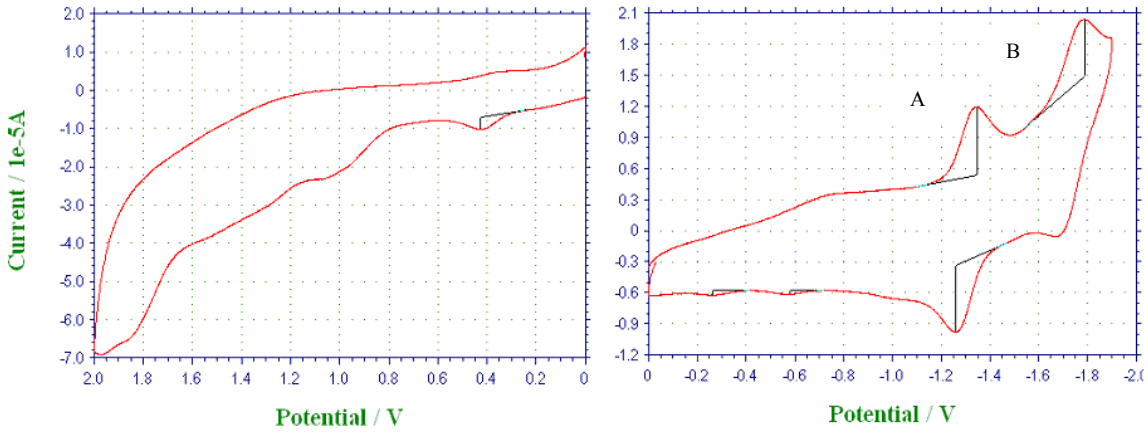

Figure 3.12: Cyclic voltammogram of the oxidation (left) and reduction (right) ofYbTPyP(LOEt) in ionic liquid with a scan rate of 0.3 V/s.

The cyclic voltammogram of YbTPPTp is in figure 3.13. There are two oxidation/reduction waves, A and B, and two reduction/oxidation waves, C and D, which are quasi reversible. The $E_{1/2}$ were determined to be –1.53 V and –1.91 V for the two reduction waves and 0.51 V for the oxidation wave. The band gap is 2.0 eV.

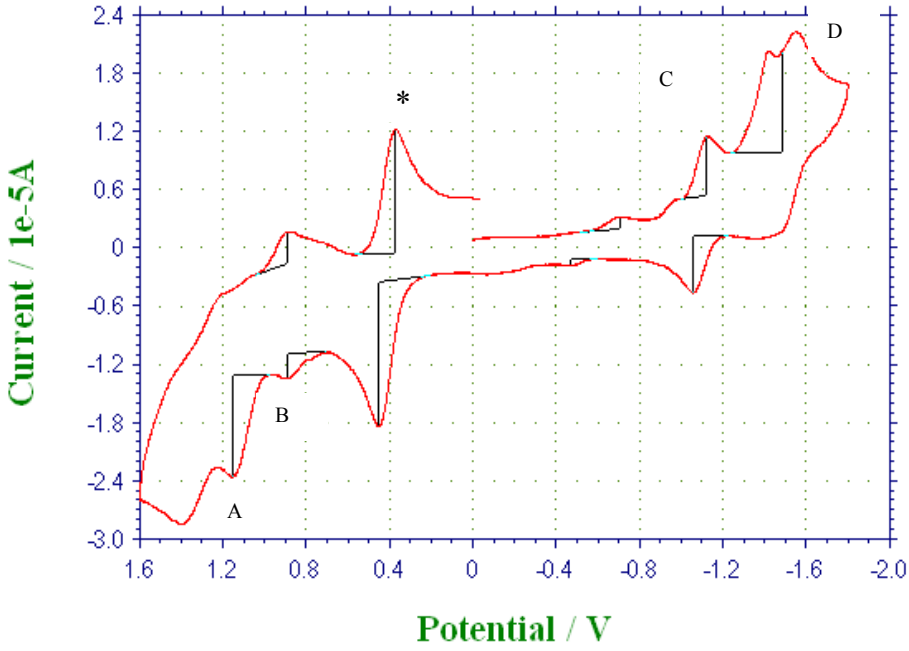

Figure 3.13: Cyclic voltammogram of YbTPPTp in ionic liquid with a scan rate of 0.2 V/s (* indicates Fc/Fc^{+}).

Figure 3.14 shows the cyclic voltammogram of the complex YbTPP(LOEt) in [BMP^+]-[NTF^-]. Similar to LnTPP(acac) complexes, there are two reduction waves and two oxidation waves. The oxidation /reduction waves, peaks A and B are reversible with E_{pa} - E_{pc} equal to 75 and 68 mV, respectively (under the conditions, the peak potential difference is equal to 75mV for the Fc/Fc^+ coupling, a well established completely reversible process). Peaks C and D are quasi reversible and peak E is irreversible. The $E_{1/2}$ for complex YbTPP(LOEt) were determined to be –1.79 V for the first reduction wave and 0.35 V for the first oxidation wave. The band gap is 2.2 eV.

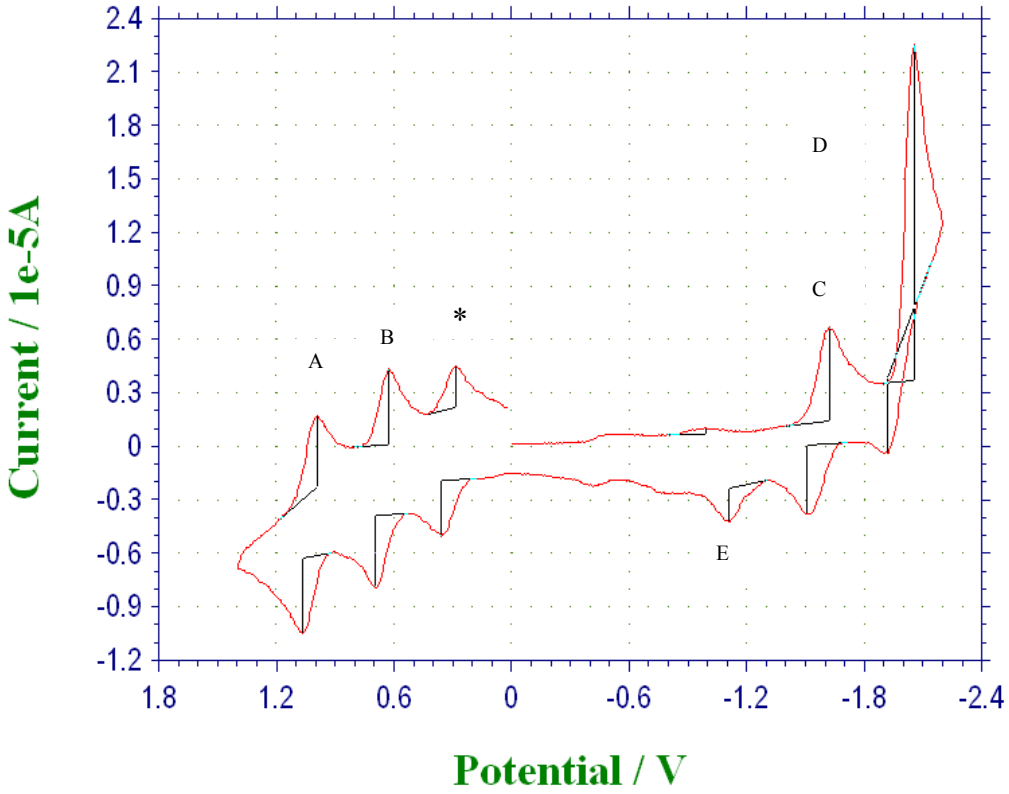

Figure 3.14: Cyclic voltammogram ofYbTPP(LOEt) in ionic liquid with a scan rate of 0.05 V/s (* indicates Fc/Fc^+).

Table 3.1 shows the half wave potentials and the band gap determined by the electrochemical studies of the lanthanide complexes and the corresponding free base porphyrins. When compared to TmPP, the redox potentials of **15** are quite similar, suggesting that reductions are occurring on the macrocycle and addition of the metal ion and Tp does not affect the electrochemistry. When comparing **15** to other Ln-porphyrin complexes such as YbTPPTp, YbTPP(LOEt) and YbTPP(acac) the oxidation reaction is not reversible and occurs at a higher potential, suggesting that substituents may destablize the oxidation products. Similar to **15**, the oxidation and reduction of **23** are affected by the substituent. Comparing **23** with YbTPP(LOEt),reduction of the complex occurs at a lower potential while the oxidation process is irreversible.

Comparing YbTPP(L) with different capping ligands also shows changes in the reduction and oxidation potentials. Reported results show that the CV of YbTPP(acac) has two reversible reduction and two reversible oxidation reactions. Complex YbTPP(Tp) has two reduction and two oxidation reactions, which occur at higher potentials and are not reversible. Complex YbTPP(LOEt) has two reduction and two reversible oxidation waves as well as another oxidation peak, which irreversible.

Table 3.1: Half wave potentials and band gaps of Ln-porphyrin complexes (potentials are reported vs Fc/Fc^+ internal standard) [a] Irreversible peak and so was determined by E_p.

Complex	Red, $E_{1/2}$ (v)		Ox, $E_{1/2}$ (v)		Eg (eV)
	1	2	1	2	
TmPP	-1.54	-1.78	0.66	-	2.6
Yb(TmPP)Tp (**15)**	-1.52	-1.97	0.68	-	2.2
TPyP	-1.62	-	0.71	-	2.3
YbTPyP(LOEt) (**23**)	-1.69	-2.12	0.22 [a]		1.9
TPP (ionic liquid)	-1.78		0.51		2.3
YbTPP(Tp)	-1.53	-1.92	0.51		2.0
YbTPP(LOEt)	-1.79	-2.31	0.35	0.7	2.1
YbTPP(acac) [47]	-1.76		0.28		2.0
TPP in CH_2Cl_2 [83]	-1.64	-1.99	0.58	0.83	2.02
ZnTPP in CH_2Cl_2 [83]	-1.76	-2.15	0.34	0.65	2.1

Photoluminescence and Electroluminescene Studies

After the synthesis and full characterization of the substituted ytterbium porphyrin complexes, the photoluminescence (PL) and electroluminescence (EL) properties of these compounds were examined. The photoluminescence studies by Garry Cunnigham showed photoluminescence from the metal-based *f*-states ($^2F_{5/2} \rightarrow {}^2F_{7/2}$) with efficiencies ranging from 0.9% for YbTPPQ to 4.1% for YbTmPPTp. With the exception of YbTPPQ, PL efficiencies were similar to other YbTPP complexes and higher than other reported Yb-complexes, with efficiencies reported in the range of 0.1%[88] to 0.8%.[72] The emission spectral properties for all of the porphyrin complexes were nearly identical,

with emission maxima at ~980 and ~1020 nm, similar to the previous YbTPP complexes studied. Light emitting diodes containing blends of the substituted Yb-porphyrin complexes and polystyrene were prepared. The configuration of all devices tested was ITO/PEDOT-PSS/PS-porphyrin complex/Ca;Al 40:100:5:200 (nm).

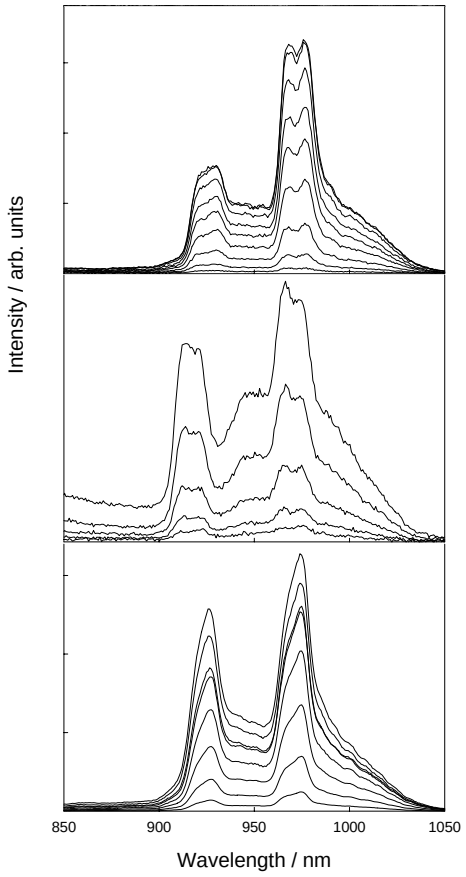

Figure 3.15: Electroluminescence of Yb(TMPP)TP (bottom), Yb(TPyP)L(OEt)$_3$ (middle), and Yb(TPPoeh)TP (top) as a function of increasing voltage, starting at 6 V to 20 V.

Electroluminescence spectra of devices containing a 2:3 wt. ratio (complex:polymer) of the porphyrin complexes dispersed in polystyrene show the ~980 nm emission of the Yb^{3+} $^2F_{5/2} \rightarrow {}^2F_{7/2}$ transition as also seen in the PL measurements with a weaker peak at ~920 nm which is attributed to the crystal field splitting of the Yb^{3+} *f*-states by the axial and porphyrin ligands (Figure 3.15). The Yb(TPyP)LOEt devices

were considerably less stable and failed at a lower voltage than devices fabricated from the other porphyrin complexes. The external quantum efficiency for each of the complexes is ~1–3 x 10^{-4} which is similar to devices constructed with Yb(TPP)TP.[73]

Summary

Lanthanide-porphyrin complexes have been synthesized and characterized with a variety of porphyrin-phenyl ring substituents in order to improve the efficiency of electron transport and consequently the luminescence of our devices. The electrochemistry of these complexes and the free base porphyrins were studied. The lanthanide complexes show a decrease in the reduction/oxidation potentials when compared with the unsubstitued YbTPPTp and YbTPP(LOEt) complexes and there is little interpretable data for the oxidation of YbTPyP(LOEt), suggesting that the substiuents affect the stability of the oxidized complexes. These electrochemical studies also showed that changing the capping ligand affects the electrochemistry of the complexes. PL and EL studies, however, show NIR luminescence with no change in device efficiencies. Because there appears to be no correlation between the electrochemical results and device efficiency suggests that the factors involved in device construction outweigh any differences that arise from the identity of the porphyrin substituents. So, for PL and EL studies, changing the porphyrin-phenyl ring substituents has little effect on the electronic properties of the complex and does little to enhance device efficiency.

Lanthanide-Phthalocyanine Complexes

Like TPP, phthalocyanine (Pc) (Figure 3.16) is an aromatic tetradentate macrocycle with a strong absorption at ~720 nm. Because of these properties, lanthanide complexes

of Pc were synthesized to investigate their luminescence properties and compare them with the LnTPP complexes.

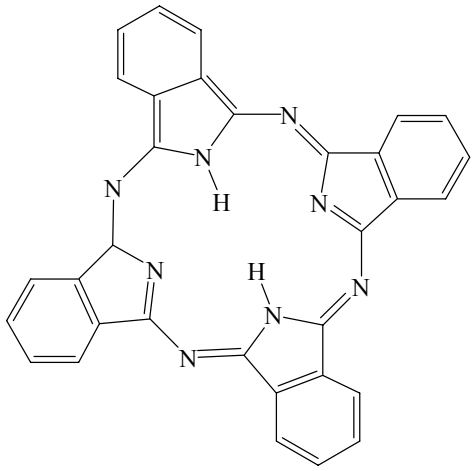

Figure 3.16: Phthalocyanine (Pc).

There are many examples of $LnPc_2$ sandwich-type complexes in the literature.[89-91] These complexes however, have a strong interligand charge transfer band at 1550 nm that would quench many of the NIR emissions under investigation.[92,93] In order to use Pc as a chromophore for the lanthanides, a convenient synthesis of the monoPc complexes would be desirable.

Synthesis and Structure of LnPc(LOEt) Complexes

The LnPc complexes were made with a methodology that was similar to that used for the LnTPP complexes. Dilithiophthalocyanine was synthesized by refluxing 1,2 dicyanobenzene and lithium in pentanol. The synthesis of LnPcCl, which is published in the patent literature,[94] consists of refluxing Li_2Pc with anhydrous $LnCl_3$ in dry DME. The LnPcCl(DME) complex was then in turn used to synthesize the LnPc(LOEt) complex. This procedure has been used to make the Ho, Er, Tm, and Yb complexes. The synthesis of LnPcTP was attempted, but the product was insoluble in all organic solvents and therefore purification and characterization was not completed.

In order to make NdPcI(DME) **(24)** and PrPcI(DME) **(25)**, Li_2Pc was was stirred at reflux with the lanthanide triiodide complex in DME for twelve hours (Figure 3.17). These complexes are insoluble in DME and were isolated by filtration.

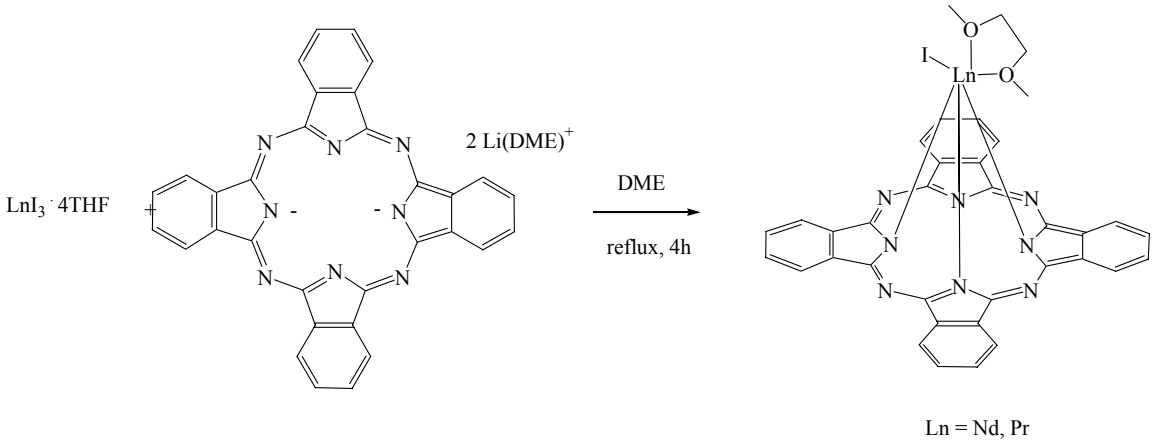

Figure 3.17: Synthesis of LnPcI(DME), Ln= Nd, Pr.

The (LOEt) complexes were then synthesized by reaction of LnPcI(DME) with K(LOEt) in THF at room temperature for twelve hours (Figure 3.18).

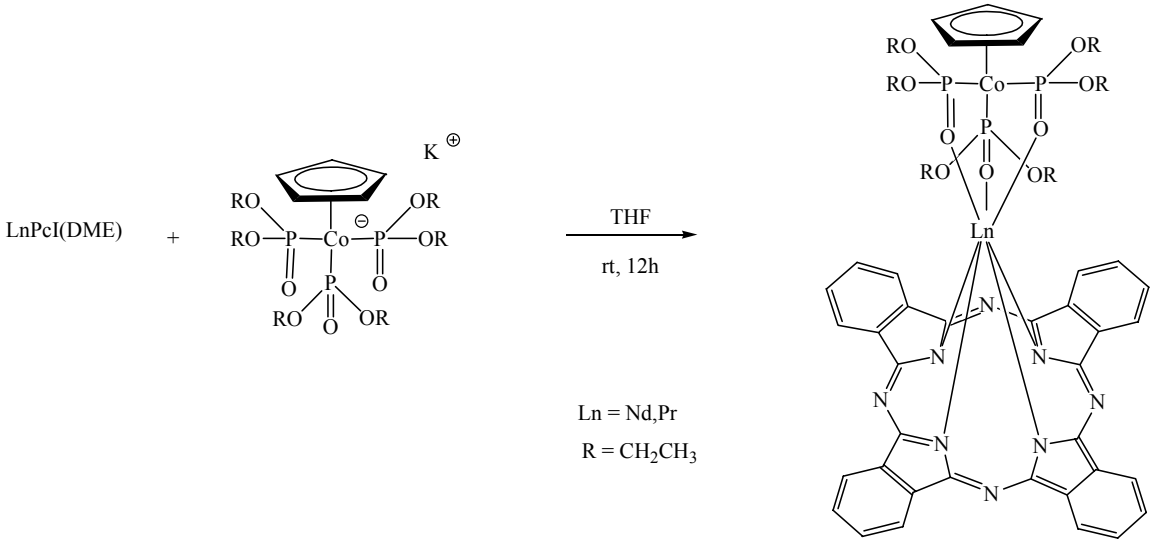

Figure 3.18: Synthesis of LnPc(LOEt) complexes, Ln = Pr, Nd.

The LnPc(LOEt) compounds were recrystallized from CH_2Cl_2 and pentane and were isolated in high yields and purity. A thermal ellipsoid plot of PrPc(LOEt) **(27)** is shown in Figure 3.19.

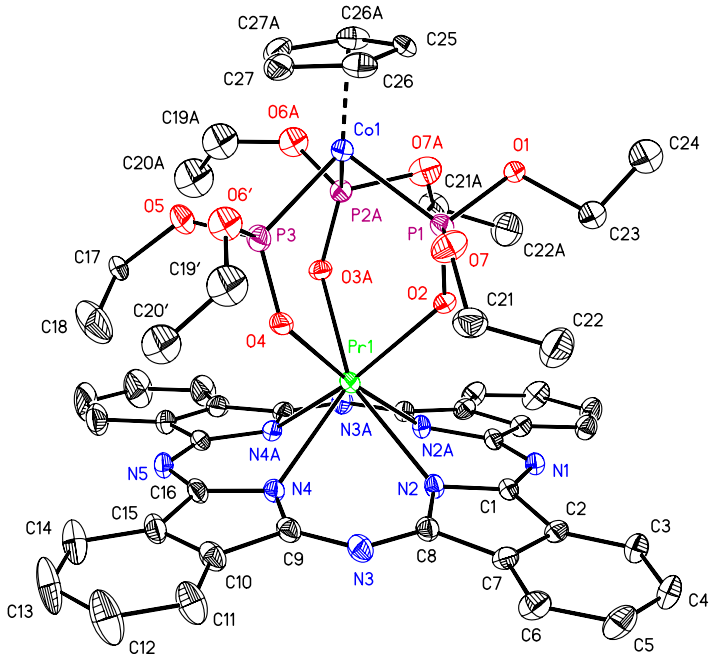

Figure 3.19: Solid state structure of PrPc(LOEt) **(27)**.

The complex is located on a mirror plane, which passes through Pr, Co, two N atoms on the Pc ring and C on the Cp ring. This plane, however, does not pass through any of the P atoms on the ligand, but between them causing them to occupy different positions and creating disorder. Due to considerable amount of disorder associated with the three $OP(OC_2H_5)_2$ groups on the ligand, a drawing was used to model the crystal structure. Bond lengths of Pr-N(2A) and Pr-N(4A) are 2.466(2) Å and 2.468(2) Å respectively. The metal sits 1.459(2) Å above the plane defined by N(2), N(2A), N(4) and N(4A). In order to accommodate the large metal, the rings of N(2) and N(4) become distorted with deviations from the plane of 10.6˚ and 5.3˚ respectively. When compared to the crystal structure of YbPc(LOEt),[92] the Pr sits 0.212(2) Å further from the plane, due to the larger ionic radius of Pr.

NMR Studies

As demonstrated with the TPP complexes, one and two-dimensional proton NMR spectra were used to identify the PC complexes. The proton NMR spectrum of PrPc(LOEt) **(27)** in figure 3.20 has 5 peaks (labeled A-E) with relative integrals of 5:8:8:12:18, respectively. With these relative integrals, the peaks were assigned as peak A corresponding to the Cp protons, peaks B and C to the protons on the Pc ring, and peaks D and E to the methylene and methyl protons on the ethoxy group respectively. There is no separation of the diastereotopic protons of the methylene in the Pr complex. The COSY spectra in figures 3.21 and 3.22 confirm the assignments made, showing one set of cross peaks between peaks B and C and another between peaks D and E, confirming the peak assignments from the 1-D spectra.

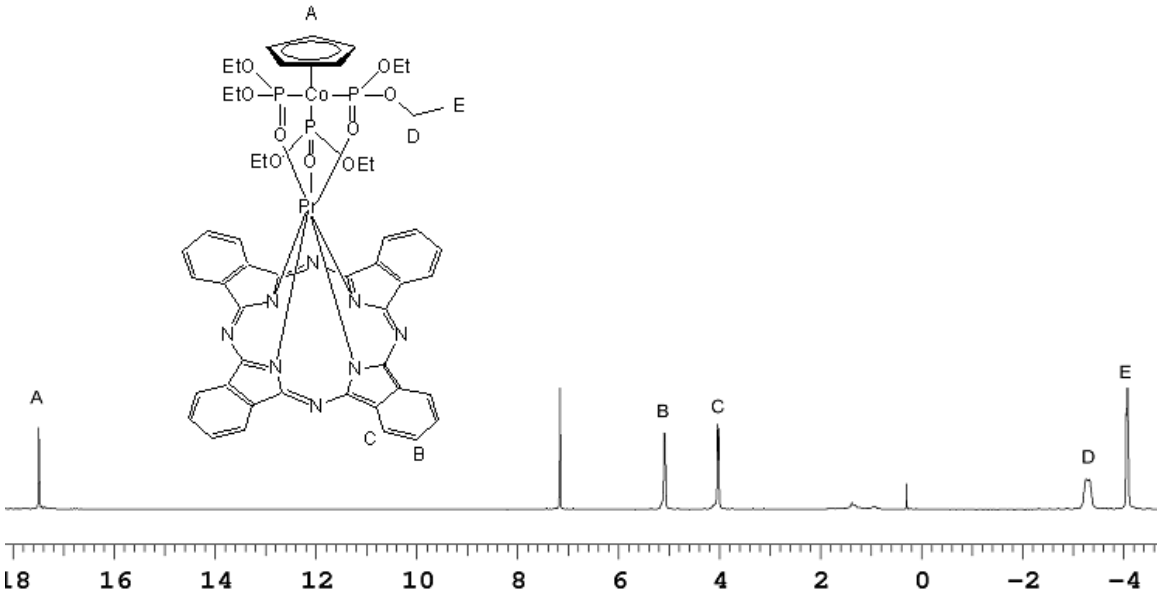

Figure 3.20: ^{1}H NMR spectrum of PrPc(LOEt) **(27)**.

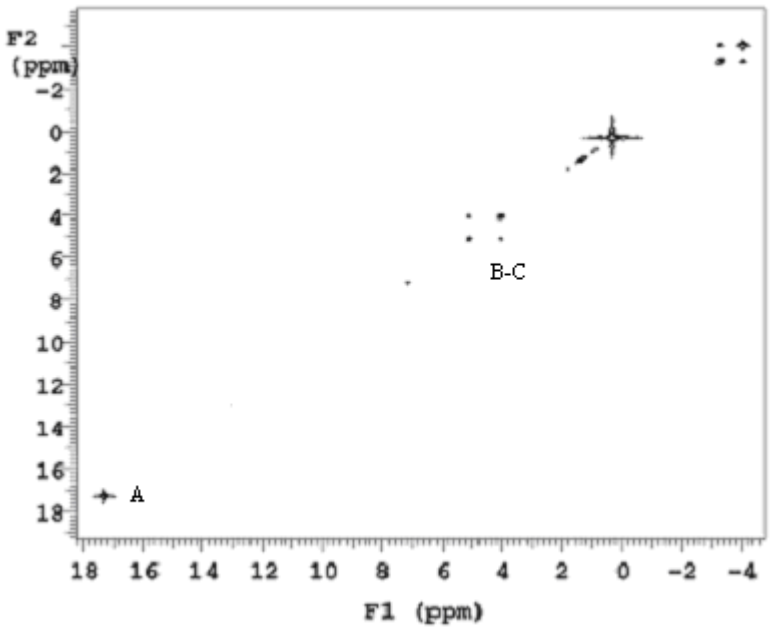

Figure 3.21: COSY NMR spectra of PrPc(LOEt) **(27)**.

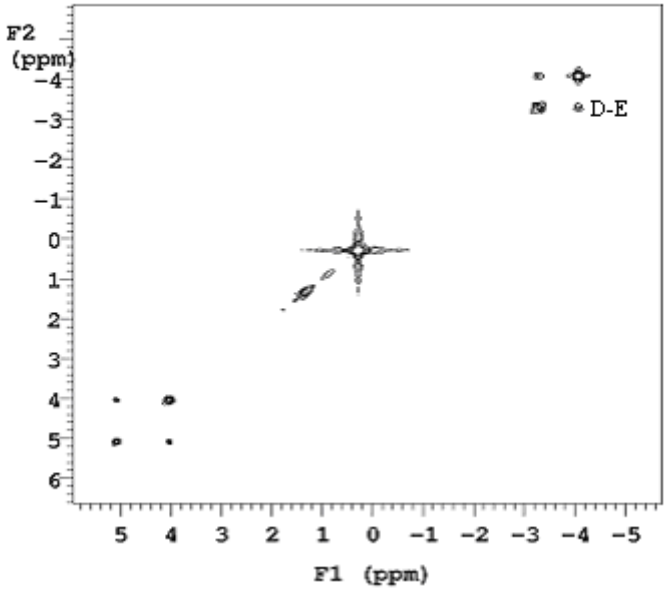

Figure 3.22: Expansion of COSY NMR spectra of PrPc(LOEt) **(27)**.

Photoluminescence Studies

PL studies were done by Gary Cunningham. Results show that there was no photoluminescence for either the neodymium or the praseodymium complexes. The

triplet state of Pc is ~1050 nm and is too low in energy to sensitize neodymium and praseodymium. Similar results were obtained with Ho-, Tm- and YbPc(LOEt) complexes. PL studies of ErPc(LOEt) observe the expected emission ~1500nm, however, the emission was extremely weak and no devices have been fabricated because of the extremely low intensity of this emission.[92]

Summary

The series of LnPc monomeric complexes was completed with the synthesis of neodymium and praseodymium complexes. These complexes were charactized by 1-D and 2-D NMR spectroscopy and crystallography. Unfortunately, PL studies show no observable luminescence for the Pr-,Nd-Ho- and TmPc(LOEt) complexes.

Experimental

Materials and Reagants

Unless otherwise stated, all syntheses were carried out on a double manifold Schlenk line under an atmosphere of nitrogen or in a N_2 filled glovebox. Glassware was oven dried prior to use. Methylene chloride, dimethoxyethane, chloroform and dimethlyforamide were purchased from Fisher Scientific and were dried with an appropriate drying agent.[77] The complexes (Cyclopentadienyl)tris(diethylphospinito)cobalt(I) (LOEt),[78] and hydridotris(1-pyrazolyl)borate (Tp^H)[79] were synthesized according to literature procedure. Tetrapyridylporphyrin (TpyP), pyrrole, 2-ethylhexyl bromide, 3-hydroxybenzaldehyde and 8-hydroxyquinoline were purchased from Aldrich and used as received. Tetra(3,4,5 trimethoxyphenyl) porphyrin (TmPP) was synthesized by the reaction of trimethoxybenzaldehyde and pyrrole in refluxing propionic acid.[95] Lithiated TmPP[81] and PC[92] were prepared using literature procedures. Elemental analyses were performed at

the University of California, Berkley, Micro-Mass Facility or University of Florida Spectroscopic Services. Proton NMR spectra were measured at 300 MHz at room temperature unless otherwise stated, on Varian, Gemini 300, VXR 300, Mercury 300 or Bruker 300 NMR spectrometers. Chemical shifts in spectra were referenced to residual solvent peaks and are reported relative to tetramethylsilane. Electrochemical investigations were carried out in an argon filled glove box using a three electrode cell with a platinum wire, platinum working and silver wire reference electrodes with the ionic liquid, 1-butyl-1-methyl-pyrrolidium NTF [BMP^+-NTF^-] (synthesized by Tony Burrell, Los Alamos National Lab) as the electrolyte solution. Electrochemical data were recorded using the electrochemical analyzer CHI730A-software. All UV/VIS spectra were run in 1 cm square quartz cuvettes in CH_3Cl (unless stated otherwise). The samples were prepared and run under N_2 on a double-beam Cary-100 UV-visible spectrometer.

Synthesis

Yb(TMPP)Cl(DME) (14)

A Schlenk flask was charged with Li_2TmPP(DME) (1 g, 0.9 mmol) and $YbCl_3(THF)_3$ (0.5 g, 0.9mmol) in a glovebox. After the addition of 40 mL of dry toluene, the flask was removed from the glovebox and the purple solution was refluxed under N_2. The progress of the reaction was monitored by UV/VIS and after 4 hours, the Soret band at 415 nm had shifted to 425 nm indicating complete metalation of the porphyrin. Toluene was removed under reduced pressure and the purple solid residue was extracted and filtered with dry CH_2Cl_2 (2 x 30 mL). The combined extracts were reduced in volume to *ca.* 20 mL and layered with pentane (*ca.* 20mL) giving 0.8 g of purple product (64%). ^{1}H NMR (300 MHz, DMSO): δ3.25 ($w_{1/2}$ = 2 Hz, 6 H, DME), 3.43($w_{1/2}$ = 2Hz, 4 H, DME), 3.82 ($w_{1/2}$ = 4 Hz,12 H, -OC*H*3), 5.10 ($w_{1/2}$ = 2 Hz,12H, -

OC*H*3), 6.07 ($w_{1/2}$ = 5 Hz,12H, -OC*H*3) 7.89 ($w_{1/2}$ = 10 Hz,4H, *H* -ortho), 14.74 ($w_{1/2}$ = 20 Hz, 8H, H-pyrrole), 15.75 ($w_{1/2}$ = 24 Hz,4H, *H* -ortho). UV/VIS (CH_2Cl_2) λ_{max} (log ε): 425 (5.27), 513 (3.77), 552 (4.34), 588 (3.81) nm. Anal. Calc. for $C_{60}H_{62}N_4O_{14}ClYb$: C, 56.69; H, 4.88; N, 4.41. Found: C, 56.58; H, 4.85; N, 4.32.

Yb(TMPP)Tp (15)

A solution of Yb(TmPP)Cl(DME) (0.1g , 0.07 mmol) in DMF (*ca*. 40 mL) was stirred while potassium hydridotris(1-pyrazolyl)borate (KTp) (0.02 g, 0.07 mmol) was added. The purple solution was allowed to stir at room temperature in the glove box for 12 hours. The solvent was removed *in vacuo* and the purple solid was extracted with *ca.* 30 mL of CH_2Cl_2 and then filtered, leaving behind a brown residue. The purple solution was reduced in volume to *ca.* 10 mL and then layered with *ca.* 20 mL of pentane. After standing overnight, 0.08 g (71% yield) of purple product was collected. ^{1}H NMR (300 MHz, C_6D_6): *δ*22.69 ($w_{1/2}$ = 79.41 Hz, 3H, H-Tp), 14.82 ($w_{1/2}$ =18.83 Hz, 4H, *H*-ortho), 14.25 ($w_{1/2}$ =15.97 Hz, 8H, *H*-pyrrole), 7.48 ($w_{1/2}$ =14 Hz, 4H, *H*-ortho), 5.21 ($w_{1/2}$ =12 Hz, 12 H, *H*- OCH_3), 5.08 ($w_{1/2}$ =6 Hz, 12H, *H*-OCH_3), 4.61 ($w_{1/2}$ =12 Hz, 3H, *H*-Tp), 3.27 ($w_{1/2}$ =10 Hz, 12H, *H*- OCH_3), -2.87($w_{1/2}$ = 12 Hz, 3H, *H*-Tp). UV/VIS (CH_2Cl_2) λ_{max} (log ε): 426 (3.11), 515 (0.22), 554 (0.39), 591 (0.20) nm. Anal. Calc. for $C_{65}H_{62}N_{10}O_{12}Yb$: C, 57.44; H, 4.60; N, 10.31. Found: C, 57.77; H, 4.60; N, 10.31.

4(2-ethylhexyloxy)benzaldehyde (16)[96]

Ethylhexyl bromide (5.64 mL, 0.032 mol) was added dropwise to a solution of 4-hydroxybenzaldehyde (3.89 g, 0.032 mol) and potassium carbonate (6.6 g, 0.048 mol) in butanone in air. The solution was refluxed for four days after which time the brown reaction mixture was filtered through Celite™ and the solvent removed to give brown oil. The oil was dissolved in ether (*ca.* 20 mL), washed with 1M NaOH (2 x 30 mL) then H_20

(2 x 30 mL,) and dried (Na_2SO_4). Purification by column chromatography [silica, methylene chloride: petroleum ether (3:2)] gave a yellow oil in 45% yield (3.54g, 1.51mmol). ^{1}H NMR (300 MHz, acetone): δ10.17 (s, 1H), 8.15 (d, J=3 Hz, 2H), 7.37 (d, J=1.8 Hz, 2H), 4.28 (d, J=5.4 Hz 2H), 1.8-1.59 (m, 9H), 1.25-1.16 (m, 6H). ^{13}C: δ190.5, 164.7, 132.1, 130.5, 115.2, 71.11, 39.7, 30.8, 29.45, 29.40, 29.39, 24.15, 23.36, 14.16, 11.19.

5,10,15,20-tetrakis [4-(2-ethylhexyloxy) phenyl]-porphyrin (TPPoeh) (17)

To a boiling solution of propionic acid, ethylhexyloxybenzaldehyde (2.5 g, 0.01 mol) and pyrrole (0.7 mL, 0.01 mol) were added together giving a solution that turned from yellow to dark brown. The solution was refluxed for one hour and the solvent was removed under reduced pressure, leaving a brown solid. The compound was then purified by column chromatography (silica, chloroform). The purple band was collected and was reduced in volume to *ca*. 10 mL and then layered with *ca*. 20 mL of methanol to give **17** in 5% yield (0.51 g, 0.4 mmol). ^{1}H NMR (300 MHz, $CDCl_3$): δ8.87 (s, 8H, *H*-pyrrole), 8.12 (d, J=8.7 Hz, 8H, *H*-phenol), 7.29 (d, J=11.7 Hz 8H, *H*-phenol), 4.15 (d, J=5.4 Hz, 8H), 1.95 (m, 8H), 1.73-1.43 (m, 28H), 1.08 (t, J =15 Hz, 12H), 0.99 (t, J=13.8 Hz, 12H) –2.76 (s, 1H). UV/VIS ($CHCl_3$) λ_{max} (log ε): 421(5.09), 520(4.06), 556(3.93), 595(3.63), 651(3.72) nm. Anal. Calc. for $C_{75}H_{92}N_4O_4$: C, 80.89; H, 8.33; N, 5.03. Found: C, 79.11; H, 8.56; N, 4.73.

Li_2TPPoeh(DME)$_4$ (18)

In a Schlenk tube, the addition of lithium hexamethyldisilazide (0.07 g, 0.46 mmol) to TPPoeh, **17**, (0.27 g, 0.23 mmol) in dry DME (*ca*. 20 mL) gave a color change from purple to blue/green. The progress of the reaction was monitored by UV/VIS and after 3 hours, the Soret band at 421 nm had shifted to 434 nm indicating complete lithiation of

the porphyrin. The solution was removed *in vacuo* and the product was extracted with pentane (2 x 20 mL), filtered, and cooled to –33° C to give **6** in 83% yield (0.278g). ^{1}H NMR (300 MHz, C_6D_6): δ9.26 (s, 8H, *H*-pyrrole), 8.39 (d, J=8.1 Hz, 8H, *H*-phenol), 7.33 (d, J=8.1 Hz, 8H, *H*-phenol), 3.96 (d, J=5.4 Hz, 8H, *H*-OCH_2), 2.12 (s, 18H, DME), 2.04 (s, 12H, DME), 1.88-1.38 (m, 36H), 1.03-0.96 (m, 24H). UV/VIS (CH_2Cl_2) λ_{max} (log ε): 434(4.74), 573(3.94), 618(2.79) nm. Anal. Calc. for $C_{91}H_{130}Li_2N_4O_{12}$: C, 73.56; H, 8.82; N, 3.77. Found: C, 72.12; H, 8.28, N, 4.22.

YbTPPoehCl(DME) (19)

To a solution of **18** (0.1 g, 0.07 mmol) in toluene (*ca.* 20 mL), $YbCl_3(THF)_3$ (0.06 g, 0.13 mmol) was added. Upon addition of $YbCl_3$, the solution turned from dark blue to red. The solution was refluxed under N_2 and the progress of the reaction was monitored by UV/VIS. After 3 hours of refluxing, the Soret band had shifted to 421 nm, indicating complete metalation of the porphyrin. The solvent was then removed *in vacuo* and the product extracted with pentane (2 x 20 mL). The solvent was removed, leaving purple oil in 70 % yield (0.07 g). ^{1}H NMR (300 MHz, C_6D_6): δ46.41 ($w_{1/2}$ =123 Hz, 6H, DME), 15.45 ($w_{1/2}$ =28 Hz, 8H, *H*-pyrrole), 14.86 ($w_{1/2}$ =30 Hz, 4H, *H*-phenol), 9.585 ($w_{1/2}$ =20 Hz, 4H, *H*-phenol), 9.24 ($w_{1/2}$ =19 Hz, 4H, *H*-phenol), 8.31 ($w_{1/2}$ =20 Hz, 4H, *H*-phenol), 4.83 ($w_{1/2}$ =10 Hz, 8H, *H*-OCH_2), 2.49-1.37 (m, 60H), -17.43 ($w_{1/2}$ =240 Hz, 4H, DME). UV/VIS (CH_2Cl_2) λ_{max} (log ε): 421(5.27), 515(3.86), 554(4.14), 594(3.92) nm.

YbTPPoeh(Tp) (20)

In the glovebox, KTp (0.015 g, 0.056 mmol) was added to a stirring solution of **19** (0.07 g, 0.056 mmol) in toluene (*ca*. 20 mL). The purple solution was stirred overnight and then the solvent removed *in vacuo*. The product was extracted with pentane (2 x 10 mL) and then filtered. The pentane solution was removed, giving **20** as red oil in 58%

yield (0.05 g). ^{1}H NMR (300 MHz, C_6D_6): δ22.7($w_{1/2}$ =120 Hz, 3H. *H*-Tp), 15.33 ($w_{1/2}$ =60 Hz, 4H, *H*-phenol), 14.29 ($w_{1/2}$ =30 Hz, 8H, *H*-pyrrole), 9.56 ($w_{1/2}$ =45 Hz, 4H, *H*-phenol), 8.19 ($w_{1/2}$ =90 Hz, 8H, *H*-phenol), 4.91 ($w_{1/2}$ =24 Hz, 8H, *H*-OCH_2), 4.80 ($w_{1/2}$ =27 Hz, 3H, *H*-Tp), 2.53-1.57 (m, 60H), -2.76 ($w_{1/2}$ =45 Hz, 3H, *H*-Tp). UV/VIS (CH_2Cl_2) λ_{max} (log ε): 424(4.83), 515(3.17), 555(3.77), 594(3.25) nm.

Li_2TPyP(DMF)$_2$ (21)

In the glovebox, lithium hexamethyldisilazide (0.86 g, 5.17 mmol) was added to a solution of TpyP (0.8, 1.3 mmol) in dry DMF (*ca.* 30 mL), which changed colors from red to green/blue. The solution was refluxed under N_2 for 12 hours. After the reaction, the solvent was removed *in vacuo* and the product was washed 3 times with *ca.* 20 mL of hexane to remove the excess lithium hexamethyldisilazide. ^{1}H NMR (300 MHz, DMSO-*d*$_6$): δ8.93 (d, J=4.8Hz, 8H, *H*-phenol), 8.54 (s, 8H, *H*-pyrrole), 8.16 (d, J=6Hz, 8H, *H*-phenol), 7.96 (s, 2H, DMF), 2.87(s, 6H, DMF), 2.72 (s, 6H, DMF). UV/VIS (CH_2Cl_2) λ_{max} (log ε): 434(5.34), 535(2.19), 575(3.34), 615(3.11) nm. Anal. Calc. for $C_{46}H_{38}N_{10}O_2Li_2$: C, 71.13; H, 4.93; N, 18.03. Found: C, 70.20; H, 4.44; N, 17.77.

YbTPyPCl(DME) (22)

In the glovebox, $YbCl_3(THF)_3$ (0.12 g, 0.25 mmol) was added to a solution of **21** (0.15 g, 0.25 mmol) in DMF (*ca*. 20 mL). The solution was refluxed for 12 hours under N_2 over which time the reaction mixture went from blue/green to red in color. The DMF was removed *in vacuo* and the red product was washed 3 times with *ca.* 20 mL of DME to give 0.15g (61% yield) of product. The poor solubility of this compound made it difficult to purify completely and so it was used as is for the next reaction. ^{1}H NMR (300 MHz, DMSO-*d*$_6$): δ16.29 ($w_{1/2}$ =78 Hz, 4H, *H*-phenol), 14.71 ($w_{1/2}$ =60 Hz, 8H, *H*-pyrrole), 11.71 ($w_{1/2}$ =60 Hz, 4H, *H*-phenol), 10.07 ($w_{1/2}$ =60 Hz, 4H, *H*-phenol), 8.67

($w_{1/2}$ =60 Hz, 4H, *H*-phenol), 3.39 (12H, DME), 3.22 (18H, DME). UV/VIS (CH_2Cl_2) λ_{max} (log ε): 425 (5.00), 513(3.45), 555(4.00), 593(3.40) nm. Anal. Calc. for $C_{44}H_{36}ClN_8O_2Yb$: C, 57.61; H, 3.96; N, 12.22. Found: C, 50.80; H, 3.88; N,11.80.

YbTPyP(LOEt) (23)

In the glovebox, K(LOEt) (0.11 g, 0.18 mmol) was added to a solution of **22** (0.2 g, 0.18 mmol) in DMF (*ca.* 10 mL) and stirred for 12 hours. The solution was then removed *in vacuo* and the desired product was extracted with CH_2Cl_2 (2 x. 10 mL). The CH_2Cl_2 extractions were filtered and reduced in volume to *ca.* 10 mL and then layered with *ca.* 20 mL of pentane to give **23** as a red powder in 41% yield (0.1 g). ^{1}H NMR (300 MHz, C_6D_6): δ16.86 ($w_{1/2}$ =72 Hz, 4H, *H*-phenol), 15.37($w_{1/2}$ =12 Hz, 8H, *H*-pyrrole), 12.03 ($w_{1/2}$ =76 Hz, 4H, *H*-phenol), 10.11 ($w_{1/2}$ =80 Hz, 4H, *H*-phenol), 8.31 ($w_{1/2}$ =36 Hz, 4H, *H*-phenol), 7.91 ($w_{1/2}$ =30 Hz, 6H, *H*-OCH_2CH$_3$), 7.34 ($w_{1/2}$ =35 Hz, 6H, *H*-OCH_2CH$_3$), 2.83 ($w_{1/2}$ =12 Hz, 18H, *H*-OCH$_2$CH_3), -4.86 ($w_{1/2}$ =6 Hz, 5H, *H*-Cp). UV/VIS (CH_2Cl_2) λ_{max} (log ε): 425 (5.24), 510(3.95), 555(4.07), 593(3.69) nm. Anal. Calc. for $C_{57}H_{55}N_8O_9YbP_3Co$: C, 51.82; H, 4.19; N, 8.48. Found: C, 49.51; H, 3.95; N, 8.02.

NdPcI(DME) (24)

$NdI_3(THF)_4$ (0.25g 0.31mmol) and Li_2Pc (0.162g, 0.31mmol) were added together in 40 mLof DME. The blue solution was refluxed for 12 hours under N_2. The solution was cooled to room temperature at which time the solvent was removed *via* canula filtration. 0.126 g (0.143 mmol, 47%) of product was isolated after filtering and drying on the Schlenk line. The complex is insoluble in all organic solvents, preventing full characterization of this material. It was used as is for the next reaction.

PrPcI(DME) (25)

The same procedure for **24** was used in this synthesis. To $PrI_3(THF)_4$ (1.00 g, 1.2 mmol), and Li_2PC (0.65 g, 1.2 mmol), 50 mL of DME was added and refluxed for 12 hours to give 0.695 g (0.8 mmol, 65%) of **25**.

NdPc(LOEt) (26)

NdPcI(DME) (0.160 g, 0.18 mmol) and the K(LOEt) (0.09 g, 0.18 mmol) were stirred together in 30 mL of dry THF. After 12 hours, the blue solution was removed *in vacuo* and the solid was extracted with about 30 mL CH_2Cl_2, leaving behind a white residue of KI. The volume of the CH_2Cl_2 solution was reduced to 15 mL and then layered with pentane and allowed to sit at room temperature until the product crystallized. After 48 hours, the blue product was isolated in 65% yield (0.142 g, 0.119 mmol) *via* cannula filteration. ^{1}H NMR (C_6D_6): δ 11.51 ($w_{1/2}$ = 5.15 Hz, 5H, *H*-Cp), 6.35 ($w_{1/2}$ = 13.36 Hz, 8H, *H*-Pc), 6.30 ($w_{1/2}$ = 12.64 Hz, 8H, *H*-Pc), -0.69 ($w_{1/2}$ = 31.27 Hz, 6H, OC*H*$_2$CH$_3$), -0.98 ($w_{1/2}$ = 32.34 Hz, 6H, OC*H*$_2$CH$_3$), -2.14 ($w_{1/2}$ = 12.67 Hz, 18H,-OCH$_2$C*H*$_3$). UV/VIS (CH_3Cl), λ_{max} (log ε) = 676(5.05), 644(2.85), 608(4.29), 342(3.86) nm. Anal. Calc. for $C_{49}H_{51}O_9N_8P_3CoNd$: C, 49.37; H, 4.31; N, 9.40. Found: C,48.25; H,4.16; N,8.73.

PrPc(LOEt) (27)

PrPcI(DME) (0.2 g, 0.2 mmol) was allowed to react with K(LOEt) (0.135 g, 0.230 mmol) in dry THF (*ca.* 20 mL) for 12 hours under inert atmosphere. The solution was removed i*n vacuo* and the complex was extracted with *ca*. 30 mL of CH_2Cl_2. The volume of the blue solution was reduced to *ca.* 10 mL and layered with pentane (*ca.* 20 mL), causing the compound to precipitate. The product was isolated in 71.3% yield (0.195 g, 0.16 mmol). ^{1}H NMR (C_6D_6): δ17.48($w_{1/2}$ = 5.61 Hz, 5H, *H*-Cp), 5.10($w_{1/2}$ = 11.65 Hz,

8H, *H*-Pc), 4.04($w_{1/2}$ = 11.60 Hz, 8H, *H*-Pc), -3.27($w_{1/2}$ = 46.90 Hz, 12H, OC*H*$_2$CH$_3$), -4.08($w_{1/2}$ = 13.18 Hz, 18H, OCH$_2$C*H*$_3$). UV/VIS (CH_3Cl), λ_{max} (log ε) = 674(4.97), 644(4.19), 610(4.23), 340(4.58) nm. Anal. Calc. for $C_{49}H_{51}O_9N_8P_3CoPr$: C, 49.51; H, 4.32; N, 9.43. Found: C, 50.42; H, 4.22; N, 8.95.

HoPc(LOEt) (28)

To a dark blue solution of HoPcCl(DME) (0.125 g,0.155 mmol) in 30 mL of THF, was added K(LOEt) (0.08 g,0.15 mmol). After stirring at room temperature for 12 hours, the solution was removed *in vacuo* and the product was extracted with CH_2Cl_2 (3 x 10 mL). The extracts were combined and the volume of the solution was reduced to *ca.* 10 mL and then layered with pentane. The blue crystals were collected in 38% yield (0.08 g, 0.065 mmol) after 12 hours. ^{1}H NMR (C_6D_6): δ 53.54($w_{1/2}$= 64.22 Hz, 5H, *H*-Cp), -4.85($w_{1/2}$= 17.62 Hz, 8H, *H*-Pc), -15.17($w_{1/2}$= 51.41 Hz, 8H, *H*-Pc), -16.98($w_{1/2}$ = 64.4 Hz, 18H, OCH$_2$C*H*$_3$), -24.02($w_{1/2}$= 15.63 Hz, 6H, O*CH*$_2$CH$_3$), -26.01 ($w_{1/2}$= 16.69 Hz, 6H, OC*H*$_2$CH$_3$). UV/VIS (CH_3Cl), λ_{max} (log ε) 672(5.72), 642(4.41), 606(5.00), 340(5.20) nm. Anal. Calc. for $C_{49}H_{51}O_9N_8P_3CoHo$: C, 48.53; H, 4.24; N, 9.24. Found: C, 47.52; H, 4.17; N, 8.0.

TmPc(LOEt) (29)

Using the same procedure as **28**, TmPcCl(DME) (0.148 g, 0.206 mmol) and K(Klaui) (0.097 g, 0.206 mmol) were stirred together in THF to give 0.05 g (0.041 mmol, 20% yield). ^{1}H NMR (C_6D_6): δ 48.62($w_{1/2}$ = 62.53 Hz, 6H, O*CH*$_2$CH$_3$), 47.86($w_{1/2}$ = 19.41 Hz, 8H, *H*-Pc), 47.56($w_{1/2}$ = 83.07 Hz, 6H, OC*H*$_2$CH$_3$), 27.62($w_{1/2}$ = 18.41 Hz, 18H, OCH$_2$C*H*$_3$), 27.02($w_{1/2}$ = 10.22 Hz, 8H, *H*-Pc), -71.83($w_{1/2}$ = 16.69 Hz, 5H, *H*-Cp). UV/VIS (CH_3Cl), λ_{max} (log ε)= 675(5.08), 673(5.17), 645(4.48), 608(4.41), 338(4.65)

nm. Anal. Calc. for $C_{49}H_{51}O_9N_8P_3CoTm$: C, 48.37; H, 4.22; N, 9.21. Found: C,48.10; H, 4.10; N,8.79.

XRAY of PrPc(LOEt)

Data were collected at 173 K on a Siemens SMART PLATFORM equipped with A CCD area detector and a graphite monochromator utilizing MoK_α radiation ($\lambda = 0.71073$ Å). Cell parameters were refined using up to 8192 reflections. A full sphere of data (1850 frames) was collected using the ω-scan method (0.3° frame width). The first 50 frames were remeasured at the end of data collection to monitor instrument and crystal stability (maximum correction on I was < 1 %). Absorption corrections by integration were applied using the measured, indexed, crystal faces.

The structure was solved by Direct Methods in *SHELXTL5,* and refined using full-matrix least squares. The non-H atoms were treated anisotropically, whereas the hydrogen atoms were calculated in ideal positions and were riding on their respective carbon atoms. The complex is located on a mirror plane which causes a disorder in the $OP(OC_2H_5)_2$ ligand bridging the Pr and Co centers. The mirror passes through Pr, Co, two N atoms on opposite side the macrocycle, and atom C25 of the cp ring and bisects the bond between C27 and its mirror equivalent C27a. The mirror symmetry does not pass through any of the P atoms but between them causing them to occupy six positions belonging to two parts of the three $OP(OC_2H_5)_2$ ligands rotated by an angle of 60° from each other. A total of 374 parameters were refined in the final cycle of refinement using 18773 reflections with $I > 2\sigma(I)$ to yield R_1 and wR_2 of 3.46% and 5.45%, respectively. Refinement was done using F^2.

CHAPTER 4
POLYERMIZABLE LANTHANIDE-PORPHYRIN COMPLEXES

Introduction

Because our systems work without a conjugated polymer, devices were prepared by spin-casting YbTPP(L) as the only active layer. These devices, however had poor film quality when compared with blended devices and produced only 20% of the near-infrared intensity of devices consisting of blends of 5 mol% metal complexes with non-cojugated polymers.[97] So, blending our complexes with a polymer, conjugated or non-conjugated enhances device efficiency probably by minimizing self-quenching effects and by improving film quality.

Blending polymers with metal complexes acting as emitting molecules has been shown to be a valuable technique in the development of efficient sources of light for LEDs. There are, however, some disadvantages to using this technique. The blending of a polymer and dopant usually results in phase separation and non-uniform dispersion of the dopant which can lead to lower luminescent efficiencies and device durability due to triplet-triplet annihilation and higher turn on voltages.[98] Minimizing phase separation should result in enhanced device performance.

Lanthanide Polymers

One way to improve film quality is to incorporate the dopant into the polymer.[99] Ling *et al.* coploymerized an Eu(vinylbenzoic acid) (thenoyltrifluoroacetone) (phenathroline) complex with a vinylcarbozole to obtain an Eu-containing copolymer for red LEDs (Figure 4.1).[100]

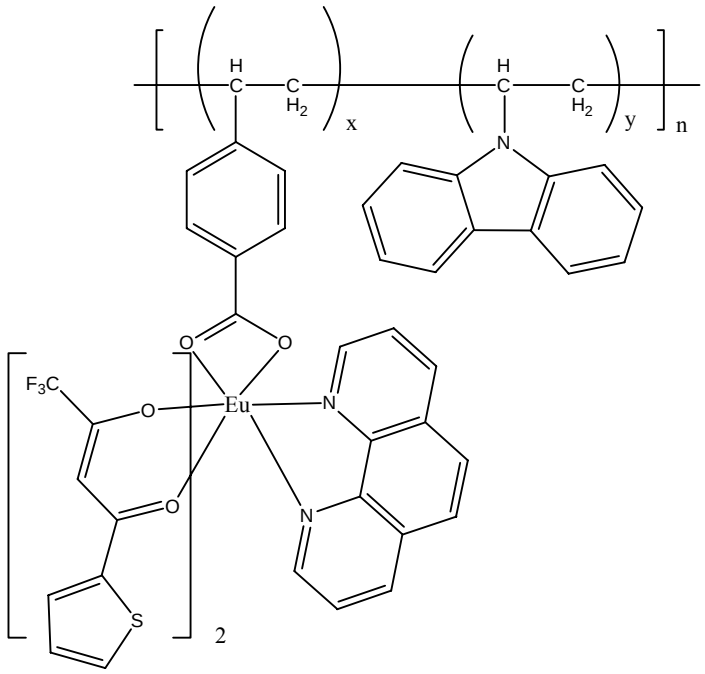

Figure 4.1: Eu(TTA)$_2$(VBA)phen-NVK copolymer.

The copolymer was prepared by free radical copolymerization of the two monomers, using AIBN as an intiator, with average molecular weights around 10,000 g/mol. Electroluminescent studies on the single-layered device produced red emission with a performance that compared favorably with those of other single layered devices and a completely homogeneous film. Other efforts to make Ln-copolymers include work by Zeng *et al.* who conducted EL studies on a Tb-containing polymer that produces green light [101] and work by Yang *et al.* who conducted EL studies on a Tb-Eu copolymer in which varying the ratio of Eu/Tb tunes the emission color.[102]

Porphyrin Polymers

In recent years, porphyrin oligomers and polymers have been studied for applications in sensing, non-linear optic materials, catalysts and artificial photosynthesis.[103] One example of a porphyrin polymer was reported by Haber and coworkers, who synthesized a porphyrin supported on a polyaniline system for studying

its catalytic activity towards the co-oxidation of styrene and iso-butyraldehyde (Figure 4.2).[104]

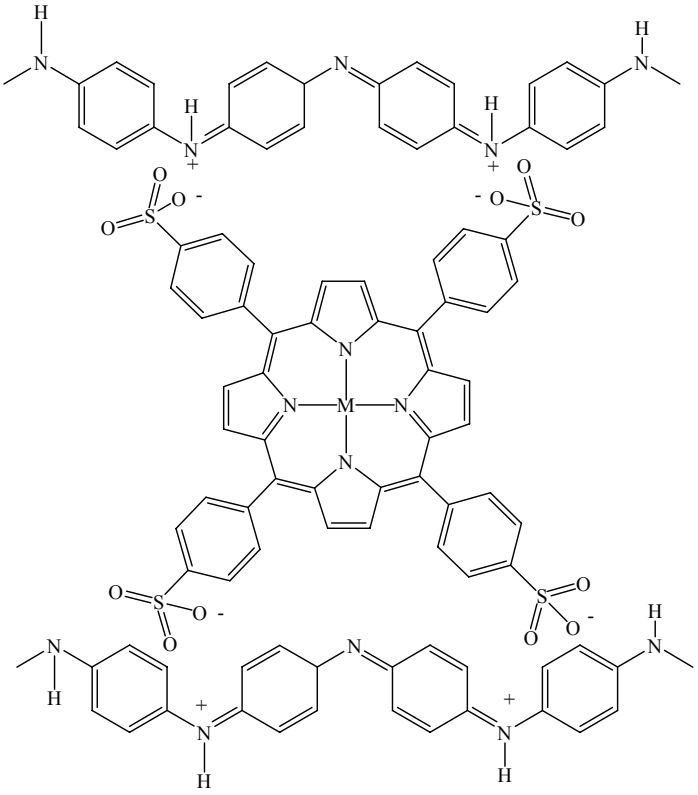

Figure 4.2: Structure of porphyrin supported in polyaniline.

Other examples consist of the copolymerization of porphyrin monomers, incorporating the porphyrin in the backbone of the polymer or as a pendant group (Figure 4.3).[105,106]

While there has been considerable research on the incorporation of lanthanides, porphyrins, and transition metalloporphyrins into polymer systems, there are no lanthanide-porphyrin polymer systems, perhaps due to the lack of convenient synthesis of suitable lanthanide porphyrin monomers. This chapter will discuss the synthesis of polymerizable lanthanide-porphyrin complexes in efforts to incorporate the complex into polymers.

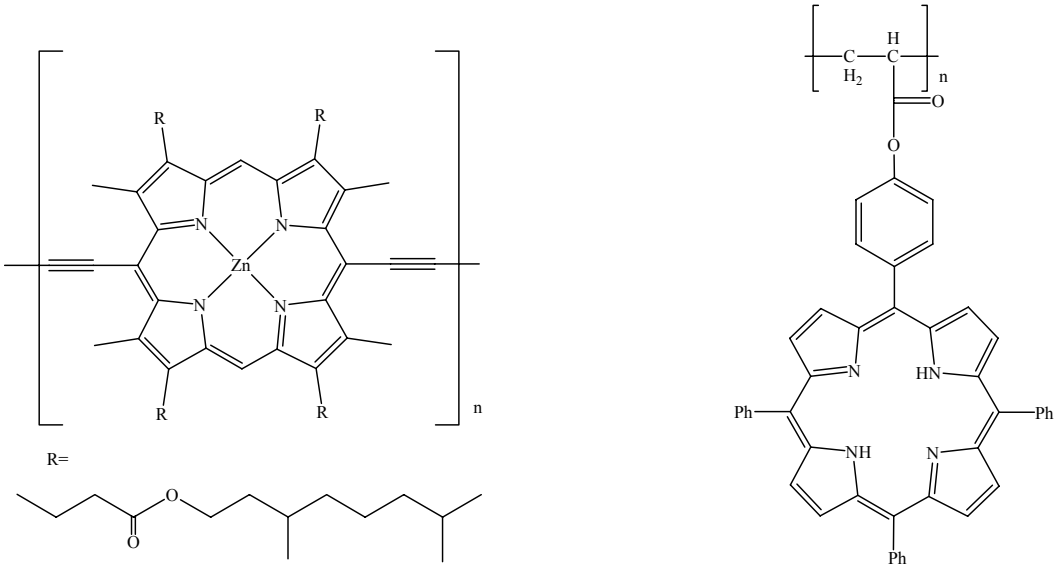

Figure 4.3: Examples of porphyrin polymers.

Lanthanide-Porphyrin Polymer Complexes

Lanthanide-vinylporphyrin Complexes

Synthesis

The vinyl porphryin, 5-(4-vinylphenyl)-10,15,20 triphenylprophyrin (TPPv) was synthesized in order to be co-polymerized into a polymer to study the effects of changes in phase segregation on device efficiency. The porphyrin was synthesized by one-pot mixed aldehyde condensation reaction between vinylbenzaldehyde, pyrrole and benzaldehyde, using $BF_3(OEt_2)$ cocatalysis (Figure 4.4). After stirring the mixture for an hour, oxidation by DDQ afforded a mixture of porphyrin isomers. The desired compound was isolated *via* column chromotagraphy, packing the column with silica gel and hexanes and eluding the desired porphyrin from CH_3Cl/hexanes. No other combinations of the condensation were isolated. After recrystallization from a CH_3Cl/methanol solution, TPPv **(30)** was collected in 14% yield.

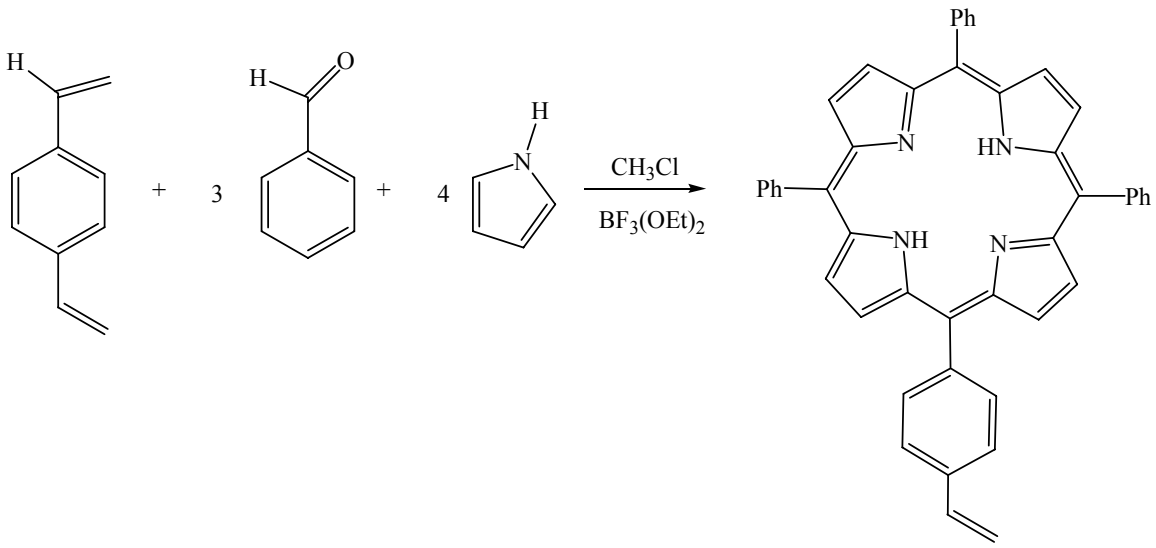

TPPv (**30**)

Figure 4.4: Synthesis of TPPv.

Lindsey and coworkers synthesized and isolated the vinylporphyrin metallated with zinc with similar results.[107] The same compound was recently synthesized by Pomogailo *et al. via* a Wittig reaction between 5-(4-formylphenyl)10,15,20- triphenylporphyrin and trimethylenephosphorane.[108] This synthetic approach, however requires a multi-step process with each stage of the reaction needing column chromotagraphy and recrystallization to separate and purify the products. The reaction starts with the mixed aldehyde condensation reaction to form a monocyanoporphyrin. After addition of zinc acetate, the metallated porphyrin is reduced to the aldehyde. The zinc is then removed and the free base porphyrin aldehyde is reacted with the ylide to form the vinylporphyrin (Figure 4.5).

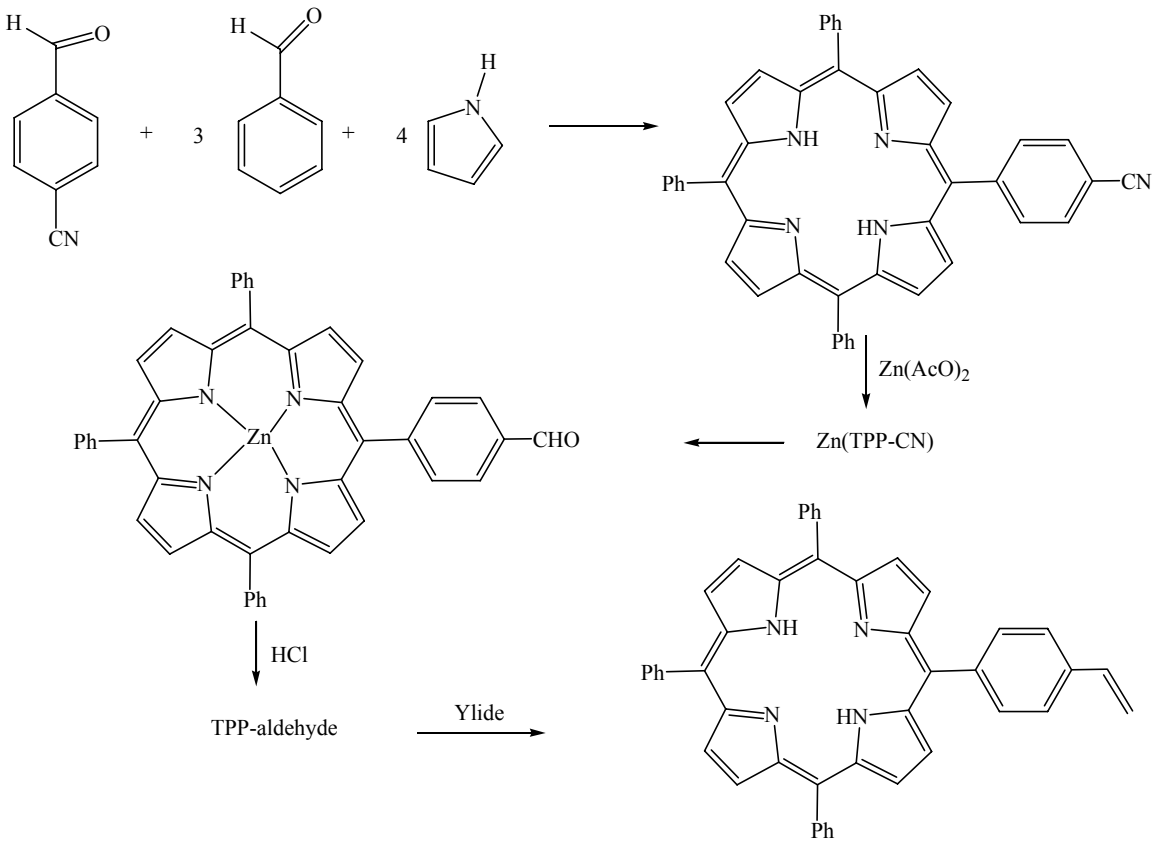

Figure 4.5: Synthesis of vinylporphyrin by Pomogailo *et al.*

With the vinyl porphyrin synthesized and characterized, similar synthetic procedures as described in the previous chapters were carried out in order to metallate the porphyrin. Firstly, the TPPv dianion was synthesized by reacting TPPv with lithium hexamethyldisilazide in refluxing DME. In a salt metathesis reaction between the dianion $Li_2TPPv(DME)_2$, **(31)** and $YbCl_3(THF)_3$, YbTPPv(Cl)DME was synthesized. After stirring the mixture of the Li salt and $YbCl_3(THF)_3$ for four hours at reflux, the UV/VIS spectrum of the reaction mixture showed an absorption at ~425 nm corresponding to metallated TPPv. The solution was then separated from KCl by hot filtration and removal of the solvent. The complex YbTPPvCl(DME) **(32)** was recrystallized from a mixture of CH_2Cl_2 and pentane to obtain the purple material in 80% yield (Figure 4.6).

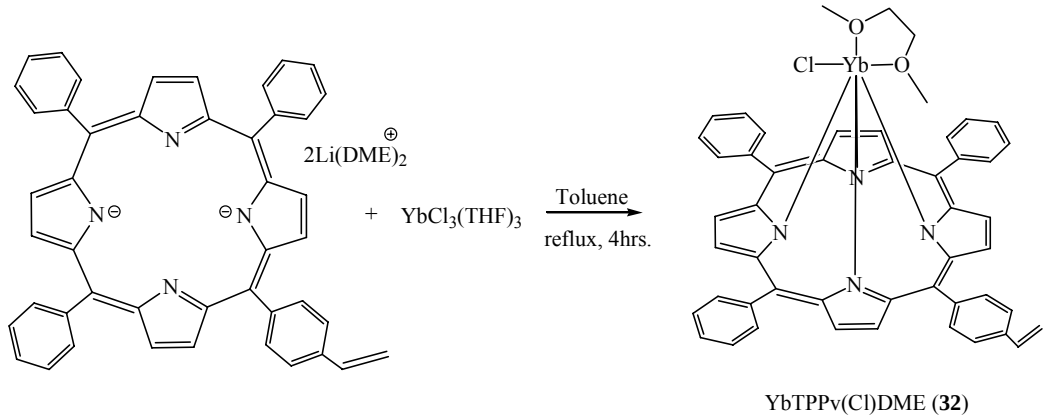

Figure 4.6: Synthesis of **32**.

In a second set of salt metathesis reactions, YbTPPv(Cl)DME was allowed to react with the capping ligands KTp or K(LOEt) to give YbTPPv(Tp) (**33**) or YbTPPv(LOEt) (**34**) (Figure 4.7), respectively. In a Schlenk flask, YbTPPv(CL)DME and the capping ligand were stirred at room temperature under nitrogen in DME. After stirring for twelve hours, complexes **33** and **34** were extracted with CH_2Cl_2 and were then isolated as purple crystalline solids in high yields by recrystallization from mixtures of CH_2Cl_2 and pentane. The purity of the bulk material was confirmed by elemental analysis.

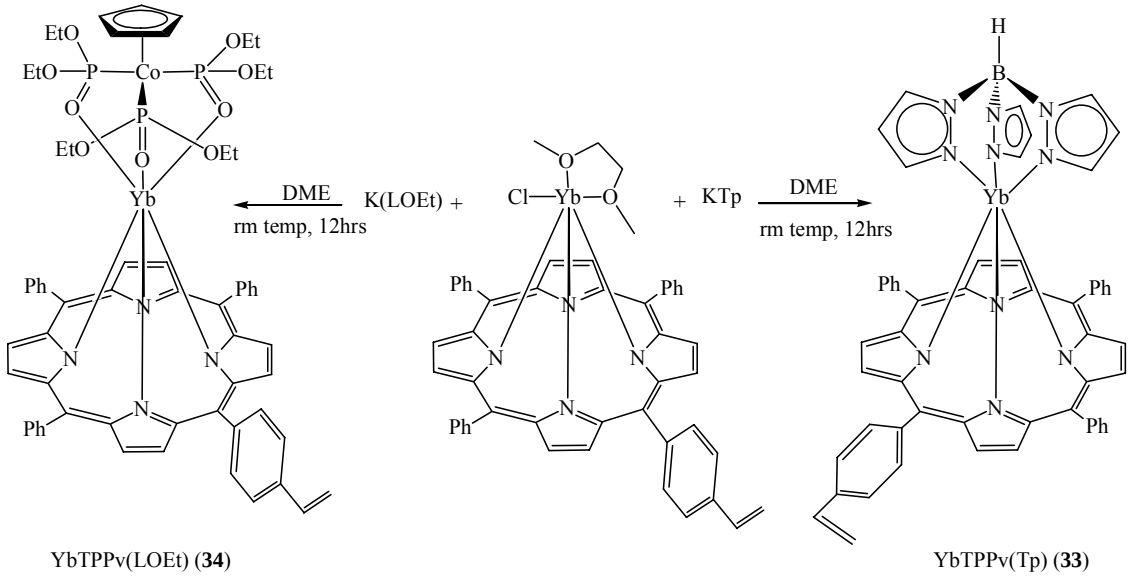

Figure 4.7: Synthesis of complexes **33** and **34**.

NMR studies

The ^{1}H NMR spectrum of YbTPPvTP **(33)** is shown in figure 4.8. Similar to the lanthanide porphyrin complexes discussed in previous chapters, the peaks were assigned by using 1-D, 2-D and variable temperature NMR techniques. The 1-D spectrum shows 12 peaks, five of the peaks correspond to the protons from the phenyl rings, three of the peaks correspond to the Tp protons, three of the peaks correspond to the vinyl group and the twelfth peak corresponds to the pyrrole protons.

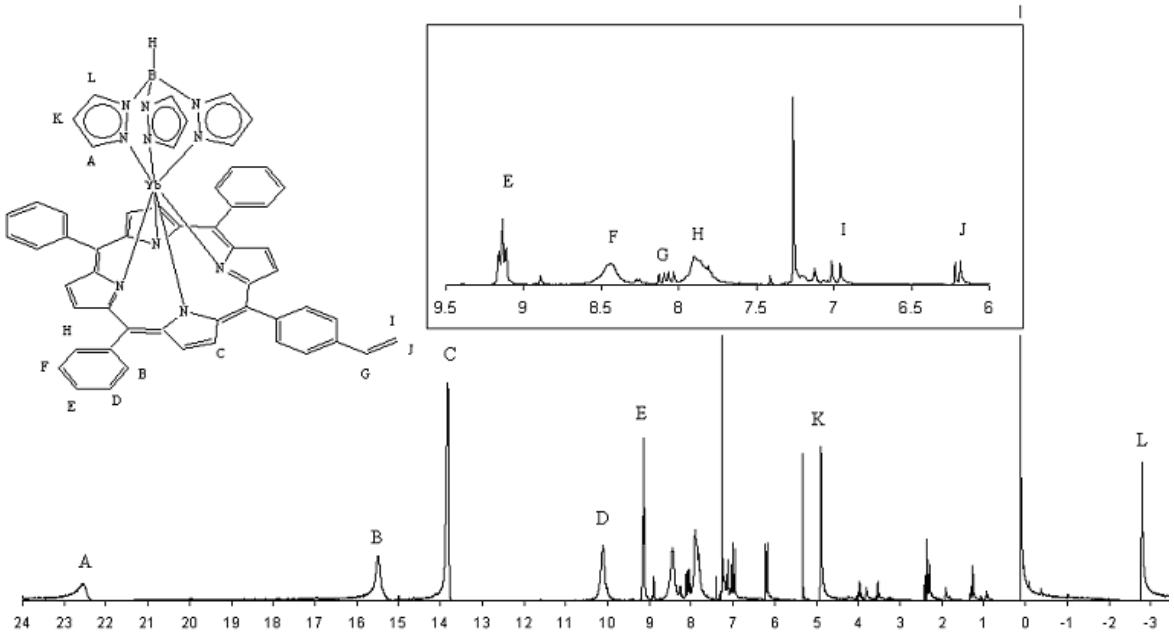

Figure 4.8: ^{1}H NMR spectrum of YbTPPvTp **(33)**

With relative integrals of three and a cross peak between K and L, as seen in the 2-D spectrum of **33** (Figure 4.9), peaks A, K, and L are assigned to the protons on the Tp ligand. Because of its proximity to the paramagnetic nucleus the relaxation time of peak A is too short to allow the appearance of the crosspeaks between A and either K or L in the NMR spectrum. Peaks B and H are assigned the *ortho* protons on the phenyl ring with relative integrals of 4 and cross peaks between only peaks D and F, respectively.

With an additional cross peak with peak E and relative integrals of 4, peaks D and E are assigned the *meta* protons on the phenyl ring. The coupling of the vinyl proton peaks can been seen in the 1-D NMR spectrum, as well as cross coupling peaks between peaks G, I, and J, allowing the assignment of these peaks as the vinyl proton peaks.

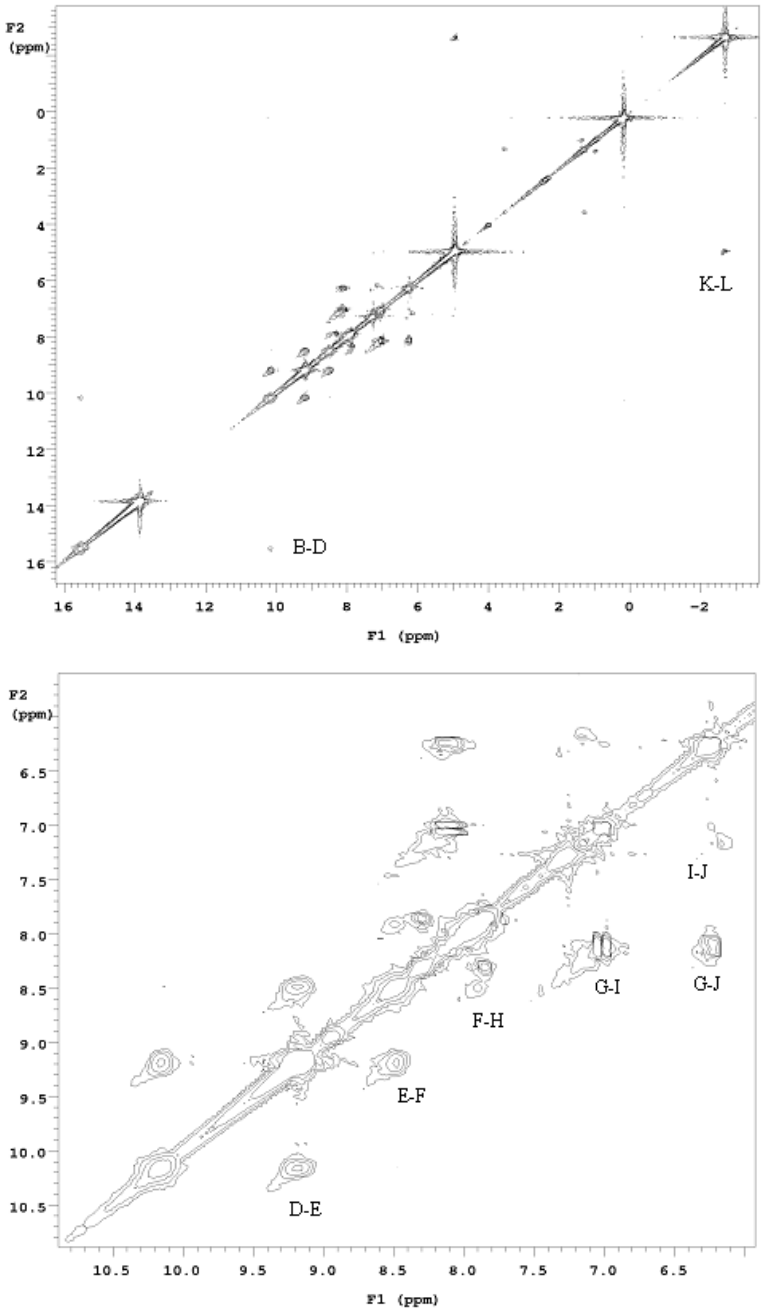

Figure 4.9: COSY NMR of **33** (top), expansion from 11-6 ppm (bottom).

Metathesis reactions

Through a metathesis reaction using the ruthenium-based second-generation Grubb's catalyst, a free base porphyrin substituted stilbene derivative was synthesized (Figure 4.10).

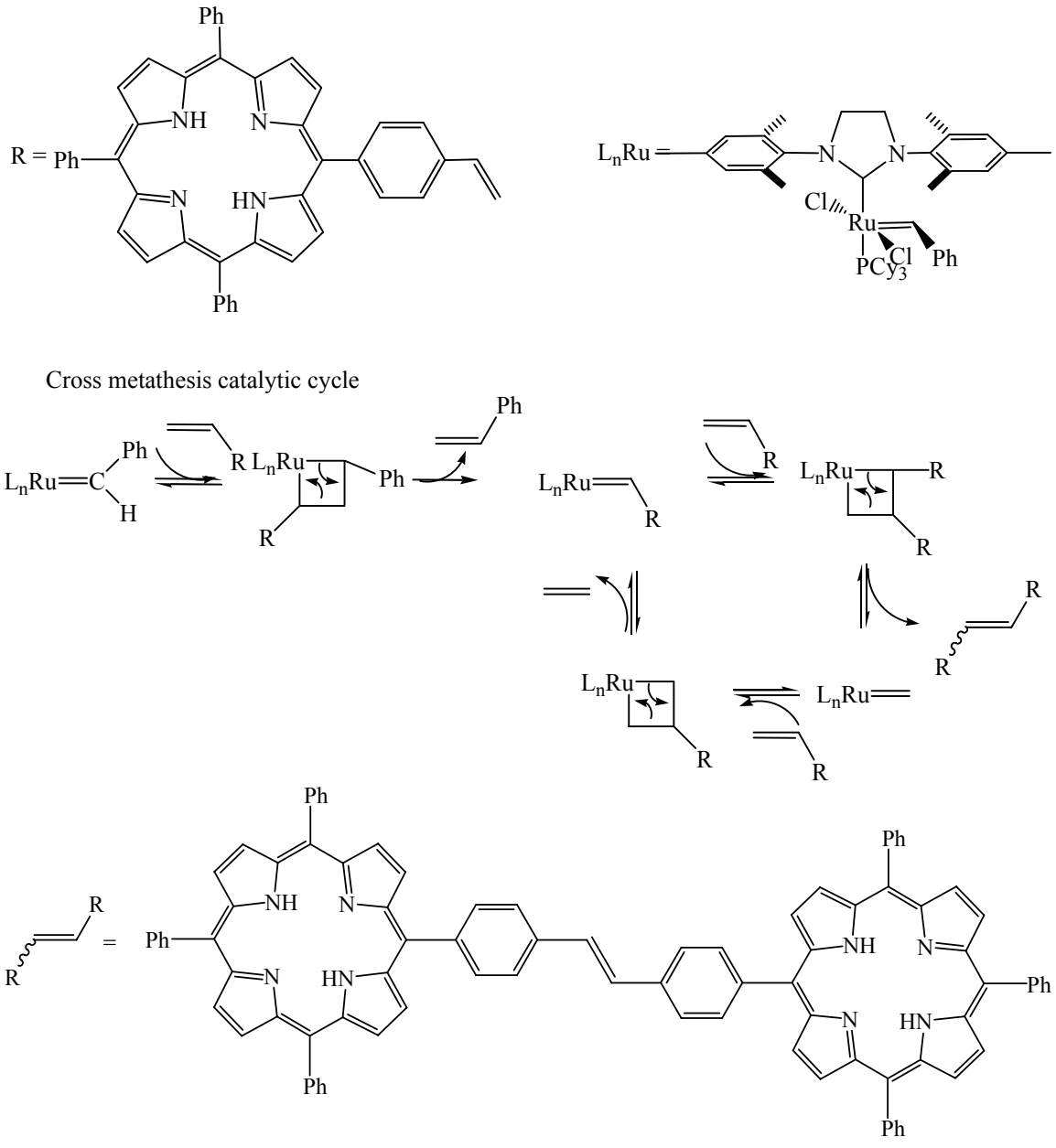

Figure 4.10: Catalytic cycle for metathesis reaction between vinyl porphyrins.

Compound **30** was treated with 10 mol% of the Ru catalyst in dry CH_2Cl_2 at reflux under N_2 for 1 hour. The solution was then removed and the purple solid was washed several times with diethyl ether to remove unreacted porphyrin and catalyst.[109] The stilbene derivative was recrystallized in a solution of CH_3Cl layered with pentane to obtain the compound in 32% yield. The ^1H NMR spectrum of compound **35** in figure 4.11 shows the disappearance of the vinyl protons of compound **30** from 5.5-7 ppm (inset) as well as the appearance of a new peak at ~8 ppm, corresponding to the vinylic proton of the compound.

While there is no precedence for self metathesis reactions between two porphyrins, Dolphin *et al.* reported the first cross metathesis reaction between vinyl porphyrins and a variety of terminal olefins.[110] They found that high loading of the catalyst was required to ensure high yields. Typical reactions used 25 mol% catalyst and when the loading was reduced to 15 mol%, the yield would drop from 100% to 70%. For the dimeraztion reaction of **30**, only 10 mol% catalyst loading was used, which perhaps accounts for the observed low yield.

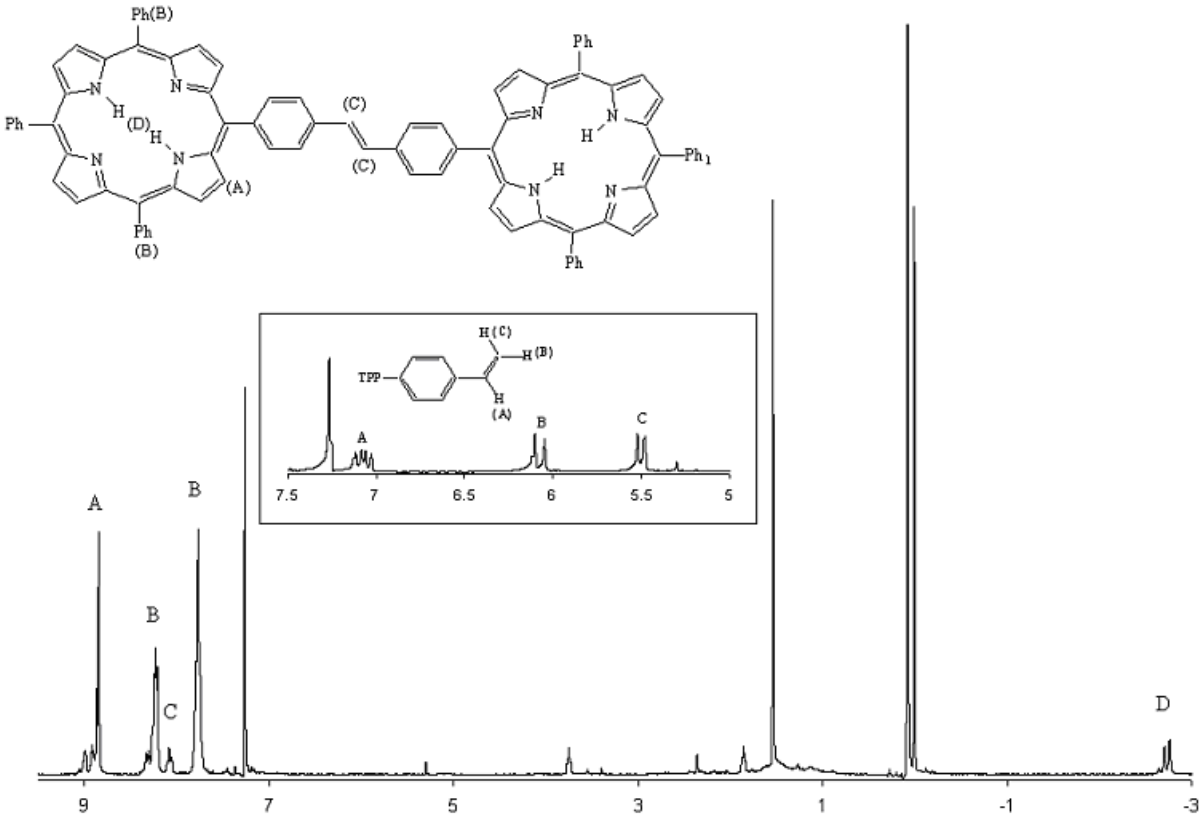

Figure 4.11: ^{1}H NMR spectrum of **35** (aromatic region of **30** in inset).

The YbTPPTp (**36**) substituted stilbene derivative was synthesized using the ruthenium-based second-generation Grubb's catalyst in the same manner as described for the free base synthetic procedure (Figure 4.12). Compound **33** was treated with 10 mol% of the Ru catalyst in dry CH_2Cl_2 at reflux under N_2 for 12 hours. The solution was then removed and the purple solid was washed several times with diethyl ether to remove unreacted porphyrin and catalyst.[109] The stilbene derivative was recrystallized in a solution of CH_2Cl_2 layered with pentane to obtain the compound in 25% yield. The ^{1}H NMR spectrum of the phenyl region of compound **36** in figure 4.13 shows the disappearance of the vinyl protons of compound **33** (inset) as well as the appearance of a new peak at ~8.9 ppm, corresponding to the vinylic protons of the compound.

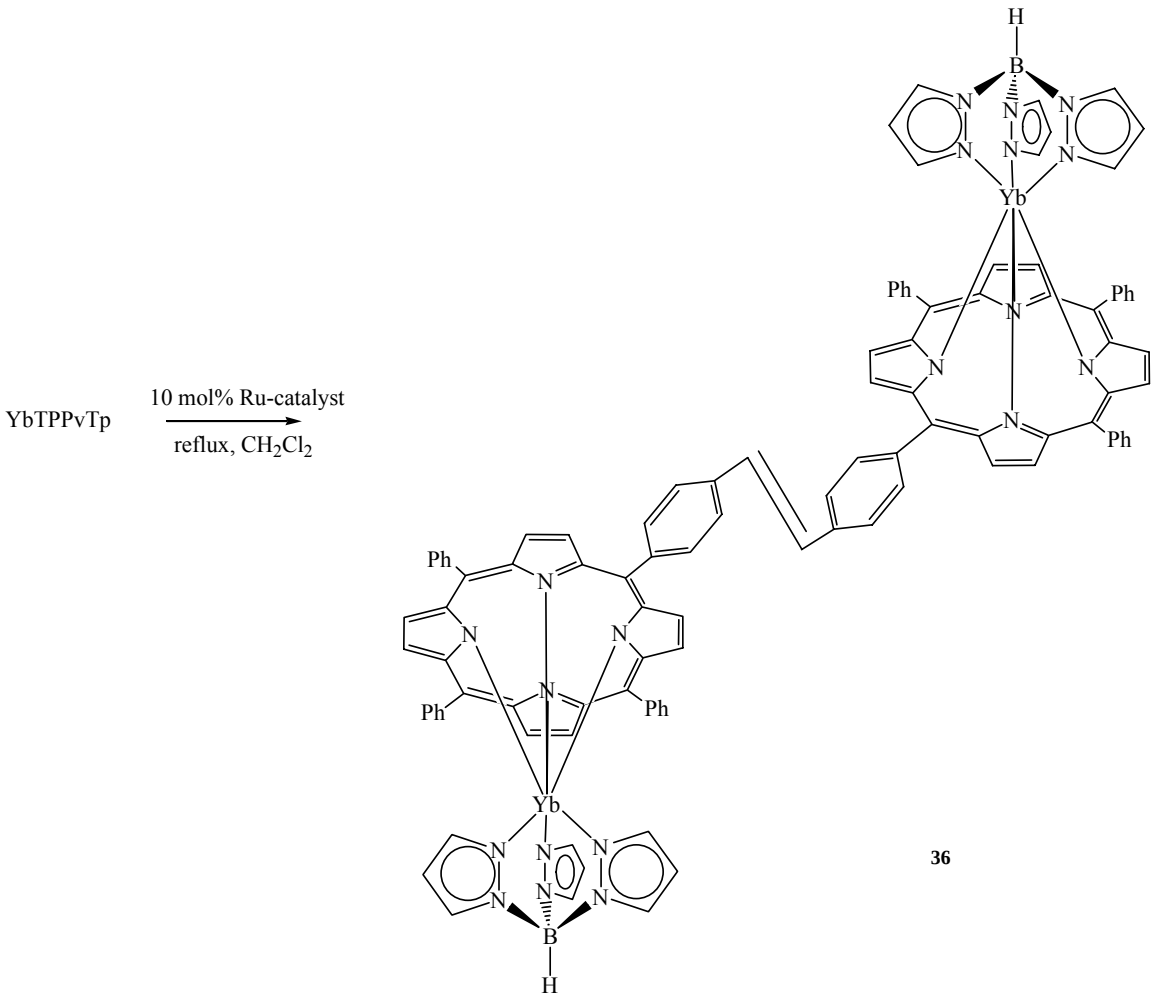

Figure 4.12: Synthesis of **36**.

Through the relative integrals in the 1-D ^{1}H NMR spectrum, comparison with the spectrum of **33** and the cross peaks in the 2-D spectrum, the eleven peaks are assigned. With relative integrals of 6, peaks G, F, E and C are assigned to the phenyl protons. These assignments are confirmed by the cross peaks between G and F, F and E, E and D, and D and C (Figure 4.14) seen in the 2-D spectrum. A cross peak between peaks B and A and relative integrals of 4 allow for the assignment of these peaks to the phenyl protons of the stilbene derivative. Peak H has a relative integral of 2 and is assigned to the vinylic protons of the stilbene derivative.

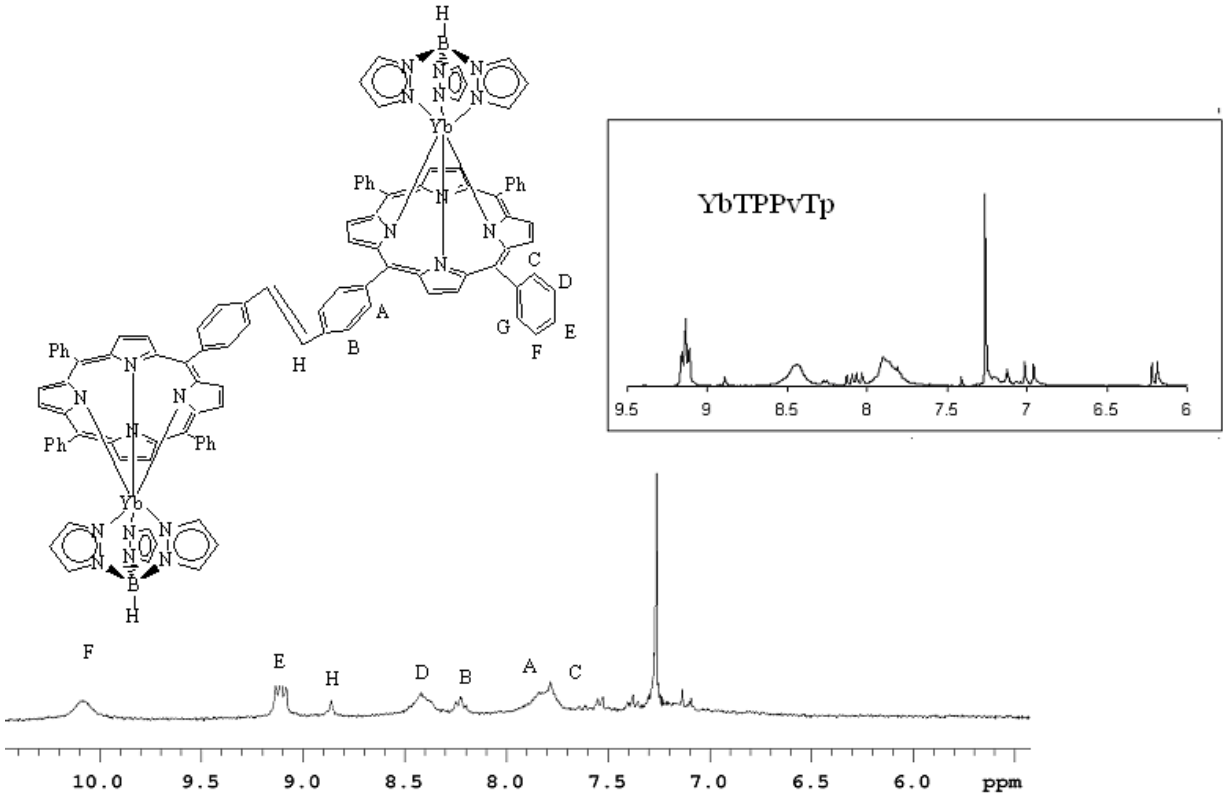

Figure 4.13: ^{1}H NMR spectrum of the phenyl region of **36** (**33** in inset).

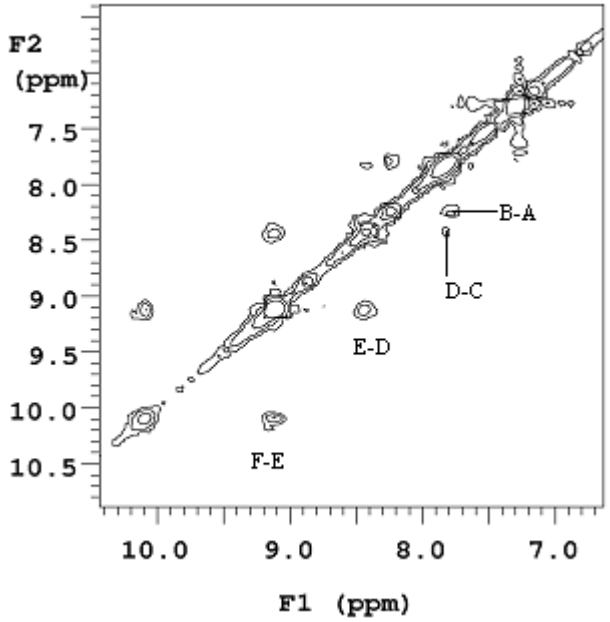

Figure 4.14: 2-D NMR spectrum of the phenyl region of **36**.

Reaction time was increased for the self metathesis reaction of **33**, however, the catalyst loading remained the same. As with the cross metathesis reaction of **30**, a low yield was obtained, perhaps due to the low catalyst loading. Due to the lack of complex **33**, optimization of the reaction could not be completed.

Polymerization

In order to incorporate the lanthanide-porphyrin complex into a polymer, YbTPPvTp was copolymerized with styrene. The copolymerization takes place *via* a free-radical chain growth mechanism in which the reaction follows the usual free radical initiated polymerization as shown in figure 4.15.

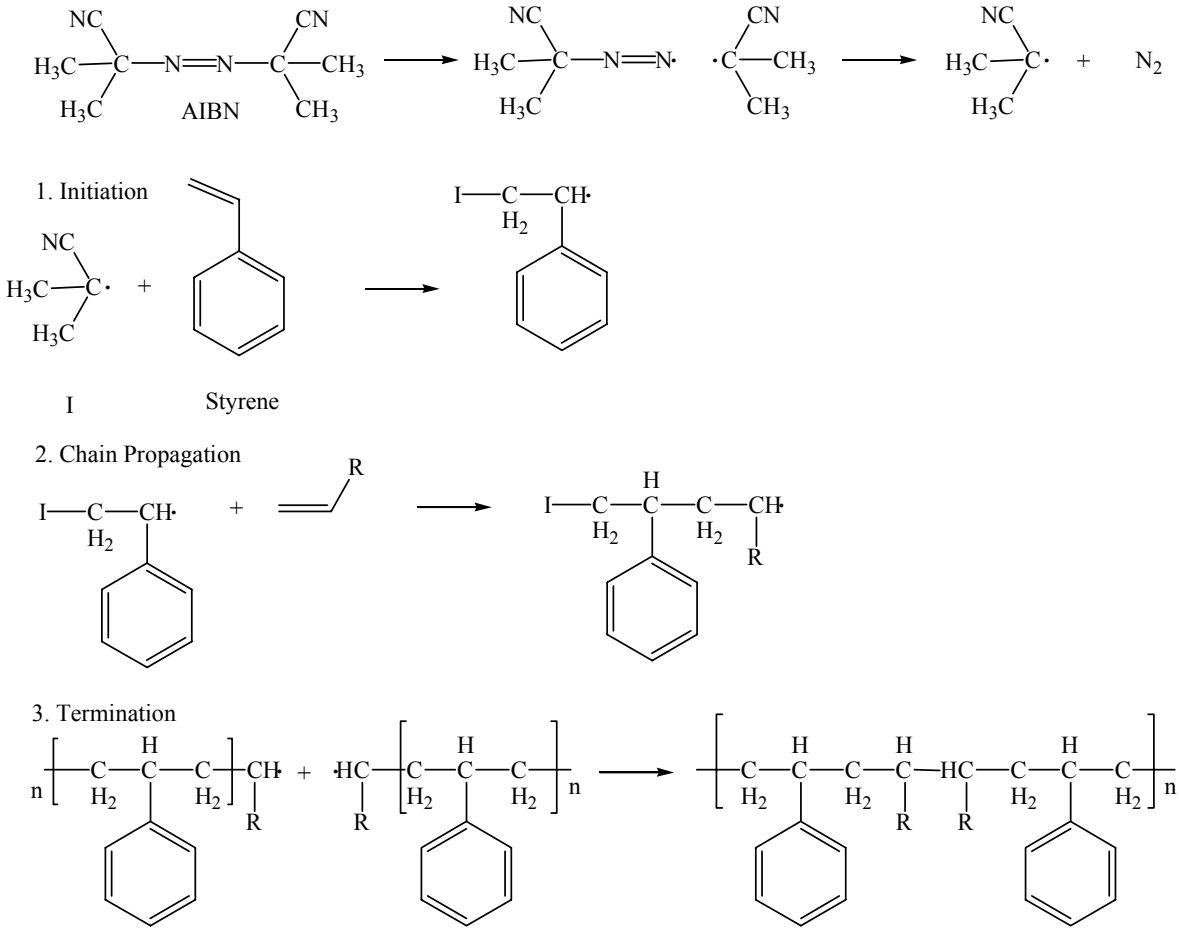

Figure 4.15: Scheme of a free radical chain growth mechanism.

Styrene and the initiator 2,2'-azobisisobutyronitrile (AIBN) were added to complex **33** with concentrations of 20, 10,and 5 mol%. The neat mixture was stirred overnight at 60 º C under N_2. After 12 hours, the purple solution turned into a solid material that was completely insoluble in most organic solvents. The solid was washed several times with THF and what was soluble in THF was analyzed by GPC and found to be monomeric species. Copolymerization reactions with styrene and the free base vinylporphyrin as well as zinc and copper complexes of the porphryin were performed by Pomogailo *et al*.[108] who showed that even when concentrations of the vinylporphyrin were ~ 0.5 mol%, THF-insoluble polymers were formed.

Studies of device construction have found that the best operating devices contained blends of lanthanide-porphyrin complex between 5 and 15 mol%.[73] In order to synthesize a soluble polymer with higher concentrations of the lanthanide-porphyrin complex, copolymerization reactions were carried out with 4-*t*-butylstyrene (*t*-BS) and 2,2,2-trifluoroethyl methacrylate (TFEM) (homopolymers containing *t*-BS are generally brittle and make a poor quality films) (Figure 4.16).[111]

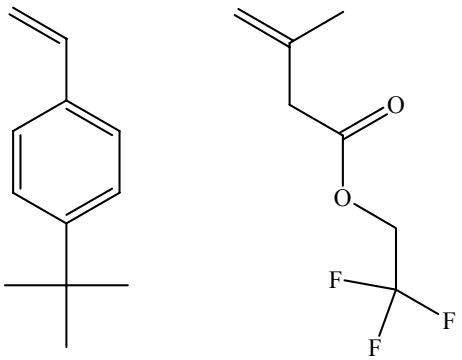

t-BS TFEM

Figure 4.16: Chemical structures of monomers.

A copolymerization reaction was carried out with equimolar amounts of *t*-BS and TFEM, 1 mol% of **33** and 0.2 mol% of the initiator AIBN in toluene (copolymerizations that were run neat produced a completely insoluble gel). After heating at 60 º C under N_2 for 20 hours, the polymer was dissolved in a small amount of CH_2Cl_2 and precipitated by addition of methanol to give a light pink powder. The polymer is soluble in most organic solvents, including CH_2Cl_2, CH_3Cl, THF and hexane. The weight average molecular weight (M_w) and the number average molecular weight (M_n) of the polymer were found to be ~ 200,000 and 90,000 with a polydispersity of 2 determined by GPC analysis. The absorption spectrum of the polymer showed the Soret band ~420nm, but the Q bands were too weak to detect. Emissions from Yb^{3+} were too weak to detect. First attempts at a polymerization reaction with 10 mol% did not yield any Ln-porphyrin containing polymer.

Tp Polymer

Polymers containing trispyrazole borate (Tp) units were synthesized by Prof. Frieder Jaekle's group, at Rutgers University, in order to incorporate LnTPP complexes into polymers (Figure 4.17).

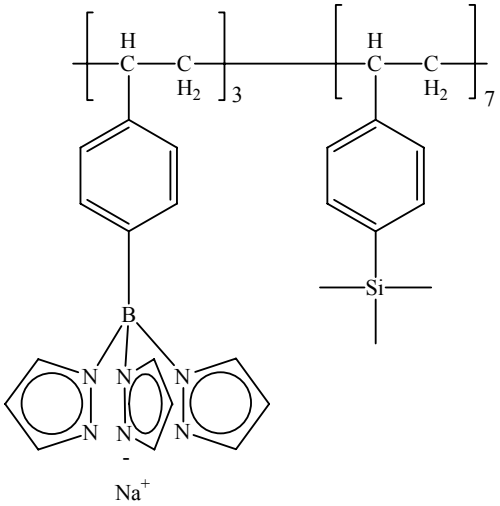

Figure 4.17: Structure of Tp polymer.

The copolymer that contained 30% Tp and a sodium counter ion was stirred with YbTPPCl(DME) in dry DMSO at 60 degrees C (Figure 4.18). After 2 days, the solution was removed *in vacuo* and the copolymer was isolated. The polymer was found to be insoluble in most organic solvents, including THF, DME, and CH_2Cl_2. The crude material was washed several times with THF and CH_2Cl_2 to remove any impurities, unreacted YbTPPCl(DME) and the by-product, KCl.

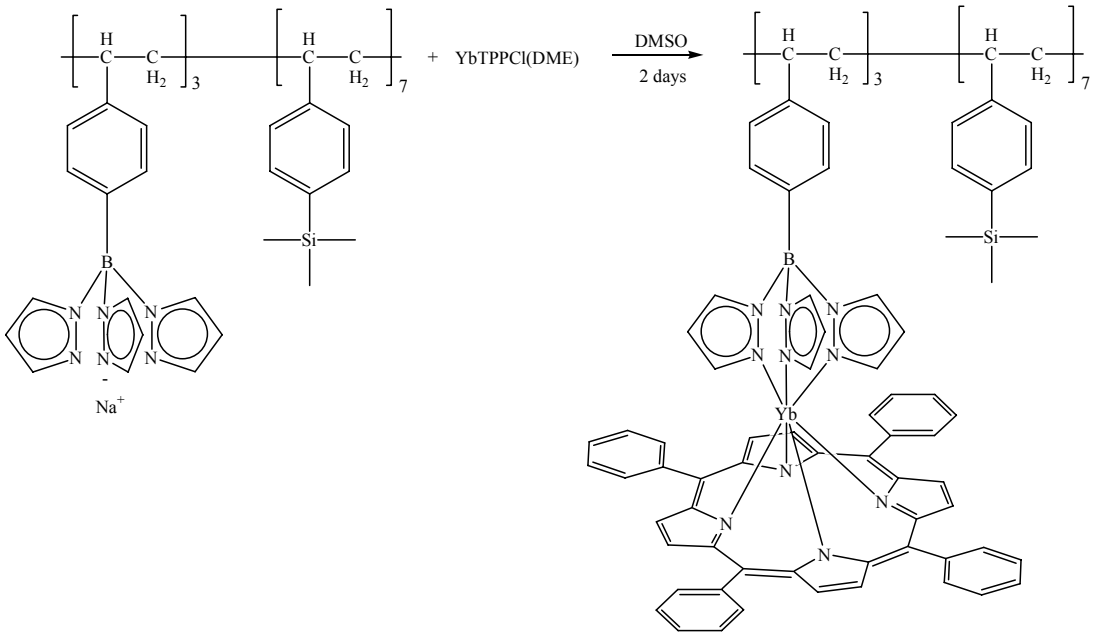

Figure 4.18: Synthesis of YbTPP-Tp (**37**) polymer.

Absorption studies performed in dichlorobenzene showed typical metallated porphyrin spectra with the Soret band ~ 423nm and three Q bands between 520 and 630nm (Figure 4.19). Emission studies showed Yb-emission ~980 nm emission of the Yb^{3+} $^2F_{5/2} \rightarrow {}^2F_{7/2}$ transition with weaker emission bands at lower wavelengths, which is attributed to the crystal field splitting of the Yb^{3+} *f*-states by the axial and porphyrin ligands (figure 4.20). Efforts to find a solvent that dissolves the polymer and is suitable for device construction are underway.

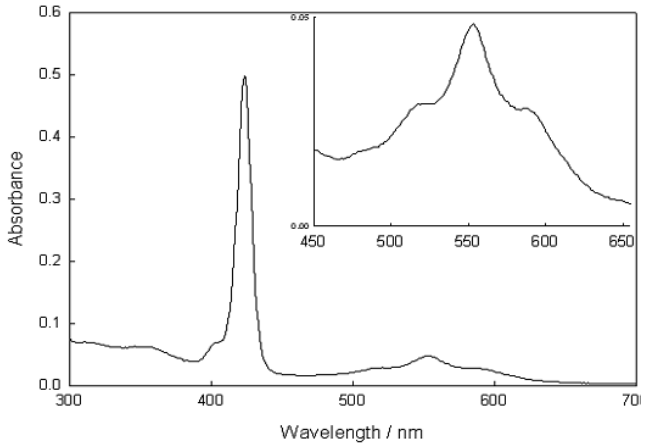

Figure 4.19: Absorption spectrum of **37** (inset shows Q bands).

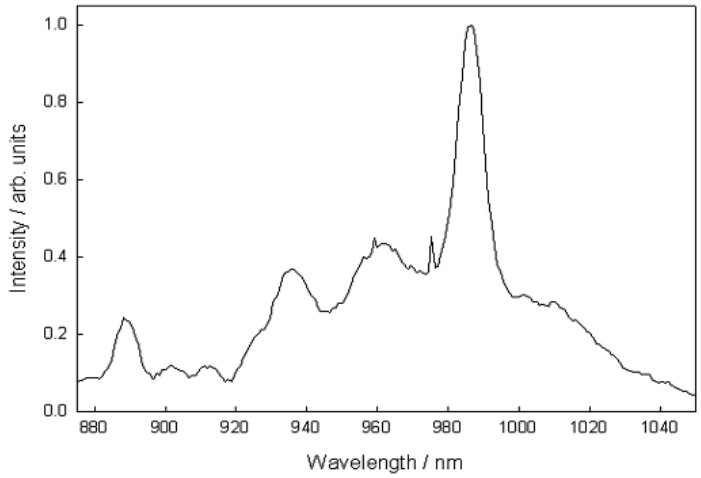

Figure 4.20: NIR emission spectrum of **37**.

Summary

An effort to incorporate a lanthanide-porphyrin complex into a polymer has led to the synthesis and characterization of new Yb-vinylporphyrin complexes. These vinylporphyrin complexes have been found to undergo a self metathesis reaction with a Ru-based Grubb's catalyst to give porphyrin and Yb-porphyrin stilbene derivatives. Attempts to copolymerize the Yb-vinylporphyrin complex with styrene produced insoluble copolymers, with loading as low as 5 mol% YbTPPvTp. Copolymerization

reactions of vinylporphyrin metal complexes with styrene or methylmethacrylate carried out by Pomogailo and coworkers produced soluble copolymers when 0.5 mol% the porphyrin monomer was used. Higher concentrations of porphyrin monomer produced insoluble polymers and as the concentration of porphyrin monomer increased, the appearance of the gel effect is increased. When the concentrations of monomers are high, the viscosity of the reaction mixture becomes high as polymer chains form. Due to the high viscosity, the diffusion of polymer chains becomes hindered and the rate of termination is decreased. Small monomers, however, can still diffuse and chains grow without terminations, producing polymers with extremely high molecular weights. Copolymerizations of YbTPPvTP and styrene were carried out neat and so concentrations of the monomers were high and perhaps producing polymers with too high of a molecular weight. Future work in the copolymerization of the lanthanide porphyrin complexes with styrene should be carried out in solution in efforts to curb the gel effect.

Copolymerization reactions of *t*BS, TFEM and YbTPPvTp were run in an effort to produce a more soluble copolymer. In toluene solution, 1 mol% of YbTPPvTp, *t*BS, TFEM and the initiator AIBN were reacted to give a soluble polymer with high molecular weight. So, changing from styrene to a more soluble *t*BS as well as running the polymerization reaction in solution afforded soluble Yb-porphyrin containing polymers. The Yb-porphyrin content in the polymer, however, was too small to detect Yb emission. The first attempt at increasing YbTPPvTP concentration in the polymer was carried out in a more dilute solution and yielded no polymers. Future work should optimize the polymerization conditions, focusing on the dilution of the solution.

The synthesis of Tp-polymers provide another means to incorporate LnTPP complexes into polymers. A salt metathesis reaction between YbTPPCl(DME) and NaTp-polymer yielded the Yb-TPP incorporated polymer. Absorption and NIR emission studies show typical LnTPP absorption and Yb-emission. The copolymer was not soluble enough in any solvents to make devices. Incorporation of a more soluble lanthanide-porphyrin complex such as Yb(TPPeoh)Cl would perhaps increase the solubility of the polymer.

Experimental

Materials and Reagents

Unless otherwise stated, all syntheses were carried out on a double manifold Schlenk line under an atmosphere of nitrogen or in a N_2 filled glovebox. Glassware was oven dried prior to use. Methylene chloride, dimethoxyethane, chloroform, DMSO and dimethlyforamide were purchased from Fisher Scientific and were dried with an appropriate drying agent.[77] Pentane, tetrahydrofuran and toluene were purchased from Aldrich Chemicals and dried by passing through a column of activated alumina. Following dehydration, all solvents were degassed and stored over 4 Å molecular sieves in resealable ampoules with fitted Teflon valves. Anhydrous dichlorobenzene was purchased from Aldrich and used as it was received. The monomers styrene and *t*-BS were purchased from Aldrich. TFEM was purchased from SynQuest Labs in Alachua, FL. All monomers were run through basic alumina prior to use. The initiator AIBN was purchased from Aldrich and recrystallized from methanol prior to use. The complexes (Cyclopentadienyl)tris(diethylphospinito)cobalt (LOEt),[78] hydridotris(1-pyrazolyl)borate (Tp^H),[79] and YbTPPCl(DME)[51] were synthesized following literature procedures. The Tp-polymer was provided by Professor Frieder Jaekle at Rutgers University. The

second-generation Grubb's catalyst was provided by Professor Ken Wagener at the University of Florida. Elemental analyses were performed at the University of California, Berkley, Micro-Mass Facility or University of Florida Spectroscopic Services. Proton NMR spectra were measured at 300 MHz at room temperature unless otherwise stated on Varian, Gemini 300, VXR 300, Mercury 300 or Bruker 300 NMR machines. Chemical shifts were referenced to residual solvent peaks and are reported relative tetramethylsilane. The spectral window was also different for each metal complex and was determined by expanding the window until peak positions remained unchanged. COSY spectra were run using the standard parameters of the instrument. All UV/VIS spectra were run in 1 cm path length quartz cuvettes in CH_3Cl unless stated otherwise. The samples were prepared and run under N_2 on a double-beam Cary-100 UV-visible spectrometer. GPC analysis was run in THF on a Dynamax GPC with the Spectroflow 757 absorbance detector set at 420 nm and calibrated to polystyrene standards.

Synthesis

TPPv (30)

Following the procedure for mixed aldehyde condensation,[107, 112] (diethylacetal)vinylphenyl (2 g, 10 mmol), pyrrole (2.8 mL, 40 mmol) and benzaldehyde (3.16 mL, 30 mmol) were condensed in *ca.* 700 mL of $CHCl_3$ in the presence of $BF_3(OEt)_2$ (0.78 mL, 6.7 mmol) at room temperature. After 1 hour, DDQ (6 g, 30 mmol) was added and solution was stirred for 5 minutes. `The solution was filtered and run through a silica column (packed with hexanes) with CH_3Cl/hexanes (3:1) as the eluant. The first purple band was collected and the solvent was removed. Recrystallization from CH_2Cl_2/ methanol (10 mL/ 30 mL) gave 0.9 g (1.4 mmol, 14% yield) of product. ^1H NMR (300 MHz, $CDCl_3$): δ8.89 (m, 8H), 8.27 (m, 8H), 7.79 (m, 12H), 7.11 (dd,

J1=10.98 Hz, J2=10.98, 1H), 6.11 (d, J=17.7 Hz, 1H), 5.52 (d, J=10.99 Hz, 1H), –2.38 (s, 2H). UV/VIS (CH_2Cl_2) λ_{max} (log ε): 422(4.55), 518(3.28), 552(2.98), 595(2.95), 662(3.18) nm. Anal. Calc. for $C_{46}H_{30}N_4$: C, 86.52; H, 4.70; N, 8.78. Found: C, 85.28; H, 4.99; N, 8.37.

Li_2TPPv(DME)$_2$ (31)

In a Schlenk flask, TPPv (0.1 g, 0.016 mmol) was added to lithium hexamethyldisilazane (0.05 g, 0.032 mmol) in *ca.* 10 mL of dry DME. The solution was refluxed under nitrogen for 12 hours, after which the color changed from red to green/blue and the product precipitated. The solution was filtered, leaving behind the product in 75% yield (0.1 g, 0.012 mmol). ^{1}H NMR (300 MHz, C_6D_6): δ9.05 (m, 8H), 8.30 (m, 8H), 7.54 (m, 12H), 6.95 (dd, J_1= 10.47 Hz, J_2= 10.47, 1H), 5.94 (d, J= 17.57 Hz, 1H), 5.32 (d, J= 10.74, 1H), 1.63 (DME, 20H). UV/VIS (CH_2Cl_2) λ_{max} (log ε): 435(5.56), 554(4.43), 603(4.44) nm.

YbTPPvCl(DME) (32)

In a Schlenk flask, Li_2TPPv(DME)$_2$ (0.1 g, 0.12 mmol) and Yb(Cl)$_3$ (0.033 g, 0.12 mmol) were added together in ca. 20 mL of toluene. The solution was refluxed under N_2 for 3 hours, during which the green/blue solution turned red. The compound was isolated by filtration and removal of the solution. Recrystallization from CH_2Cl_2 (10 mL) layered with hexane (30 mL) gave 0.09 g (80% yield, 0.096 mmol) of product. ^{1}H NMR (300 MHz, $CDCl_3$): δ44.23 ($w_{1/2}$ = 5.47 Hz, 4H, DME), 15.81 ($w_{1/2}$ = 10 Hz, 5H, H-phenyl), 14.68 ($w_{1/2}$ = 23 Hz, 8H, H-pyrrole), 10.27 ($w_{1/2}$ = 21 Hz, 5H, H-phenyl), 9.34 ($w_{1/2}$ = 17 Hz, 9H, H-phenyl), 8.25 (dd, J_1= 10.9 Hz, J_2= 10.9, 1H), 7.09(d, J= 18 Hz, 1H), 6.30 (d, J= 11 Hz, 1H), -19.74($w_{1/2}$ = 3 Hz, 6H, DME). UV/VIS (CH_2Cl_2) λ_{max} (log ε): 422(4.07),

512(2.64), 551(2.97), 590 (2.64) nm. Anal. Calc. for $C_{50}H_{40}N_4O_2ClYb$: C, 64.10; H, 4.27; N, 5.98. Found: C, 64.32; H, 4.27; N, 5.56.

YbTPPv(Tp) (33)

In DME (*ca*. 10 mL), YbTPPvCl(DME) (0.35 g, 0.38 mmol) and KTp (0.094 g, 0.35 mmol) were added together and stirred overnight at room temperature. The solvent was then removed *in vacuo* and the product was extracted with *ca.* 20 mL of CH_2Cl_2. The CH_2Cl_2 solution was reduced in volume to *ca*. 5 mL and then layered with pentane (*ca*. 10 mL). After being cooled to -10^0 C for 12 hours, the solution was filtered, leaving a purple solid. The mother liquor was reduced in volume (*ca.*10 mL) to allow more product to precipitate. The combined solids were collected giving a yield of 69% (0.25 g, 0.24 mmol). ^{1}H NMR (300 MHz, $CDCl_3$): δ22.5($w_{1/2}$ = 16 Hz, 3H, *H*-Tp), 15.60($w_{1/2}$ = 4 Hz, 4H, *o*-C_6H_5 Tpp), 13.81($w_{1/2}$ = 16 Hz, 8H, *H*-pyrrole), 10.11($w_{1/2}$ = 29 Hz, 4H, *m*-C_6H_5 Tpp), 9.13($w_{1/2}$ = 5 Hz, 4H, *p*-C_6H_5 Tpp), 8.44($w_{1/2}$ = 30 Hz, 4H, *m*-C_6H_5 Tpp), 8.07(dd, J_1= 11 Hz, J_2= 11 Hz 1H, *H*-vinyl) 7.86($w_{1/2}$ = 15 Hz, 4H, *o*-C_6H_5 Tpp), 7.01(d, J=17 Hz, 1H, *H*-vinyl), 6.18(d, J=11 Hz, 1H, *H*-vinyl), 4.89($w_{1/2}$ = 8 Hz, 3H, *H*-Tp), -2.68($w_{1/2}$ = 15 Hz, 3H, *H*-Tp). UV/VIS (CH_2Cl_2) λ_{max} (log ε): 423(5.07), 513(3.56), 552(3.92), 589(3.55) nm. Anal. Calc. for $C_{55}H_{40}N_{10}BYb$: C, 64.46; H, 3.91; N, 13.61. Found: C, 64.25; H,3.88; N,13.53.

YbTPPv(LOEt) (34)

Using a procedure similar to that used for the preparation of **33**, **34** was synthesized by stirring YbTPPvCl(DME) (0.2 g, 0.2 mmol) and K(LOEt) (0.1 g, 0.2 mmol) together in DME (*ca*. 10 mL) at room temperature. After 12 hours of stirring, the purple solution was removed *in vacuo* and the product was extracted with *ca.* 20 mL of CH_2Cl_2, leaving behind a residue of KCl. The CH_2Cl_2 solution was reduced in volume (*ca.* 5 mL) and

layered with pentane (10 mL) to precipitate the product in 60% yield (0.16 g, 0.12 mm0l). ^{1}H NMR (300 MHz, C_6D_6 10 degrees C): δ17.14 ($w_{1/2}$ = 22 Hz, 4H, *o*-C_6H_5 Tpp), 15.56 ($w_{1/2}$ = 8 Hz, 8H, *H*-pyrrole), 10.48 ($w_{1/2}$ = 20 Hz, 4H, *m*-C_6H_5 Tpp), 9,18($w_{1/2}$ = 4 Hz, 3H, *p*-C_6H_5 Tpp), 8.74($w_{1/2}$ = 13 Hz, 4H, *m*-C_6H_5 Tpp), 8.53($w_{1/2}$ = 22 Hz, 4H, *o*-C_6H_5 Tpp), 8.19($w_{1/2}$ = 29 Hz, 6H, OC*H*$_2$CH$_3$) 8.07 ($w_{1/2}$ = 6 Hz 1H, *H*-vinyl) 7.39($w_{1/2}$ = 3 Hz, 6H, OC*H*$_2$CH$_3$), 7.01(d, J=17 Hz, 1H, *H*-vinyl), 6.14(d, J=11 Hz, 1H, *H*-vinyl), 2.85($w_{1/2}$ = 10 Hz, 18H, OCH$_2$C*H*$_3$), -4.83($w_{1/2}$ = 4 Hz, 5H, *H*-Cp). UV/VIS (CH_2Cl_2) λ_{max} (log ε): 425(4.58), 514(3.12), 557(3.46), 596(3.12) nm.

TPP-TPP (35)

In a Sclenk flask, TPPv (0.168g, 0.26mmol) and 10 mol % of second-generation Grubb's catalyst were added together in *ca*. 3 mL of CH_2Cl_2. The flask was fitted with a reflux condenser and the solution was stirred at reflux under nitrogen for one hour. The solution was removed *in vacuo* and the product was washed with diethyl ether (3 x 10 mL). The product was recrystallized from CH_2Cl_2 layered with pentane to give the stilbene derivative in 32% yield (0.1 g, 0.07 mmol). ^{1}H NMR (300 MHz, $CDCl_3$): δ8.99(m, 16H), 8.22(m, 16H), 8.08(d, 2H), 7.79(m, 24H), -2.69(s, 2H), -2.75(s, 2H). UV/VIS (CH_2Cl_2) λ_{max} (log ε): 416(5.30), 514(4.25), 550(4.01), 588(3.84), 644(3.81) nm. Anal. Calc. for $C_{90}H_{60}N_8$: C, 86.24; H, 4.82; N, 8.94. Found: C, 82.47; H, 4.78; N, 8.18.

YbTPPTp-YbTPPTp (36)

In a Sclenk flask, YbTPPvTp (0.02g, 0. 02mmol) and 10 mol % of second-generation Grubb's catalyst were added together in *ca*. 3 mL of CH_2Cl_2. The flask was fitted with a reflux condenser and the solution was stirred at reflux under nitrogen for 12 hours. The solution was removed *in vacuo* and the product was washed with diethyl

ether (3 x 10 mL). The product was recrystallized from CH_2Cl_2 layered with pentane to give **36** in 24% yield (0.01 g, 0.005 mmol). ^{1}H NMR (300 MHz, $CDCl_3$): δ22.6($w_{1/2}$ = 8 Hz, 6H, *H*-Tp), 15.5($w_{1/2}$ = 24 Hz, 6H, *o*-C_6H_5 Tpp), 13.81($w_{1/2}$ = 16 Hz, 16H, *H*-pyrrole), 10.11($w_{1/2}$ = 30 Hz, 6H, *m*-C_6H_5 Tpp), 9.13($w_{1/2}$ = 5 Hz, 6H, *p*-C_6H_5 Tpp), 8.86($w_{1/2}$ = 15 Hz, 4H, *H*-vinyl), 8.42($w_{1/2}$ = 30 Hz, 6H, *m*-C_6H_5 Tpp), 8.20($w_{1/2}$ = 15, 4H, *H*-stilbene derivative), 7.78($w_{1/2}$ = 15 Hz, 10H, *o*-C_6H_5 Tpp, *H*-stilbene), 4.89($w_{1/2}$ = 8 Hz, 6H, *H*-Tp), -2.84($w_{1/2}$ = 15 Hz, 6H, *H*-Tp). UV/VIS (CH_2Cl_2) λ_{max} (log ε): 421(5.32), 513(3.88), 550(4.31), 590(3.88) nm.

YbTPP-Tp polymer (37)

In a Schlenk flask in the glove box, YbTPPCl(DME) (0.06 g, 0.07mmol) was added to a solution of the 30% NaTp-polymer (0.07 g) in d_6-DMSO (10 mL). The solution was stirred at room temperature for 12 hours. ^{1}H NMR revealed no change to the polymer spectrum. The solution was heated to 60 degrees C for 12 hours. The solution was then removed *in vacuo* and a pink and white solid were present in the flask. The crude material was washed with CH_2Cl_2, DME and THF, leaving behind the pink product, which is insoluble in most organic solvents. UV/VIS and emission studies were carried out in dichlorobenzene.

Copolymerizations

All polymerizations were performed in a Schlenk flask stoppered with a septum under an atmosphere of N_2. YbTPPvTp (0.04 g, 0.03 mmol, 1 mol%) was introduced to the flask and the monomers, *t*-BS (0.35 mL, 1.9 mmol) and TFEM (0.27mL, 1.9 mmol) were dissolved in toluene (2 x monomer volume) and added to the YbTPPvTp complex. The initiator, AIBN (0.0012g, 0.0076 mmol, 0.2 mol% of AIBN relative to the total mass of monomers) was then added to the stirring toluene solution of YbTPPvTP and the

monomers. The solution was heated to 60 degrees C for 48 hours. The solution was removed and CH_2Cl_2 (1 mL) was added to the crude material. Methanol was added to the solution until the polymer precipitated. GPC analysis (in THF, polystyrene standards): M_w: 200,000, M_n: 90,000 with a polydispersity of 2.

CHAPTER 5
CONCLUSIONS

In conclsuion, novel lanthanide-porphyrin complexes have been synthesized and characterized for emitting materials in NIR LEDs. Through a simple salt metathesis reaction with the corresponding lanthanide trihalides and dilithio-porphyrin complexes, LnPorphyrin(X)(DME) complexes were cleanly isolated in good yields. From this starting material, the lanthanide compounds were easily complexed with a number of ancillary ligands including Tp, LOEt and quinolate. Through these synthetic procedures, lanthanide-porphyrin complexes with a variety of capping ligands and porphyrin-phenyl ring substituents were easily synthesized and isolated in yields ranging from 30% to 75%. These compounds have been fully characterized through crystallographic methods, proton and COSY NMR studies, UV/Vis spectroscopy and elemental analysis.

PL studies of the complexes found that NdTPP(Tp) and NdTPP(LOEt) complexes produced NIR emission around 900 nm, 1069 nm and 1300 nm with quantum efficiencies around 2.4%. The Yb(porphyrin)L complexes produced NIR emission around ~980 and ~1020 nm with quantum efficiencies as high as 4.1%. Emission spectra are easily tuned by changing the lanthanide ion in the porphyrin complex. There is little change, however, in PL efficiency when the capping ligands or porphyrin-phenyl ring substituents are varied. These lanthanide-porphyrin complexes have higher NIR quantum yields than other reported lanthanide complexes, perhaps due to the effective sensitization of the porphyrin chromophore and the effective shielding of the capping ligand. New LnPc monomeric complexes were synthesized and fully characterized, but produced no NIR

emission because the triplet state of Pc (1050 nm) is too low in energy to sensitize Nd-, Pr-, Ho-, Tm- and YbPc(LOEt) complexes. When the capping ligand is not sterically encumbering enough to hinder solvent coordination, in the instance of YbTPPQ(THF), the solvent molecule facilitates nonradiative decay and lowers quantum efficiency. Future efforts to improve PL quantum efficiency should perhaps focus on designing Ln(porphyrin)L complexes with fewer C-H and O-H molecules in close proximity to the lanthanide ion.

EL studies carried out with blends of Ln(porphyrin)L and PS show that these complexes act as the charge carrier as well as the emitting species. Devices produced NIR emission with external quantum efficiencies around ~1–3 x 10^{-4} (with exception to YbTPPQTHF which was 2 x 10^{-5}). There is no change in emission or device efficiency when the capping ligands or porphyrin-phenyl ring substituents are varied, perhaps because the factors involved in device construction outweigh any differences that arise from the identity of the porphyrin substituents. Studies on devices blended with AlQ_3, produce NIR emission with quantum efficiencies ten times higher than devices without AlQ_3, suggesting that LnTPP(L) is more efficient in the transport of holes than electrons therefore, creating a charge imbalance and lowering of device efficiencies. Improvement of device efficiencies could then perhaps be obtained by incorporating an electron transport layer.

An effort to incorporate a lanthanide-porphyrin complex into a polymer has led to the synthesis and characterization of new Yb-vinylporphyrin complexes. Attempts to copolymerize the Yb-vinylporphyrin complex with styrene produced insoluble copolymers, with loading as low as 5 mol% YbTPPvTp. Copolymerization reactions of

vinylporphyrin metal complexes with styrene or methylmethacrylate carried out by Pomogailo and coworkers produced soluble copolymers when 0.5 mol% the porphyrin monomer was used. Higher concentrations of porphyrin monomer produced insoluble polymers and as the concentration of porphyrin monomer increased, the appearance of the gel effect is increased. When the concentrations of monomers are high, the viscosity of the reaction mixture becomes high as polymer chains form. Due to the high viscosity, the diffusion of polymer chains becomes hindered and the rate of termination is decreased. Small monomers, however, can still diffuse and chains grow without terminations, producing polymers with extremely high molecular weights. Copolymerizations of YbTPPvTP and styrene were carried out neat and so concentrations of the monomers were high and perhaps producing polymers with too high of a molecular weight. Future work in the copolymerization of the lanthanide porphyrin complexes with styrene should be carried out in solution in efforts to curb the gel effect.

Copolymerization reactions of *t*BS, TFEM and YbTPPvTp were run in an effort to produce a more soluble copolymer. In toluene solution, 1mol% of YbTPPvTp, *t*BS, TFEM and the initiator AIBN were reacted to give a soluble polymer with M_w and M_n around ~ 200,000 and 90,000, respectively. The Yb-porphyrin content in the polymer, however, was too small to detect Yb emission. The first attempt at increasing YbTPPvTP concentration in the polymer was carried out in a more dilute solution and yielded no polymers. Future work should optimize the polymerization conditions, focusing on the dilution of the solution.

The synthesis of Tp-polymers provide another means to incorporate LnTPP complexes into polymers. Absorption studies performed in dichlorobenzene showed

typical metallated porphyrin spectra with the Soret band ~ 423nm and three Q bands between 520 and 630nm and NIR emission studies showed Yb-emission at ~980 nm emission. The copolymer was not soluble enough in any solvents to make devices. Incorporation of a more soluble lanthanide-porphyrin complex such as Yb(TPPeoh)Cl would perhaps increase the solubility of the polymer.

APPENDIX
CRYSTALLOGRAPHIC INFORMATION

Information for the crystal structure of **3**

Table 1. Crystal data and structure refinement for **3**.

Identification code	ak02	
Empirical formula	C56 H52 I N4 Nd O3	
Formula weight	1100.16	
Temperature	173(2) K	
Wavelength	0.71073 Å	
Crystal system	Triclinic	
Space group	P-1	
Unit cell dimensions	a = 12.4470(11) Å	□= 69.585(2)°.
	b = 14.5765(13) Å	□= 74.880(2)°.
	c = 14.6837(13) Å	□ = 89.225(2)°.
Volume	2401.5(4) $Å^3$	
Z	2	
Density (calculated)	1.521 Mg/m^3	
Absorption coefficient	1.772 mm^{-1}	
F(000)	1106	
Crystal size	0.24 x 0.08 x 0.05 mm^3	
Theta range for data collection	1.54 to 27.50°.	
Index ranges	-16≤h≤15, -18≤k≤18, -18≤l≤19	
Reflections collected	21110	
Independent reflections	10631 [R(int) = 0.0462]	
Completeness to theta = 27.50°	96.5 %	
Absorption correction	Integration	
Max. and min. transmission	0.9243 and 0.7470	
Refinement method	Full-matrix least-squares on F^2	
Data / restraints / parameters	10631 / 0 / 548	
Goodness-of-fit on F^2	0.964	

Final R indices [I>2sigma(I)]	R1 = 0.0406, wR2 = 0.1031 [7861]
R indices (all data)	R1 = 0.0562, wR2 = 0.1075
Extinction coefficient	0.0061(4)
Largest diff. peak and hole	1.162 and -0.790 e.Å^{-3}

$R1 = \sum(||F_o| - |F_c||) / \sum|F_o|$

$wR2 = [\sum[w(F_o^2 - F_c^2)^2] / \sum[wF_o^{22}]]^{1/2}$

$S = [\sum[w(F_o^2 - F_c^2)^2] / (n-p)]^{1/2}$

$w= 1/[\sigma^2(F_o^2)+(m*p)^2+n*p]$, $p = [\max(F_o^2,0)+ 2* F_c^2]/3$, m & n are constants.

Table 2. Atomic coordinates (x 10^4) and equivalent isotropic displacement parameters (Å^{2}x 10^3) for **3** U(eq) is defined as one third of the trace of the orthogonalized U^{ij} tensor.

	x	y	z	U(eq)
Nd1	6901(1)	2213(1)	714(1)	19(1)
I1	5044(1)	492(1)	2158(1)	40(1)
I2	5127(11)	3785(10)	222(10)	99(4)
O1	5556(3)	2458(3)	-392(2)	34(1)
O2	5553(3)	3180(2)	1583(2)	34(1)
N1	7881(3)	2447(2)	1869(3)	21(1)
N2	8030(3)	841(2)	1069(3)	19(1)
N3	8047(3)	2222(2)	-913(3)	19(1)
N4	7936(3)	3838(2)	-134(2)	20(1)
C1	8078(4)	3309(3)	2011(3)	22(1)
C2	8370(4)	3076(3)	2955(3)	26(1)
C3	8349(4)	2100(3)	3362(3)	28(1)
C4	8062(3)	1691(3)	2679(3)	22(1)
C5	8063(3)	694(3)	2800(3)	21(1)
C6	8045(3)	306(3)	2048(3)	20(1)
C7	8074(4)	-715(3)	2185(3)	24(1)
C8	8109(4)	-800(3)	1285(3)	26(1)
C9	8105(3)	185(3)	578(3)	22(1)
C10	8258(3)	439(3)	-470(3)	21(1)
C11	8310(3)	1411(3)	-1161(3)	21(1)

C12	8663(4)	1694(3)	-2251(3)	27(1)
C13	8624(4)	2681(3)	-2638(3)	29(1)
C14	8233(3)	3019(3)	-1810(3)	22(1)
C15	8159(3)	4005(3)	-1908(3)	23(1)
C16	8012(4)	4377(3)	-1126(3)	23(1)
C17	8028(4)	5411(3)	-1266(3)	28(1)
C18	8003(4)	5488(3)	-384(3)	29(1)
C19	7975(4)	4505(3)	340(3)	23(1)
C20	8060(4)	4269(3)	1330(3)	23(1)
C21	8197(4)	5085(3)	1688(3)	25(1)
C22	9112(4)	5796(3)	1171(3)	29(1)
C23	9246(5)	6575(3)	1498(4)	36(1)
C24	8476(5)	6633(4)	2341(4)	41(1)
C25	7572(5)	5935(4)	2862(4)	41(1)
C26	7438(4)	5158(3)	2527(4)	31(1)
C27	8235(4)	-5(3)	3757(3)	25(1)
C28	7394(5)	-290(4)	4639(4)	43(1)
C29	7581(6)	-948(5)	5536(4)	59(2)
C30	8601(6)	-1307(4)	5533(4)	53(2)
C31	9460(6)	-1016(4)	4659(4)	54(2)
C32	9261(5)	-370(4)	3778(4)	38(1)
C33	8429(3)	-365(3)	-895(3)	22(1)
C34	9265(3)	-1003(3)	-720(3)	24(1)
C35	9408(4)	-1747(3)	-1097(3)	29(1)
C36	8747(4)	-1876(3)	-1674(4)	34(1)
C37	7914(4)	-1240(4)	-1861(4)	34(1)
C38	7753(4)	-501(3)	-1468(3)	29(1)
C39	8396(4)	4742(3)	-2966(3)	25(1)
C40	7636(4)	4820(4)	-3540(4)	35(1)
C41	7874(5)	5517(4)	-4520(4)	47(2)
C42	8844(5)	6111(4)	-4933(4)	48(1)
C43	9600(6)	6015(4)	-4391(4)	53(2)
C44	9375(5)	5336(4)	-3405(4)	40(1)
C45	5580(5)	1812(5)	-964(5)	55(2)
C46	4419(6)	1646(7)	-973(7)	86(3)
C47	3862(5)	2523(5)	-855(5)	58(2)

C48	4438(4)	2795(4)	-188(4)	39(1)
C49	5132(5)	4114(4)	1135(4)	42(1)
C50	4795(5)	4541(4)	1944(4)	50(2)
C51	4386(5)	3643(5)	2894(5)	57(2)
C52	5181(5)	2898(4)	2685(4)	42(1)

Information for the crystal structure of **7**

Table 1. Crystal data and structure refinement for sk01.

Identification code	sk01	
Empirical formula	C108.50 H82 B2 N20 Nd2	
Formula weight	1976.04	
Temperature	193(2) K	
Wavelength	0.71073 Å	
Crystal system	Triclinic	
Space group	P-1	
Unit cell dimensions	a = 12.6145(5) Å	□= 84.067(2)°.
	b = 13.7314(6) Å	□= 78.022(2)°.
	c = 27.843(2) Å	□ = 74.461(2)°.
Volume	4539.5(3) $Å^3$	
Z	2	
Density (calculated)	1.446 Mg/m^3	
Absorption coefficient	1.194 mm^{-1}	
F(000)	2006	
Crystal size	0.17 x 0.05 x 0.05 mm^3	
Theta range for data collection	1.71 to 27.50°.	
Index ranges	-16≤h≤16, -17≤k≤17, -36≤l≤35	
Reflections collected	40834	
Independent reflections	20287 [R(int) = 0.0548]	
Completeness to theta = 27.50°	97.2 %	
Absorption correction	Analuy	
Max. and min. transmission	0.9471 and 0.8203	
Refinement method	Full-matrix least-squares on F^2	
Data / restraints / parameters	20287 / 0 / 1208	
Goodness-of-fit on F^2	0.840	
Final R indices [I>2sigma(I)]	R1 = 0.0369, wR2 = 0.0642 [12451]	

R indices (all data)	R1 = 0.0756, wR2 = 0.0697
Extinction coefficient	0.00003(3)
Largest diff. peak and hole	0.584 and -0.836 e.Å^{-3}

$R1 = \sum(||F_o| - |F_c||) / \sum|F_o|$

$wR2 = [\sum[w(F_o^2 - F_c^2)^2] / \sum[wF_o^{22}]]^{1/2}$

$S = [\sum[w(F_o^2 - F_c^2)^2] / (n-p)]^{1/2}$

$w= 1/[\sigma^2(F_o^2)+(0.0176*p)^2+0.00*p]$, $p = [\max(F_o^2,0)+ 2* F_c^2]/3$

Table 2. Atomic coordinates (x 10^4) and equivalent isotropic displacement parameters (Å^{2}x 10^3) for **7**. U(eq) is defined as one third of the trace of the orthogonalized U^{ij} tensor.

	x	y	z	U(eq)
Nd	5271(1)	7773(1)	8574(1)	20(1)
B	4016(4)	8029(3)	7456(2)	31(1)
N1	7263(2)	7536(2)	8574(1)	22(1)
N2	5873(2)	6127(2)	8983(1)	22(1)
N3	4071(2)	7789(2)	9376(1)	20(1)
N4	5440(2)	9210(2)	8986(1)	21(1)
N5	5444(3)	6661(2)	7850(1)	34(1)
N6	4773(2)	6958(2)	7505(1)	30(1)
N7	3268(2)	8125(2)	8375(1)	30(1)
N8	3065(2)	8235(2)	7911(1)	28(1)
N9	5248(2)	8939(2)	7774(1)	27(1)
N10	4716(2)	8820(2)	7408(1)	26(1)
C1	7804(3)	8303(3)	8468(1)	23(1)
C2	8995(3)	7854(3)	8335(1)	29(1)
C3	9162(3)	6844(3)	8391(1)	29(1)
C4	8077(3)	6637(3)	8536(1)	23(1)
C5	7904(3)	5660(3)	8647(1)	23(1)
C6	6868(3)	5429(3)	8836(1)	23(1)
C7	6696(3)	4421(3)	8908(1)	29(1)
C8	5597(3)	4514(3)	9092(1)	29(1)

C9	5090(3)	5580(2)	9160(1)	22(1)
C10	4008(3)	5998(3)	9417(1)	22(1)
C11	3597(3)	7002(2)	9562(1)	20(1)
C12	2642(3)	7353(3)	9936(1)	26(1)
C13	2529(3)	8347(3)	9974(1)	27(1)
C14	3424(3)	8628(3)	9615(1)	23(1)
C15	3576(3)	9620(3)	9534(1)	21(1)
C16	4530(3)	9876(3)	9246(1)	23(1)
C17	4734(3)	10870(3)	9200(1)	25(1)
C18	5768(3)	10789(3)	8919(1)	27(1)
C19	6227(3)	9751(3)	8793(1)	22(1)
C20	7319(3)	9336(3)	8539(1)	22(1)
C21	8917(3)	4784(3)	8591(1)	26(1)
C22	9572(3)	4539(3)	8136(2)	42(1)
C23	10500(4)	3739(4)	8091(2)	63(2)
C24	10787(4)	3185(3)	8500(2)	62(2)
C25	10168(4)	3410(3)	8956(2)	52(1)
C26	9228(3)	4221(3)	9005(2)	36(1)
C27	3211(3)	5328(3)	9575(1)	24(1)
C28	3454(3)	4469(3)	9881(1)	31(1)
C29	2708(3)	3875(3)	10020(1)	39(1)
C30	1713(3)	4133(3)	9848(2)	47(1)
C31	1451(3)	4995(3)	9544(2)	42(1)
C32	2201(3)	5587(3)	9411(1)	31(1)
C33	2620(3)	10431(3)	9768(1)	25(1)
C34	1581(3)	10579(3)	9640(2)	38(1)
C35	649(3)	11250(3)	9888(2)	53(1)
C36	740(4)	11787(3)	10258(2)	48(1)
C37	1775(4)	11671(3)	10376(1)	38(1)
C38	2709(3)	10993(2)	10135(1)	28(1)
C39	8072(3)	10031(2)	8374(1)	24(1)
C40	8563(3)	10128(3)	7886(1)	30(1)
C41	9294(3)	10743(3)	7730(2)	37(1)
C42	9510(3)	11299(3)	8064(2)	43(1)
C43	9038(3)	11219(3)	8551(2)	44(1)
C44	8328(3)	10578(3)	8708(1)	35(1)

C45	5983(3)	5700(3)	7770(2)	42(1)
C46	5668(4)	5357(3)	7383(2)	47(1)
C47	4899(4)	6172(3)	7232(2)	42(1)
C48	2260(3)	8408(3)	8672(2)	32(1)
C49	1418(3)	8720(3)	8399(2)	35(1)
C50	1962(3)	8592(3)	7923(2)	36(1)
C51	5708(3)	9713(3)	7611(1)	29(1)
C52	5486(3)	10089(3)	7151(1)	33(1)
C53	4850(3)	9507(3)	7030(1)	31(1)
Nd'	13538(1)	3349(1)	6665(1)	22(1)
B'	14135(4)	2960(3)	7931(2)	28(1)
N1'	13750(2)	1883(2)	6172(1)	22(1)
N2'	14947(2)	3507(2)	5941(1)	25(1)
N3'	12875(2)	5037(2)	6288(1)	26(1)
N4'	11682(2)	3432(2)	6498(1)	25(1)
N5'	15324(2)	2895(2)	7072(1)	30(1)
N6'	15255(2)	2802(2)	7567(1)	30(1)
N7'	13066(2)	4427(2)	7428(1)	29(1)
N8'	13406(2)	4046(2)	7862(1)	28(1)
N9'	13090(2)	2175(2)	7441(1)	26(1)
N10'	13519(2)	2170(2)	7852(1)	25(1)
C1'	12963(3)	1352(2)	6169(1)	21(1)
C2'	13508(3)	455(2)	5889(1)	24(1)
C3'	14584(3)	476(2)	5722(1)	24(1)
C4'	14733(3)	1371(2)	5897(1)	21(1)
C5'	15735(3)	1703(3)	5754(1)	25(1)
C6'	15819(3)	2702(3)	5775(1)	26(1)
C7'	16815(3)	3054(3)	5592(1)	36(1)
C8'	16529(3)	4060(3)	5631(1)	38(1)
C9'	15351(3)	4362(3)	5835(1)	29(1)
C10'	14701(3)	5373(3)	5875(1)	29(1)
C11'	13544(3)	5669(3)	6058(1)	29(1)
C12'	12838(3)	6676(3)	6014(2)	38(1)
C13'	11778(3)	6645(3)	6200(1)	35(1)
C14'	11795(3)	5614(3)	6372(1)	28(1)
C15'	10834(3)	5265(3)	6577(1)	26(1)

C16'	10798(3)	4248(3)	6647(1)	26(1)
C17'	9806(3)	3896(3)	6840(1)	31(1)
C18'	10083(3)	2891(3)	6787(1)	31(1)
C19'	11243(3)	2605(3)	6552(1)	24(1)
C20'	11821(3)	1642(3)	6383(1)	22(1)
C21'	16741(3)	937(3)	5521(1)	27(1)
C22'	17304(3)	1112(3)	5050(2)	40(1)
C23'	18244(3)	404(4)	4839(2)	50(1)
C24'	18633(3)	-482(4)	5092(2)	50(1)
C25'	18080(3)	-680(3)	5560(2)	44(1)
C26'	17146(3)	29(3)	5774(1)	32(1)
C27'	15273(3)	6186(3)	5657(1)	30(1)
C28'	15253(3)	6986(3)	5931(2)	39(1)
C29'	15803(3)	7725(3)	5719(2)	45(1)
C30'	16357(4)	7680(3)	5246(2)	49(1)
C31'	16379(3)	6907(3)	4967(2)	48(1)
C32'	15821(3)	6167(3)	5172(1)	40(1)
C33'	9736(3)	6046(3)	6692(1)	30(1)
C34'	9523(3)	6702(3)	7058(1)	35(1)
C35'	8473(3)	7398(3)	7164(2)	43(1)
C36'	7667(3)	7449(3)	6901(2)	50(1)
C37'	7870(4)	6799(3)	6529(2)	61(1)
C38'	8897(3)	6094(3)	6423(2)	49(1)
C39'	11152(3)	875(3)	6407(1)	24(1)
C40'	11491(3)	-88(3)	6626(1)	30(1)
C41'	10855(3)	-780(3)	6659(1)	39(1)
C42'	9882(3)	-540(3)	6481(2)	43(1)
C43'	9541(3)	416(3)	6256(2)	42(1)
C44'	10177(3)	1108(3)	6217(1)	32(1)
C45'	16415(3)	2701(3)	6876(2)	42(1)
C46'	17047(3)	2478(4)	7241(2)	63(2)
C47'	16285(3)	2552(3)	7675(2)	50(1)
C48'	12497(3)	5392(3)	7511(2)	33(1)
C49'	12480(3)	5629(3)	7979(2)	39(1)
C50'	13063(3)	4761(3)	8192(2)	38(1)
C51'	12624(3)	1388(3)	7513(1)	28(1)

C52'	12752(3)	883(3)	7963(1)	29(1)
C53'	13332(3)	1393(3)	8166(1)	29(1)
C90	10320(9)	6735(9)	5103(4)	89(4)
C91	9865(7)	6354(6)	4726(3)	153(3)
C92	9489(6)	5325(6)	4912(3)	164(4)

Information for the crystal structure of **13**

Table 1. Crystal data and structure refinement for **13**

Identification code	ak07	
Empirical formula	C66 H62 N5 O2 Yb	
Formula weight	1130.25	
Temperature	173(2) K	
Wavelength	0.71073 Å	
Crystal system	Triclinic	
Space group	P-1	
Unit cell dimensions	a = 12.339(2) Å	□= 78.046(2)°.
	b = 14.745(2) Å	□= 88.104(3)°.
	c = 15.857(3) Å	□ = 80.710(3)°.
Volume	2785.4(8) $Å^3$	
Z	2	
Density (calculated)	1.348 Mg/m^3	
Absorption coefficient	1.728 mm^{-1}	
F(000)	1158	
Crystal size	0.27 x 0.13 x 0.08 mm^3	
Theta range for data collection	1.31 to 27.50°.	
Index ranges	-16≤h≤15, -18≤k≤19, -20≤l≤20	
Reflections collected	24756	
Independent reflections	12365 [R(int) = 0.0372]	
Completeness to theta = 27.50°	96.8 %	
Absorption correction	Integration	
Max. and min. transmission	0.8860 and 0.6757	
Refinement method	Full-matrix least-squares on F^2	
Data / restraints / parameters	12365 / 0 / 585	
Goodness-of-fit on F^2	0.950	
Final R indices [I>2sigma(I)]	R1 = 0.0398, wR2 = 0.0920 [9866]	
R indices (all data)	R1 = 0.0502, wR2 = 0.0943	

Largest diff. peak and hole 3.632 and -0.908 e.Å^{-3}

$R1 = \sum(||F_o| - |F_c||) / \sum|F_o|$

$wR2 = [\sum[w(F_o^2 - F_c^2)^2] / \sum[wF_o^{22}]]^{1/2}$

$S = [\sum[w(F_o^2 - F_c^2)^2] / (n-p)]^{1/2}$

$w= 1/[\sigma^2(F_o^2)+(m*p)^2+n*p]$, $p = [\max(F_o^2,0)+ 2* F_c^2]/3$, m & n are constants.

Table 2. Atomic coordinates (x 10^4) and equivalent isotropic displacement parameters (Å^{2}x 10^3) for **13**. U(eq) is defined as one third of the trace of the orthogonalized U^{ij} tensor.

	x	y	z	U(eq)
Yb1	3251(1)	3110(1)	3381(1)	34(1)
O1	2603(2)	4461(2)	2571(2)	42(1)
O2	1534(3)	2684(2)	3074(2)	60(1)
N1	4344(3)	1640(2)	3533(2)	40(1)
N2	2686(2)	2293(2)	4710(2)	34(1)
N3	3338(2)	4136(2)	4308(2)	32(1)
N4	4998(2)	3490(2)	3130(2)	36(1)
N5	3479(3)	3079(3)	1790(2)	54(1)
C1	5259(3)	1436(2)	3054(3)	47(1)
C2	5380(4)	464(3)	2979(3)	63(1)
C3	4567(4)	92(3)	3434(3)	57(1)
C4	3924(3)	813(2)	3808(3)	42(1)
C5	3076(3)	688(2)	4411(2)	39(1)
C6	2563(3)	1361(2)	4869(2)	36(1)
C7	1875(3)	1168(2)	5616(2)	42(1)
C8	1602(3)	1967(2)	5905(2)	41(1)
C9	2093(3)	2679(2)	5337(2)	35(1)
C10	2004(3)	3610(2)	5429(2)	35(1)
C11	2581(3)	4282(2)	4942(2)	33(1)
C12	2488(3)	5240(2)	5049(2)	38(1)
C13	3182(3)	5664(2)	4484(2)	38(1)
C14	3744(3)	4961(2)	4030(2)	32(1)

C15	4608(3)	5091(2)	3443(2)	32(1)
C16	5223(3)	4383(2)	3073(2)	34(1)
C17	6252(3)	4460(3)	2625(2)	41(1)
C18	6634(3)	3625(2)	2430(2)	42(1)
C19	5857(3)	3012(2)	2737(2)	39(1)
C20	5956(3)	2067(2)	2679(3)	46(1)
C21	2728(3)	-264(2)	4640(3)	41(1)
C22	3471(4)	-1070(2)	4980(3)	47(1)
C23	3134(4)	-1941(3)	5184(3)	57(1)
C24	2057(5)	-2013(3)	5062(3)	69(2)
C25	1316(4)	-1235(3)	4746(4)	66(1)
C26	1646(3)	-353(3)	4532(3)	53(1)
C27	1284(3)	3895(2)	6138(2)	37(1)
C28	1734(3)	3963(3)	6899(3)	55(1)
C29	1078(4)	4232(4)	7553(3)	69(1)
C30	-36(4)	4426(3)	7454(3)	59(1)
C31	-501(4)	4359(3)	6706(3)	54(1)
C32	160(3)	4091(3)	6049(3)	48(1)
C33	4924(3)	6051(2)	3202(2)	35(1)
C34	4921(4)	6496(2)	2337(2)	45(1)
C35	5224(4)	7381(3)	2103(3)	59(1)
C36	5516(4)	7832(3)	2718(3)	57(1)
C37	5501(3)	7406(3)	3567(3)	50(1)
C38	5223(3)	6508(2)	3817(3)	40(1)
C39	6952(4)	1679(3)	2212(3)	62(1)
C40	7788(5)	1059(4)	2678(5)	113(3)
C41	8709(7)	664(5)	2265(6)	155(4)
C42	8790(7)	913(4)	1397(6)	134(4)
C43	7980(6)	1543(4)	922(4)	98(2)
C44	7062(5)	1921(3)	1345(4)	74(2)
C45	3848(5)	2395(4)	1377(4)	79(2)
C46	4131(6)	2569(6)	503(4)	106(2)
C47	4043(6)	3466(7)	52(4)	119(3)
C48	3623(5)	4226(5)	431(3)	85(2)
C49	3467(6)	5171(6)	16(4)	111(3)
C50	3024(6)	5844(5)	455(4)	107(2)

C51	2717(4)	5629(4)	1319(3)	70(1)
C52	2872(3)	4703(3)	1770(3)	48(1)
C53	3329(4)	3987(4)	1313(3)	56(1)
C54	573(4)	2903(5)	3544(4)	96(2)
C55	-389(5)	3015(5)	3018(5)	117(3)
C56	180(15)	2135(14)	2566(13)	152(8)
C57	1309(9)	2173(8)	2450(7)	74(3)
C56'	-151(9)	3120(8)	2220(7)	65(3)
C57'	974(16)	2929(17)	2197(13)	142(7)

Information for the crystal structure of **27**

Table 1. Crystal data and structure refinement for **27**

Identification code	ak06	
Empirical formula	C49 H51 Co N8 O9 P3 Pr	
Formula weight	1188.73	
Temperature	173(2) K	
Wavelength	0.71073 Å	
Crystal system	Orthorhombic	
Space group	Pnma	
Unit cell dimensions	a = 15.7281(7) Å	□= 90°.
	b = 22.3431(11) Å	□= 90°.
	c = 14.0630(6) Å	□ = 90°.
Volume	4941.9(4) $Å^3$	
Z	4	
Density (calculated)	1.598 Mg/m^3	
Absorption coefficient	1.472 mm^{-1}	
F(000)	2416	
Crystal size	0.18 x 0.08 x 0.08 mm^3	
Theta range for data collection	1.71 to 27.49°.	
Index ranges	-8≤h≤20, -29≤k≤12, -18≤l≤13	
Reflections collected	18773	
Independent reflections	5793 [R(int) = 0.0668]	
Completeness to theta = 27.49°	99.4 %	
Absorption correction	Integration	
Max. and min. transmission	0.8955 and 0.7901	
Refinement method	Full-matrix least-squares on F^2	

Data / restraints / parameters	5793 / 0 / 374
Goodness-of-fit on F^2	0.803
Final R indices [I>2sigma(I)]	R1 = 0.0346, wR2 = 0.0545 [3452]
R indices (all data)	R1 = 0.0744, wR2 = 0.0586
Largest diff. peak and hole	0.812 and -0.549 e.$Å^{-3}$

$R1 = \sum(||Fo| - |Fc||) / \sum|Fo|$

$wR2 = [\sum[w(Fo^2 - Fc^2)^2] / \sum[wFo^{22}]]^{1/2}$

$S = [\sum[w(Fo^2 - Fc^2)^2] / (n-p)]^{1/2}$

$w= 1/[\sigma^2(Fo^2)+(m*p)^2+n*p]$, $p = [\max(Fo^2,0)+ 2* Fc^2]/3$, m & n are constants.

Table 2. Atomic coordinates (x 10^4) and equivalent isotropic displacement parameters ($Å^2$x 10^3) for **27**. U(eq) is defined as one third of the trace of the orthogonalized U^{ij} tensor.

	x	y	z	U(eq)
Pr1	1020(1)	2500	4190(1)	20(1)
Co1	3468(1)	2500	5528(1)	22(1)
P1	2328(1)	2862(1)	6202(1)	22(1)
P2	2762(1)	3310(1)	5158(1)	24(1)
P3	3190(1)	2943(1)	4184(1)	26(1)
O1	2340(6)	2500	7277(6)	18(2)
O1'	2346(7)	2719(4)	7264(8)	13(2)
O2	1463(2)	2735(2)	5768(2)	23(1)
O3	2055(3)	3248(2)	4426(3)	22(1)
O4	2273(3)	3075(2)	3936(3)	29(1)
O5	3619(2)	2500	3378(2)	44(1)
O6	3363(3)	3860(2)	4837(3)	40(2)
O6'	3720(3)	3545(3)	4058(4)	40(2)
O7	2399(1)	3578(1)	6220(2)	38(1)
N1	-915(2)	2500	5773(2)	19(1)
N2	-214(2)	3129(1)	4602(2)	20(1)
N3	68(2)	4010(1)	3636(2)	26(1)
N4	608(2)	3128(1)	2821(2)	22(1)

N5	1156(2)	2500	1550(2)	27(1)
C1	-719(2)	3026(1)	5383(2)	20(1)
C2	-1062(2)	3592(1)	5729(2)	21(1)
C3	-1566(2)	3741(2)	6505(2)	27(1)
C4	-1761(2)	4337(2)	6642(2)	33(1)
C5	-1480(2)	4778(2)	6011(2)	36(1)
C6	-990(2)	4630(1)	5227(2)	31(1)
C7	-774(2)	4034(1)	5096(2)	23(1)
C8	-263(2)	3724(1)	4387(2)	22(1)
C9	456(2)	3722(2)	2916(2)	25(1)
C10	763(2)	4036(2)	2068(2)	30(1)
C11	759(2)	4639(2)	1808(2)	44(1)
C12	1125(3)	4788(2)	948(3)	63(1)
C13	1474(3)	4352(2)	362(3)	64(1)
C14	1464(2)	3753(2)	609(2)	47(1)
C15	1097(2)	3597(2)	1473(2)	29(1)
C16	963(2)	3026(2)	1952(2)	26(1)
C17	3414(5)	2348(4)	2321(4)	37(4)
C18	3213(6)	2940(4)	1910(6)	63(3)
C19	3769(6)	3913(4)	3974(5)	60(3)
C19'	3350(7)	4122(5)	3866(7)	56(3)
C20	3390(6)	4342(5)	3317(7)	75(3)
C20'	3178(6)	4248(5)	2918(6)	51(3)
C21	1773(2)	4031(2)	6060(2)	38(1)
C22	1094(2)	4020(2)	6800(2)	57(1)
C23	1622(14)	2808(9)	7882(14)	30(7)
C23'	1649(11)	2671(7)	7913(12)	15(6)
C24	1798(14)	2500	8803(14)	46(6)
C24'	1796(15)	2291(8)	8735(15)	31(4)
C25	4170(3)	2500	6800(3)	29(1)
C26	4369(2)	3008(2)	6254(2)	35(1)
C27	4699(2)	2813(2)	5382(2)	42(1)

LIST OF REFERENCES

1.) Kohle, A.; Wilson, J. S.; Friend, R. H. *Adv. Mater.* **2002**, *14*, 701-707.

2.) Forrest, S. R. *IEEE Journal on Selected Topics in Quantum Electronics* **2000**, *6*, 1072-1083.

3.) Helfrich, W.; Schneider, W. G. *Phys. Rev. Lett.* **1965**, *14*, 229.

4.) Bulovic, V.; Burrows, P. E.; Forrest, S. R. *Electroluminescence:Semiconductors and semimetals*. ed.; Academic Press: San Diego, 2000.

5.) Tang, C. W.; vanSlyke, S. A. *Appl. Phys. Lett.* **1987**, *51*, 913-915.

6.) Zhu, D. B.; Liu, Y. Q.; Bai, F. L. *Thin Solid Films* **2000**, *363*, 51-54.

7.) Burroughes, J. H.; Bradley, D. D. C.; Brown, A. R.; Marks, R. N.; Mackay, K.; Friend, R. H.; Burns, P. L.; Holmes, A. B. *Nature* **1990**, *347*, 539-41.

8.) Yu, G.; Liu, Y. Q.; Wu, X.; Zhu, D. B.; Li, H. Y.; Jin, L. P.; Wang, M. Z. *Chem. Mater.* **2000**, *12*, 2537-2541.

9.) Van Slyke, S. A.; Chen, C. H.; Tang, C. W. *Appl. Phys. Lett.* **1996**, *69*, 2160.

10.) Kido, J.; Okamoto, Y. *Chem. Rev.* **2002**, *102*, 2357-2368.

11.) Kulkarni, A. P.; Tonzola, C. J.; Babel, A.; Jenekhe, S. A. *Chem. Mater.* **2004**, *16*, 4556-4573.

12.) Cleave, V. Y.; Barny, P.; Friend, R. H.; Tessler, N. *Adv. Mater.* **1999**, *11*, 258-288.

13.) McGehee, M. D.; Bergstedt, T.; Zhang, C.; Saab, A. P.; O'Regan, M. B.; Bazan, G. C.; Srdanov, V. I.; Heeger, A. J. *Adv. Mater.* **1999**, *11*, 1349-1354.

14.) Lamansky, S.; Djurovich, P.; Murphy, D.; Abdel-Razzaq, F.; Lee, H. E.; Adachi, C.; Burrows, P. E.; Forrest, S. R.; Thompson, M. E. *J. Am. Chem. Soc.* **2001**, *123*, 4304-4312.

15.) Quici, S.; Marzanni, G.; Forni, A.; Accorsi, G.; Barigelletti, F. *Inorg. Chem.* **2004**, *43*, 1294-1301.

16.) Lippard, S. J. *Progress in Inorganic Chemistry*. ed.; John Wiley and Sons: New Yorkl, 1984.

17.) Kido, J.; Nagai, K.; Ohashi, Y. *Chem. Lett.* **1990**, 657-660.

18.) Yonezawa, Y. *Chem. Lett.* **1991**, 1267-1270.

19.) Hong, Z.; Li, W.; Zhao, D.; Liang, C.; Liu, X.; Peng, J.; Zhao, D. *Synth. Met.* **1999**, *104*, 165-168.

20.) Kido, J.; Ikeda, H.; Kimura, M.; Katsutoshi, N. *Jpn. J. Appl. Phys., Part 2* **1996**, *35*, L394-L396.

21.) Kido, J.; Hayase, H.; Hongawa, K.; Nagai, K.; Okuyama, K. *Appl. Phys. Lett.* **1994**, *65*,

22.) Gao, X.-C.; Cao, H.; Huang, C.-H.; Li, B. *Appl. Phys. Lett.* **1998**, *72*, 2217.

23.) Gao, X.-C.; Cao, H.; Huang, C.-H.; Umitani, S.; Chen, G.-Q.; Jiang, P. *Synth. Met.* **1999**, *99*, 127-132.

24.) Zhang, J.; Badger, P. D.; Geib, S. J.; Petoud, S. *Angew. Chem. Int. Ed.* **2005**, *44*, 2508-2512.

25.) Sun, R. G.; Wang, Y. Z.; Zheng, Q. B.; Zhang, H. J.; Epstein, A. J. *J. Appl. Phys.* **2000**, *87*, 7589-7591.

26.) Slooff, L. H.; Polman, A.; Cacialli, F.; Friend, R. H.; Hebbink, G. A.; van Veggel, F. C. J. M.; Reinhoudt, D. N. *Appl. Phys. Lett.* **2001**, *78*, 2122-2124.

27.) Spyroulias, G. A.; Coutsolelos, A. G.; Raptopoulou, C. P.; Terzis, A. *Inorg. Chem.* **1995**, *34*, 2476-9.

28.) Burrows, P. E.; Forrest, S. R.; Sibley, S. P.; Thompson, M. E. *Appl. Phys. Lett.* **1996**, *69*, 2959.

29.) Shoustikov, A.; You, Y.; Burrows, P. E.; Thompson, M. E.; Forrest, S. R. *Synth. Met.* **1997**, *91*,217-221.

30.) Higgins, R. W. T.; Monkman, A. P.; Nothofer, H. G.; Scherf, U. *J. Appl. Phys.* **2002**, *91*, 99-105.

31.) Kwong, R. C.; Sibley, S.; Dubovoy, T.; Baldo, M.; Forrest, S. R.; Thompson, M. E. *Chem. Mater.* **1999**, *11*, 3709-3713.

32.) Xiang, H. F.; Yu, S. C.; Che, C. M.; Lai, P. T. *Appl. Phys. Lett.* **2003**, *83*, 1518-1520.

33.) Sabbatini, N.; Guardigli, M. *Coord. Chem. Rev.* **1993**, *123*, 201-228.

34.) Tsvirko, M. P.; Stelmakh, G. F.; Pyatosin, V. E.; Solovev, K. N.; Kachura, T. F.; Piskarskas, A.; Gadonas, R. A. *Chem. Phys.* **1986**, *106*, 467-476.

35.) Martarono, L. A.; Wong, C. P.; Horrocks, W. D.; Goncalves, M. P. *J. Phys. Chem.* **1976**, *80*, 2389-2393.

36.) Korovin, Y.; Rusakova, N. *Reviews in Inorganic Chemistry* **2001**, *21*, 299-329.

37.) Pizzoferrato, R.; Lagonigro, L.; Ziller, T.; Di Carlo, A.; Paolesse, R.; Mandoj, F.; Ricci, A.; Lo Sterzo, C. *Chem. Phys.* **2004**, *300*, 217-225.

38.) Kang, T. S.; Harrison, B. S.; Bouguettaya, M.; Foley, T. J.; Boncella, J. M.; Schanze, K. S.; Reynolds, J. R. *Advanced Function Materials* **2003**, *13*, 205-210.

39.) Harrison, B. S.; Foley, T. J.; Bouguettaya, M.; Boncella, J. M.; Reynolds, J. R.; Schanze, K. S.; Shim, J.; Holloway, P. H.; Padmanaban, G.; Ramakrishnan, S. *Appl. Phys. Lett.* **2001**, *79*, 3770-3772.

40.) Fukuzumi, S. *J. Porphyrins Phthalocyanines* **1999**, *4*, 398-400.

41.) Kadish, K. M.; Smith, K. M.; Roger, G. *The Porphyrin Handbook*. ed.; Academic Press: San Diego, 2000.

42.) Wong, C.-P.; Venteicher, R. F.; Horrocks, W. D., Jr. *J. Am. Chem. Soc.* **1974**, *96*, 7149-7150.

43.) Horrocks, W. D., Jr.; Wong, C.-P. *J. Am. Chem. Soc.* **1976**, *98*, 7157-7162.

44.) Horrocks, W. D.; Hove, E. G. *J. Am. Chem. Soc.* **1978**, *100*, 4386-4392.

45.) Tsukube, H.; Shinoda, S.; Tamiaki, H. *Coord. Chem. Rev.* **2002**, *226*, 227-234.

46.) Tsukube, H.; Shinoda, S. *Chem. Rev.* **2002**, *102*, 2389-2403.

47.) Iwase, A.; Igarashi, A. *Electrochim. Acta* **1992**, *38*, 689-693.

48.) Li, D. M.; Zhao, Z. X.; Sun, H. R.; Liu, G. F.; Shi, T. S.; Liu, X. X.; Dong, S. J. *Synth. React. Inorg. Met.-Org. Chem.* **2000**, *30*, 1899-1915.

49.) Kadish, K. M.; Moninot, G.; Barbe, J. M.; Guilard, R. *Chem. Commun.* **1991**, 1124-1127.

50.) Wong, W.-K.; Zhang, L.; Wong, W.-T.; Xue, F.; Mak, T. C. W. *J. Chem. Soc., Dalton Trans.* **1999**, 615-622.

51.) Foley, T. J.; Abboud, K. A.; Boncella, J. M. *Inorg. Chem.* **2002**, *41*, 1704-1706.

52.) Long, D. P. C.; Day, R. O.; Bianconi, P. A.; Rheingold, A. L. *Inorg. Chem.* **2000**, *39*, 4476-4487.

53.) Hazin, P. N. H.; Bruno, J. *Organometallics* **1987**, *6*, 23-27.

54.) Werts, M. H. V.; Woudenberg, R. H.; Emmerink, P. G.; van Gassel, R.; Hofstraat, J. W.; Verhoeven, J. W. *Angew. Chem. Int. Ed.* **2000**, *39*, 4542-4544.

55.) Korovin, Y. V.; Rusakova, N. V. *J. of Fluorescence* **2002**, *12*, 159-161.

56.) Curry, R. J.; Gillin, W. P. *Curr. Opin. Solid State Mater. Sci.* **2001**, *5*, 481-486.

57.) Piers, W. E.; Emslie, D. J. H. *Coord. Chem. Rev.* **2002**, *233*, 131-155.

58.) Marques, N.; Sella, A.; Takats, J. *Chem. Rev.* **2002**, *102*, 2137-2159.

59.) Foley, T. J.; Harrison, B. S.; Knefely, A. S.; Abboud, K. A.; Reynolds, J. R.; Schanze, K. S.; Boncella, J. M. *Inorg. Chem.* **2003**, *42*, 5023-5032.

60.) Wong, W. Y.; Cheah, K. W.; Lo, W. K.; Li, K. F.; Guo, J.; Wong, W. K.; He, H. *Aust. J. Chem.* **2004**, *57*, 803-810.

61.) Harder, V.; Dubler, H.; Werner, J. *J. Organomet. Chem.* **1974**, *71*, 427.

62.) Klaui, W. *Angew. Chem. Int. Ed.* **1990**, *29*, 627.

63.) Reissmann, U.; Edelmann, F. T. *Z. Anorg. Allg. Chem.* **2003**, *629*, 2433-2434.

64.) Meng, J. X.; Li, K. F.; Yuan, J.; Zhang, L. L.; Wong, W. K.; Cheah, K. W. *Chem. Phys. Lett.* **2000**, *332*, 313-318.

65.) Wong, W.-K.; Hou, A.; Guo, J.; He, H.; Zhang, L.; Wong, W.-Y.; Li, K.-F.; Cheah, K.-W.; Xue, F.; Mak, T. C. W. *J. Chem. Soc., Dalton Trans.* **2001**, 3092-3098.

66.) Colle, M.; Garditz, C.; Muckl, A. G. *Synth. Met.* **2004**, *147*, 97-100.

67.) Baldo, M. A.; Forrest, S. R. *Phys. Rev. B: Condens. Matter* **2000**, *62*, 10958.

68.) Bertini, I.; Coutsolelos, A.; Dikiy, A.; Luchinat, C.; Spyroulias, G.; Troganis, A. *Inorg. Chem.* **1996**, *35*, 6308-6315.

69.) Behere, D. V. B.; Mitra, A. *Inorg. Chem.* **1982**, *21*, 386-390.

70.) Jenkins, B. G.; Lauffer, R. B. *Inorg. Chem.* **1988**, *27*, 4730-4738.

71.) Shavaleev, N. M.; Moorcraft, L. P.; Pope, S. J. A.; Bell, Z. R.; Faulkner, S.; Ward, M. D. *Chemistry, A European Journal* **2003**, *9*, 5283-5291.

72.) Imbert, D.; Comby, S.; Chauvin, A.; Bunzli, J. G. *Chem. Commun.* **2005**, 1432-1434.

73.) Harrison, B. S.; Foley, T. J.; Knefely, A. S.; Mwaura, J. K.; Cunningham, G. B.; Kang, T. S.; Bouguettaya, M.; Boncella, J. M.; Reynolds, J. R.; Schanze, K. S. *Chem. Mater.* **2004**, *16*, 2938-2947.

74.) Kang, T.-S.; Harrison, B. S.; Foley, T. J.; Knefely, A. S.; Boncella, J. M.; Reynolds, J. R.; Schanze, K. S. *Adv. Mater.* **2003**, *15*, 1093-1097.

75.) Wang, J. F.; Wang, R. Y.; Yang, J.; Zheng, Z. P.; Carducci, M. D.; Cayou, T.; Peyghambarian, N.; Jabbour, G. E. *J. Am. Chem. Soc.* **2001**, *123*, 6179-6180.

76.) Adachi, C.; Baldo, M. A.; Forrest, S. R. *J. Appl. Phys.* **2000**, *87*, 8049-8055.

77.) Gordon, A. J.; Ford, R. A. *The Chemist's Companion : A Handbook of Practical Data, Techniques, References*. ed.; Wiley: New York, 1972.

78.) Klaui, W.; Dehnicke, K. *Chem. Ber.* **1978**, *111*, 451-468.

79.) Trofimenko, S. *J. Am. Chem. Soc.* **1967**, *89*, 6288-94.

80.) Adler, A. D.; Longo, F. R.; Finarell, J. D.; Goldmach, J. A.; Korsakof, J. *J. Org. Chem.* **1967**, *32*, 476.

81.) Arnold, J.; Dawson, D. Y.; Hoffman, C. G. *J. Am. Chem. Soc.* **1993**, *115*, 2707-2713.

82.) Kadish, K. M.; Morrison, M. M. *J. Am. Chem. Soc.* **1976**, *98*, 3326-3328.

83.) Kadish, K. M.; Morrison, M. M. *Bioinorg. Chem.* **1977**, *7*, 107-115.

84.) Korovin, Y. V.; Kuz'min, V. E.; Rusakova, N. V.; Zhilina, Z. I.; Vodzinsky, S. V.; Yudanova, I. *Russ. J. Inorg. Chem.* **2003**, *48*, 410-414.

85.) Foley Timothy, J.; Harrison Benjamin, S.; Knefely Alison, S.; Abboud Khalil, A.; Reynolds John, R.; Schanze Kirk, S.; Boncella James, M. *Inorganic chemistry,* **2003,** *42*, 5023-32.

86.) Bonhote P; Dias AP; Papageorgiou N; Kalyanasundaram K; M, G. *Inorg. Chem.* **1996**, *35*, 1168-1178.

87.) Mazurkiewicz, J. H.; Innis, P. C.; Wallace, G. G.; MacFarlane, D. R.; Forsyth, M. *Synth. Met.* **2003**, *135-136*, 31-32.

88.) Quici, S.; Cavazzini, M.; Marzanni, G.; Accorsi, G.; Armaroli, N.; Ventura, B.; Barigelletti, F. *Inorg. Chem.* **2005**, *44*, 529-537.

89.) Trojan, K. L.; Hatfield, W. E.; Kepler, K. D.; Kirk, M. L. *J. Appl. Phys.* **1991**, *69*, 6007-6009.

90.) Nalwa, H. S. *Supramolecular Photosensitive and Electroactive Materials*. ed.; Academic Press: San Diego, 2001.

91.) Clarisse, C.; Riou, M. T. *Inorg. Chim. Acta* **1987**, *130*, 139-144.

92.) Foley Timothy, J. *Dissertation*, University of Florida, Gainesville, 2001.

93.) Orti, E.; Bredas, J. L.; Clarisse, C. *J. Chem. Phys.* **1990**, *92*, 1228-1235.

94.) Frigerio, N. A. 3027391, 1962.

95.) Adler, A. D.; Longo, F. R.; Finarell, J. D.; Goldmach, J. A.; Korsakof, J. *Journal of Organic Chemistry* **1976**, *32*, 476.

96.) Dooling, C. M.; Worsford, O.; Richardson, T. H.; Tregonning, R.; Vysotsky, M. O.; Hunter, C.; Kato, K.; Shinbo, K.; Kaneko, F. *J. Mater. Chem.* **2001**, *11*, 392-398.

97.) Harrison Benjamin, S. *Dissertation*, University of Florida, Gainesville, 2003.

98.) Segura, J. L. *Acta Polymer* **1998**, *49*, 319-344.

99.) Ling, Q. D.; Yang, M.; Zhang, W.; Lin, H.; Yu, G.; Bai, F. L. *Thin Solid Films* **2002**, *417*, 127-131.

100.) Ling, Q. D.; Cai, Q. J.; Kang, E. T.; Neoh, K. G.; Zhu, F. R.; Huang, W. *J. Mater. Chem.* **2004**, *14*, 2741-2748.

101.) Zeng, L.; Yang, M.; Wu, P.; Ye, H.; Liu, X. *Synth. Met.* **2004**, *144*, 259-263.

102.) Yang, M. J.; Zeng, L. C.; Zhang, C. H.; Wu, P.; Ye, H.; Liu, X. *J. Mater. Sci.* **2004**, *39*, 1407-1409.

103.) Jiang, B.; Jones, W. E. *Macromolecules* **1997**, *30*, 5575-5581.

104.) Haber, J.; Klosowski, M.; Poltowicz, J. *J. Mol. Catal. A: Chem.* **2003**, *201*, 167-178.

105.) Kamachi, M.; Cheng, X. S.; Kida, T.; Kajiwara, A.; Shibasaka, M.; Nagata, S. *Macromolecules* **1987**, *20*, 2665-2669.

106.) Kuebler, S. M.; Denning, R. G.; Anderson, H. L. *J. Am. Chem. Soc.* **2000**, *122*, 339-347.

107.) Liu, Z.; Yasseri, A. A.; Loewe, R. S.; Lysenko, A. B.; Malinovskii, V. L.; Zhao, Q.; Surthi, S.; Li, Q.; Misra, V.; Lindsey, J. S.; Bocian, D. F. *J. Org. Chem.* **2004**, *69*, 5568 - 5577.

108.) Pomogailo, A. D.; Razumov, V. F.; Voloshanovskii, I. S. *J. Porphyrins Phthalocyanines* **2000**, *4*, 45-64.

109.) Shoji, O.; Okada, S.; Satake, A.; Kobuke, Y. *J. Am. Chem. Soc.* **2005**, *127*, 2201-2210.

110.) Liu, X.; Sternberg, E.; Dolphin, D. *Chem. Commun.* **2004**, 852-853.

111.) Kose, M. E. *Dissertation*, Univeristy of Florida, Gainesville, 2005.

112.) Lindsey, J. S.; Wagner, R. W.; Prathapan, S.; Johnson, T. E. *Tetrahedron* **1994**, *50*, 8941-8968.

BIOGRAPHICAL SKETCH

Alison Steele Knefely, daughter of George and Carolyn Knefely, is a native of Pensacola, FL. She attended the International Baccelaurate (IB) program at Pensacola High School (PHS) from 1992-1996 and was captain of the girls' tennis team. After graduating from PHS with an IB diploma, she attented Eckerd College (EC), in St. Petersburg, FL, from 1996 to 2000. At EC, Alison was the captain of the women's tennis team and a chemistry major. While at EC, she had the opportunity to conduct research under the advisement of Dr. R. Chris Schanbel at EC and Los Alamos National Laboratory (LANL), and under the advisement of Dr. Mike Scott at the University of Florida (UF) in Gainesville, FL and Dr. Marcel Wesolek at the University of Louis Pasteur in Strasbourg, France. After graduating from EC with a BS in Chemistry, Alison started graduate school at UF. She became a member of Jim Boncella's group in October 2000 and had the opportunity to conduct research under his advisement at UF and LANL. After graduating from UF, Alison and her husband, Rob, will move to the Philadelphia area.